PHOSPHORYLATION INDEPENDENT ACTIVATION OF BETA ARRESTIN 2 AND BETA ADRENOCEPTOR TYPE 2 BY MEANS OF SMALL MOLECULES

A THESIS SUBMITTED TO
THE GRADUATE SCHOOL OF NATURAL AND APPLIED SCIENCES
OF
MIDDLE EAST TECHNICAL UNIVERSITY

BY

ALİ AKYOL

IN PARTIAL FULFILLMENT OF THE REQUIREMENTS
FOR
THE DEGREE OF MASTER OF SCIENCE
IN
BIOCHEMISTRY

SEPTEMBER 2021

Approval of the thesis:

PHOSPHORYLATION INDEPENDENT ACTIVATION OF β-ARRESTIN 2 AND BETA ADRENOCEPTOR TYPE 2 BY MEANS OF SMALL MOLECULES

submitted by **ALİ AKYOL** in partial fulfillment of the requirements for the degree of **Master of Science** i**n Biochemistry, Middle East Technical University** by,

Prof. Dr. Halil Kalıpçılar
Dean, Graduate School of **Natural and Applied Sciences** _____

Assoc. Prof. Dr. Yeşim Soyer
Head of the Department, **Biochemistry** _____

Assoc. Prof. Dr. Çağdaş Devrim Son
Supervisor, **Biochemistry, METU** _____

Assoc. Prof. Dr. Can Özen
Co-Supervisor, **Biotechnology, METU** _____

Examining Committee Members:

Assoc. Prof. Dr. Tülin Yanık
Biology, METU _____

Assoc. Prof. Dr. Çağdaş Devrim Son
Biochemistry, METU _____

Prof. Dr. Sreeparna Banerjee
Biology, METU _____

Assist.Prof. Dr. Özge Şensoy
Computer Eng., İstanbul Medipol Uni. _____

Assist. Prof. Dr. Ahmet Acar
Biology, METU _____

Date: 08.09.2021

I hereby declare that all information in this document has been obtained and presented in accordance with academic rules and ethical conduct. I also declare that, as required by these rules and conduct, I have fully cited and referenced all material and results that are not original to this work.

Name Last name: Ali Akyol

Signature:

ABSTRACT

PHOSPHORYLATION INDEPENDENT ACTIVATION OF β-ARRESTIN 2 AND BETA ADRENOCEPTOR TYPE 2 BY MEANS OF SMALL MOLECULES

Akyol, Ali
Master of Science, Biochemistry
Supervisor: Assoc.Prof. Dr. Çağdaş Devrim Son
Co-Supervisor: Assoc. Prof. Dr. Can Özen

September 2021, 102 pages

The activities of neurohormones such as epinephrine are mediated by Adrenoceptors. In physiological processes, these messengers play an essential role; thus, Adrenoceptors are commonly found across the body. Agonist stimulated Adrenoceptor type 2 (β-2AR) works primarily by activating adenylyl cyclase through the stimulatory G protein (G_s), inducing an increase in the intracellular level of cAMP. This second messenger ultimately mediates downstream physiological effects.

After few seconds of agonist stimulation, β-2ARs rapidly get phosphorylated by kinases (GRKs, PKA A, and C), resulting in uncoupling from G_s. High exposure to agonist, B2AR undergoes downregulation, mediated by a cytoplasmic adapter protein called Beta Arrestin. The magnitude of this interaction is determined by the receptor's phosphorylation level. This intensity of interaction influences the fate of the receptor, which can either be recycled back to the cell membrane or degraded in the cytoplasm, causing its downregulation. Mutations in the receptor at the amino

acid residues that can be phosphorylated could prevent phosphorylation and the interaction with Arrestin. Therefore, the signal cannot be terminated.

In this study, we try to facilitate phospho-deficient (P.D.) B2AR and wild-type β-Arrestin 2 interaction with the help of small molecules. Our aim is to find such compounds that promote the binding of β-Arrestin 2 to P.D.-β-2AR. We used Förster Resonance Energy Transfer (FRET) to monitor the interaction between P.D. or wild type β-2AR and Beta Arrestin 2. For co-localization and FRET studies, C-tail mCherry tagged β-2AR or P.D. β-2AR and 177^{th} aa. position mEGFP tagged β–Arrestin 2 and GRK2 co-transfected in N2a cells were imaged using a spinning disc confocal microscope. Results showed that one of the tested chemicals increased FRET between P.D-β-2AR and β Arrestin 2, suggesting an interaction between these proteins.

The kinetic of this chemical on β-2AR and Arrb2 interaction can be further investigated using the techniques optimized in this thesis study.

Keywords Beta-2 Adrenoceptor, Beta-Arrestin 2, Phospho-deficient Beta-2-Adrenoceptor, FRET

ÖZ

KÜÇÜK MOLEKÜLLERLE FOSFORİLASYONDAN BAĞIMSIZ β-ARRESTİN 2 VE BETA ADRENERJİK RESEPTÖR 2 NİN AKTİVASYONU

Akyol, Ali
Yüksek Lisans, Biyokimya
Tez Yöneticisi: Doç. Dr. Çağdaş Devrim Son
Ortak Tez Yöneticisi: Doç. Dr. Can Özen

Eylül 2021, 102 sayfa

Adrenoseptörler, epinefrin gibi nörohormonların aktivitelerine aracılık eder. Farklı fizyolojik süreçlerde, bu haberciler önemli bir rol oynar; bu nedenle, adrenoseptörler yaygın olarak vücudumuzda bulunur. Agonistle uyarılmış Beta Adrenoseptör tip 2 esas olarak, uyarıcı G proteini (G_s) aracılığıyla adenilil silazı aktive ederek ikincil haberci (cAMP)'nin hücre içi seviyesinde bir artışa neden olur. sonrasında ise hücre içinde bazı sinyal yolakları aktive edilmiş olur.

Agonist stimülasyonundan hemen sonra, β-2AR'lar kinazlarla (GRK'ler, PKA A ve C) hızla fosforile olur ve bu olay β-2AR'ın G_s'den ayrılmasına neden olur. Agoniste yüksek düzeyde maruz kalma, β-2AR'ün Beta Arrestin adı verilen bir sitoplazmik adaptör proteinin aracılık ettiği aşağı regülasyona uğramasına sebep olur. Reseptör bağlı arrestin etkileşiminin süreci, reseptörün fosforilasyon seviyesi ile belirlenir. Bu etkileşim yoğunluğuna bağlı olarak, Reseptör hücre zarına geri dönebilir veya sitoplazmada parçalanabilir (down regulation). Reseptör

fosforilasyon bölgesindeki amino asit mutasyonları fosforilasyonu engelleyebilir, bu durumda reseptörün Arrestin'e bağlanması engellenir ve sinyal sonlandırılamaz.

Bu çalışmada, fosforilasyondan yoksun (P.D.) olan β-2AR ve yabanıl tip β-Arrestin 2 arasındaki etkileşimi küçük moleküller yardımıyla tekrardan sağlamaya çalışıyoruz. Amacımız, β-Arrestin 2'nin P.D. β-2AR'a bağlanmayı teşvik edecek bir kimyasal bulmaktır. Bu iki protein arasındaki etkileşimi ve β-Arrestin 2 nin kolokalizyonunu, C terminal den mCherry işaretli β-2AR veya P.D.-β-2AR, 177. aa. pozisyonundan mEGFP etiketli β–Arrestin 2 ve yabanil tip GRK2 N2a hücrelerinde birlikte transfekte edilerek, Förster Rezonans Energy Transfer (FRET) gibi floresan mikroskopi teknikleri ile izlendi. Sonuç olarak, test edilen kimyasallardan birinin P.D-β-2AR ve β Arrestin 2 arasında FRET'i arttırdığı dolayısı ile bu iki protein arasında etkileşime yol açtığı görülmüştür.

Gelecek çalışmalarda bu kimyasalın β-2AR ve Arrb2 etkileşimi üzerindeki kinetiği bu çalışmada geliştirilen teknikler ile detaylı bir şekilde araştırılabilecektir.

Anahtar Kelimeler: Beta-2 Adrenoceptor, Beta-Arrestin 2, Fosforilasyondan yoksun β-2 Adrenoseptör, FRET

To Samira Assafiri…

ACKNOWLEDGMENTS

Firstly, I would like to express my great gratitude to my supervisor Assoc. Prof. Dr. Çağdaş D. SON for his patient and guidance. He introduced and guided me through numerous techniques. I am also thankful for his tolerance for me disturbing him any time I have questions. Secondly, I am grateful for working on this project with Assist. Prof. Dr. Özge Şensoy from Istanbul Medipol University and thankful for her constant support.

I also want to thank the members of my thesis examining committee; Prof. Dr. Sreeparna Banerjee, Assoc. Prof. Dr. Tülin Yanık, Assist. Prof. Dr. Ahmet Acar for their useful suggestions to evolve this thesis into its best version.

I appreciate the company and their great support of my Lab mates Cansu Şebnem Özyapıcıel, Tolga Suat Sezen, İrem Aydın, Öykü Yaman and Algı Demirbaş. They often helped me through the experiments and they often seeded cells for me. I also thank former Son Lab member Hüseyin Evci for preparing Gap43–mCh-mEGFP, β-2AR-P.D-mCh, and β-2AR-mCh. carrying plasmids that were used in this study.

I need to thank a former member of SON Lab. Sara Mingu for helping me with microscope imaging. She showed me how to work on the microscope at the very beginning of this work. I want to thank my best friend Onur Özbir for his great support for my personal life and academic life in the last ten years and Mehmet Altundağ for proofreading this thesis. I also thank the members of Mayda Gürsel's Lab for their support and Dr. Orkun Cevheroğlu from stem cell institute, Ankara University for lending Poly-L-Lysine which is used in this study. And Zeynep Eda Akyıldız from Lab 254 for lending me any pieces of equipment and chemicals whenever I needed them.

I would like to acknowledge that this thesis was supported by TUBİTAK with project number 117Z245.

TABLE OF CONTENTS

LIST OF TABLES

TABLES

LIST OF FIGURES

FIGURES

LIST OF ABBREVIATIONS

ABBREVIATIONS	
AA	Amino acid
AC	Adenylyl Cyclase
ADP	Adenosine Diphosphate
AGE	Agarose Gel Electrophoresis
Arrb2	β-2 Arrestin
ATP	Adenosine Triphosphate
β1AR	β-1 Adrenergic Receptor
β2AR	β-2 Adrenergic Receptor
bp	base pair
cAMP	cyclic AMP
D-MEM	Dulbecco's Modified Eagle Medium
DMSO	Dimethyl Sulfoxide
DNA	Deoxyribonucleic Acid
EDTA	Ethylenediaminetetraacetic acid
FBS	Fetal Bovine Serum
FP	Fluorescent protein
FRET	Förster Resonance Energy Transfer
GEF	Guanine Nucleotide Exchange Factor
GFP	Green Fluorescent Protein

GPCR	G Protein-Coupled Receptor
GRK2	G Protein Receptor Kinase
Kb	Kilobase
LB	Luria Bertani
MAPK	Mitogen-Activated Protein Kinase
mCherry	monomeric Cherry
mEGFP	monomeric Enhanced Green Fluorescent Protein
N2a	Neuro2a
NMR	Nuclear Magnetic Resonance
PBS	Phosphate Buffer Saline
PCR	Polymerase Chain Reaction
PKA	Phospho Kinase A
SDM	Site-Directed Mutagenesis
TAE	Tris –Acetate EDTA

CHAPTER 1

INTRODUCTION

1.1 G-Protein Coupled Receptors

G protein (heterotrimeric guanine nucleotide-binding protein)-coupled receptors (GPCRs) or 7-transmembrane helical Receptors compose the largest and widely distributed membrane proteins. They play crucial roles in the regulation and wide range of physiological processes in mammalian and nonmammalian systems (Pierce, Premont, and Lefkowitz 2002), including communication among cells. Stimulation of these receptors from the extracellular domain trigger G protein recruitment in the intracellular carboxyl-terminal. In terms of both, ligands and G proteins, GPCRs show high plasticity regarding numerous interacting proteins. Therefore, a single GPCR is considered to function in many different signaling pathways (Gahbauer and Böckmann 2016). A large number of experimental pieces of evidence indicate that the specificity of GPCR signaling is achieved by the selective compartmentalization of its components within specific microdomains on the cell membrane (Anderson 1998; Chini and Parenti 2004). Based on structural predictions, it is estimated that the human genome carries nearly 1000 GPCRs, and the biological functions of these are yet to be discovered. Many diseases such as psychiatric disorders, cancer, autoimmune diseases, and diabetes are often due to one or more GPCR signaling anomalies (Zhang & Eggert, 2013). Therefore, they are an important target for drug research, and conceivably nearly 40% of the drugs in the market target GPCRs (Schiöth and Lagerström 2008).

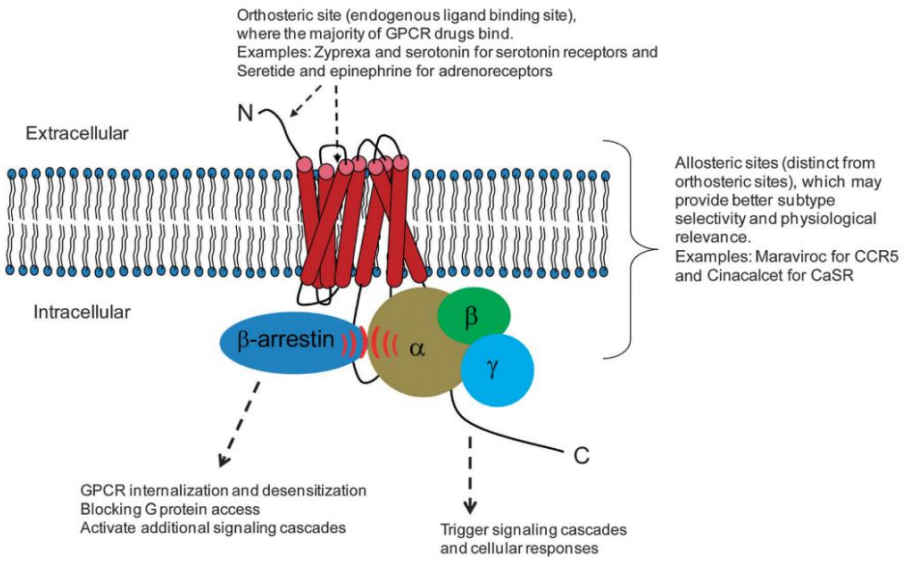

Figure 1.1. A GPCR and its interaction partners, G protein and Arrestin proteins. The ligand-binding site of the receptor may differ, and the allosteric site of the receptor can be at any region of the receptor that is distinct from its Orthosteric sites. G protein or Arrestin bound receptor activates different pathways. (Taken from (Zhang & Eggert, 2013)).

The 7 of 19 licensed drug products with the greatest sales revenue that reached their peak sale up to the year 2013 were targeted towards GPCRs. The Plavix (**1** in figure 2), an antithrombotic drug reached up to 9 billion $ annual sale that followed by Salmeterol (phenylethanolamine) a β-2AR-R agonist that has been used to treat asthma with 8 billion $ (**2** in figure2). From 2013 to 2015 15 new compounds that also target GPCRs, were approved by FDA as new chemical entities (shown in figure 2) (Jacobson 2015).

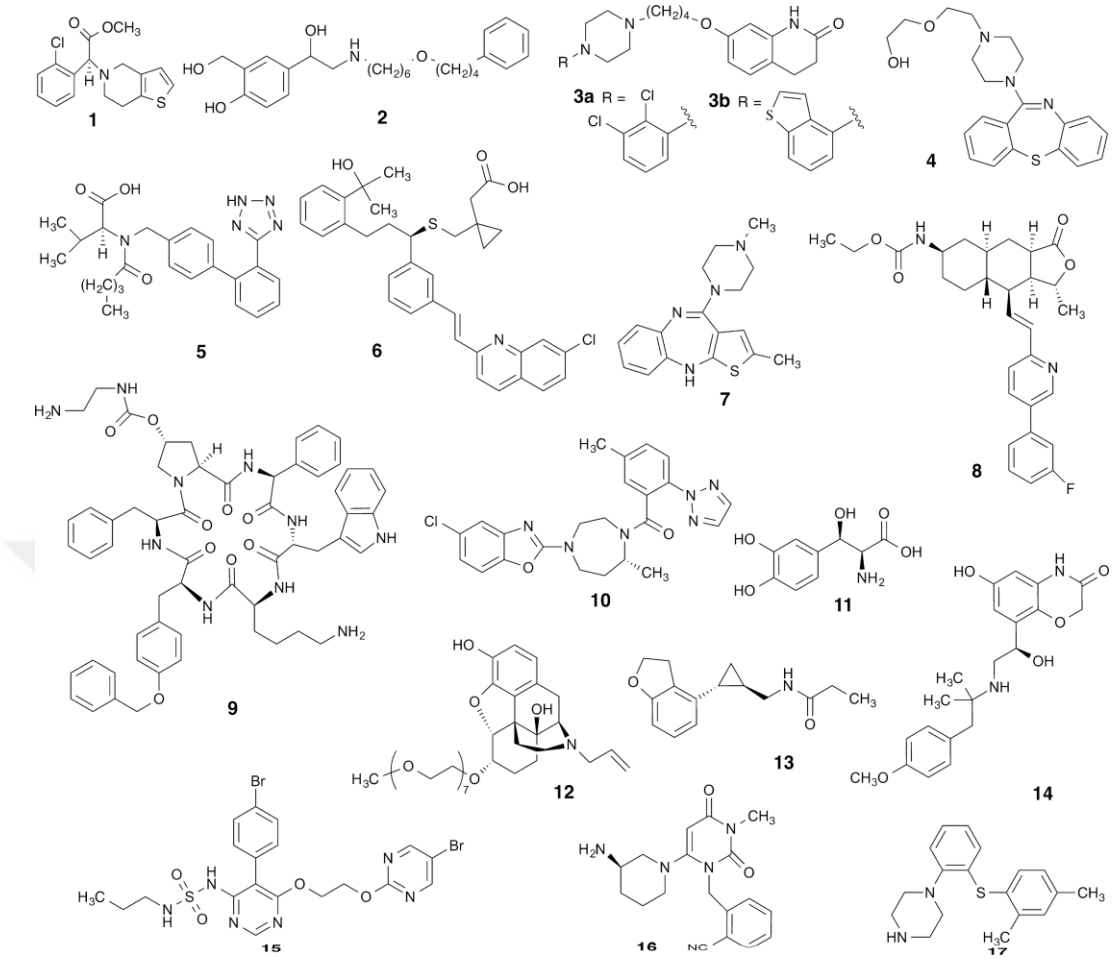

Figure 1.2 The most successful small molecular GPCR ligands. (1–7) as of 2013 and the small molecular GPCR ligands that have been approved between 2013-2015 (3b, 8–17) taken from (Jacobson, 2015).

1.1.1 Active States of GPCRs

The remarkable progress in GPCR structural biology has greatly aided our understanding of GPCR signaling, including the determination of above 170 structures from 40 unique GPCR members in active or inactive states and complex with G_s or arrestin (Kang *et al.* 2018). The cytoplasmic part of the seven-transmembrane-helix domain (TMD) is closed in inactive states (Rosenbaum *et al.* 2007; Cherezov *et al.* 2007; Palczewski *et al.* 2000), preventing GPCRs from being efficient and effectively couple with cellular signaling transducers. Agonist binding

results in a conformational change, such as an outward movement of transmembrane helix 6 (TM6) at the cytoplasmic end, (Xu *et al.* 2011; Lebon *et al.* 2011; Choe *et al.* 2011; Funk JL, Frye JB, Oyarzo JN 2014; Standfuss *et al.* 2011; Rosenbaum *et al.* 2011), which creates a cavity in the TMD that exposed for interaction with one or more unique modulator proteins. This mechanism of action was revealed by the G_s-bound β2-adrenergic receptor (β2AR) structure and recent cryo-electron microscopy structures of G_s-bound class B GPCRs. As a result of these studies, it was found that agonist binding results in a 14–18 Å outward movement of TM6 at the cytoplasmic side (Sŏren G.F. Rasmussen *et al.* 2011; Li *et al.* 2017; Liang *et al.* 2017).

Activated GPCRs by their ligands exist in a wide spectrum of functional states. Upon stimuli, depending on the type of ligand may activate more than one isoform of G proteins or even specifically activate β-Arrestin, independent from G protein-mediated pathways. Even without stimulation GPCRs may display basal, agonist independent activity towards G protein or β-Arrestin mediated signaling pathways. Orthosteric compounds that occupy the native hormone-binding cavity can be categorized according to their effect on receptor signaling through a specific pathway. A compound that inhibits basal activity is called an Inverse agonist. While full agonists activate the receptor at the maximum level, partial agonists activate the receptor up to a certain level, which, unlike full agonists, never reach maxima even at very high concentrations.

On the other hand, neutral antagonists sterically block other ligands to bind to the receptor while they do not affect the receptor's basal activity. The existence of the receptor's basal activity suggests that the receptor exhibits a low energy barrier between those mentioned conformational states and the possibility of transition between those states. Ligands with different effects act through stabilizing one of those conformations (Søren G F Rasmussen *et al.* 2011).

.

1.1.2 The Classical View of GPCR Signal Transduction

The three components of the most studied transmembrane GPCR signaling are GPCRs, G proteins, and adenylyl cyclases (ACs). The classical and yet still widely accepted sequential model of GPCR-mediated signal transduction involves AC activation. Upon binding of an agonist molecule to the receptor induces to G protein coupling in its GDP-bound heterotrimeric Gαβγ form to the receptor then triggers guanylyl nucleotide exchange, GDP for GTP, that causes a rapid release of Gα from the heterotrimeric complex with its GTP-bound active form. Subsequently, it binds to the AC that eventually promotes the production of cAMP. Because Gα binding site of AC overlaps with the Gα binding site of Gβγ, suggest AC activation requires dissociation of Gα from Gβγ to allow effector activation The termination of the signal starts with the hydrolysis of GTP to GDP by Gα protein's GTPase activity, which results in the dissociation of Gα from AC and re-forming of the free heterotrimeric Gαβγ protein. Since the rate of cAMP production is much greater than GTP hydrolysis, multiple cAMP molecules can be produced by one agonist-induced GPCR activation per minute (Freeman 2018).

1.1.3 GPCR Biased Agonism

As the name implies, over decades, GPCRs were thought to couple only to the heterotrimeric G proteins, which regulate the activation of phospholipase C or adenylyl cyclase, which eventually starts downstream signaling through second messengers such as cAMP. Later, it was discovered that GPCRs also trigger G protein-independent activation of ERK1/2 and other kinases through β-Arrestin pathways (figure 1.3) (McDonald *et al.* 2000; Luttrell *et al.* 2001; Charest and Bouvier 2003; Beaulieu *et al.* 2005; Lefkowitz and Shenoy 2005). The discovery of this complexity of the GPCR signaling changed the classical view of GPCR signal transduction. The unveiling of such molecules that are able to induce a signal only

a fraction of these possible responses had led to an update on pharmacological terminology. In addition to "balanced agonists" which activate both G protein and β-Arrestin mediated signaling equally; now it is well accepted the existence of some compounds that preferentially activate only one of these pathways referred to as "biased agonists" (Kahsai *et al.* 2011; Azzi *et al.* 2003; Audet and Bouvier 2012; Lefkowitz and Shenoy 2005; Galandrin, Oligny-Longpré, and Bouvier 2007; Kenakin 2007; Drake *et al.* 2008; Shukla *et al.* 2008b).

In the last two decades, three independent groups have shown the existence of biased character of some ligands. The first of these was in 2003, Robert Lefkowitz's group published on AngII analog, [Sar1-Ile4-Ile8]-AngII (SII), triggers β-Arrestin recruitments to angiotensin AT1 receptor without inducing ERK1/2 phosphorylation. Within two months, another group showed that previously considered as a β-2AR antagonist, propranolol, was, in fact, a β-Arrestin biased agonist (Azzi *et al.* 2003). These findings were corroborated by another group (Baker, Hall, and Hill 2003). Based on these shreds of evidence, it is conceivable that some of the current clinically used drugs, which are mostly antagonists, would be a G protein or Arrestin biased agonists. Expected features of these compounds could explain the distinct outcomes in patients treated with different antagonists, even though they target the same receptor. Drugs in the β-blocker category can be given as an example. Drugs in this category are generally used for myocardial infarction (Kopecky 2006). Surprisingly some β-blockers also have beneficial effects on heart failure. One of which is, carvedilol showed to be most efficient (Packer *et al.* 1996; Poole-Wilson *et al.* 2003). Further studies revealed that carvedilol acts as a β-arrestin biased agonist (Wisler *et al.* 2007). Later on, it was shown that even β–arrestins biased ligands can result in distinct patterns of downstream signaling, possibly by inducing different conformations of β-arrestins (Santos *et al.* 2015). These studies reveal the need for further characterization of biased compounds because the actions of these compounds may comprise highly complex mechanisms and functional selectivity rather than simply categorized by G protein or β-arrestins biased ligands (Calebiro *et al.* 2009).

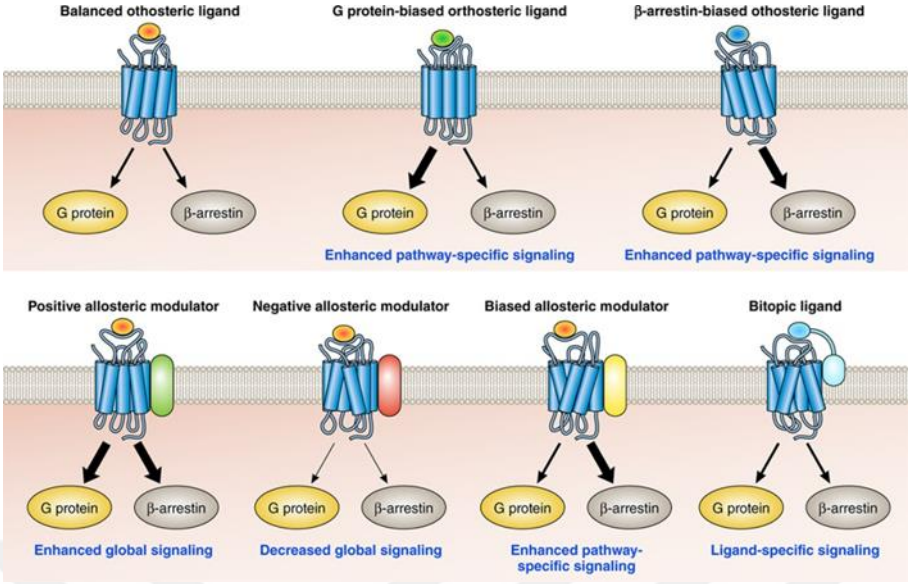

Figure 1.3 Mechanisms of biased GPCR signaling. Several classes of biased compounds targeting GPCRs have been revealed. These include orthosteric ligands that occupy the binding site of the endogenous ligand, allosteric modulators that bind to a site distinct from the endogenous ligand of the receptor, and bitopic ligands that bind at both orthosteric and allosteric sites. Taken from (Wisler, Rockman, and Lefkowitz 2018).

1.2 Arrestins

Arrestins belong to a four-member small homologous protein family (arrestin 1–4), that carry out an essential position in regulating GPCR signaling. Arrestin 1 (or visual arrestin) and arrestin 4 (or cone arrestin) are only expressed in the visual system. In contrast, arrestin 2 (or b-arrestin 1) and arrestin 3 (or β-Arrestin 2) are ubiquitously expressed (Park *et al.* 2016). Arrestin 1 was first named "S- antigen" due to its immunogenicity in uveitis (Wacker *et al.* 1977). The name was revised to Arrestin because of the discovery of its involvement in interfering (or "arresting") rhodopsin signaling in further studies (Zuckerman and Cheasty 1986; Wilden *et al.* 1986). According to a series of experiments, visual arrestin interacts with light-activated and phosphorylated rhodopsin, inhibiting rhodopsin signal transduction (Kuhn, n.d.; Bennett and Sitaramayya 1988). Soon after, arrestin 2 was discovered

to disrupt Beta 2- adrenergic receptor signaling (β-2AR) in a similar way to visual arrestin and was given the name β-arrestin (later renamed as β-arrestin 1) (Martin J Lohse *et al.* 2017; Benovic *et al.* 1987; M. J. Lohse *et al.* 1990). cDNA homology cloning led to the discovery of a new non-visual arrestin (arrestin 3 or β-arrestin 2) and a second visual arrestin (arrestin 4, cone arrestin, or X-arrestin) (Craft, Whitmore, and Wiechmann 1994; Attramadal *et al.* 1992; Sterne-Marr *et al.* 1993; Murakami *et al.* 1993).

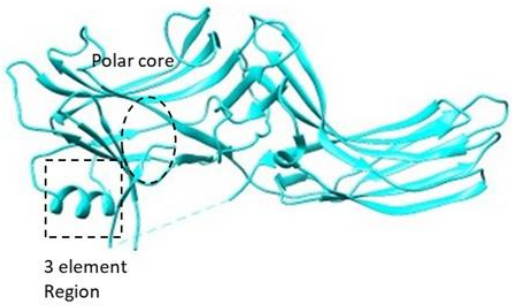

Figure 1.4 Crystal structure of β- arrestin 2. PDB code: 3P2D.

Four members of arrestins typically share over 75 % amino acid sequence similarity (Figure 1.5). The 3D structure of these proteins has two distinct lobes (N-lobe and C-lobe), each composed of mainly β-sandwich protein motif, yet each member has significantly different requirements for receptor phosphorylation in order to bind to the receptor. While Arr1 shows the most sensitivity to receptor phosphorylation β-Arrestin 2 (Arr3) shows less sensitivity. Arr1 can only form a high-affinity complex with phosphorylated and activated receptors regardless of receptor types. Phosphorylation requirement for β-Arrestin 2 receptor complex differs from receptor to receptor. For instance, β-Arrestin 2 can not bind to phosphodeficient (P.D.) β2-AR, yet it forms complex with M2R (Muscarinic Receptor) without phosphorylation (Gimenez *et al.* 2012).

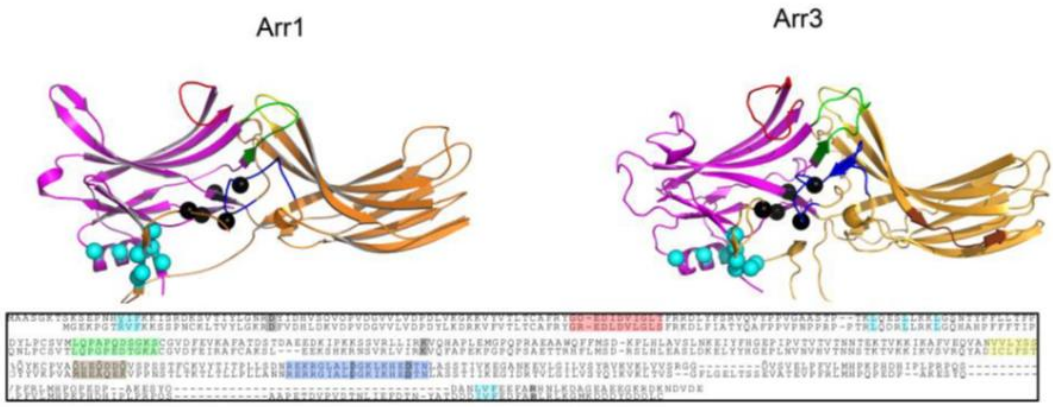

Figure 1.5: Crystal structures of Arr1 and Arr3. N-lob and C-lob of the protein are shown in purple and orange, respectively. Regions that change upon binding to the receptor are shown in different colors. Cα atoms of the polar core are shown in black balls. Sequence alignment of Arr1 and Arr3 in the lower panel (Sensoy, Moreira, and Morra 2016).

β-Arrestin-Receptor complex forms in a two-step binding mechanism (Pierce *et al.*, 2002; Freedman &Lefkowitz, 1996; Gurevich *et al.*, 1995; Kovoor, Celver, Abdryashitov, Chavkin, & Gurevich, 1999). In the first step N lobe of β-Arrestin attaches the phosphorylated amino acids of the receptor, which results in an outwards movement of the C lobe from the N lobe leading to a conformational change of the protein. This movement releases C-tail from the polar core and three-element region called the "structural determinants" that are necessary for the second step binding of the β-Arrestin to the receptor (Nobles *et al.* 2007; Shukla *et al.* 2008a; Yun *et al.* 2015).

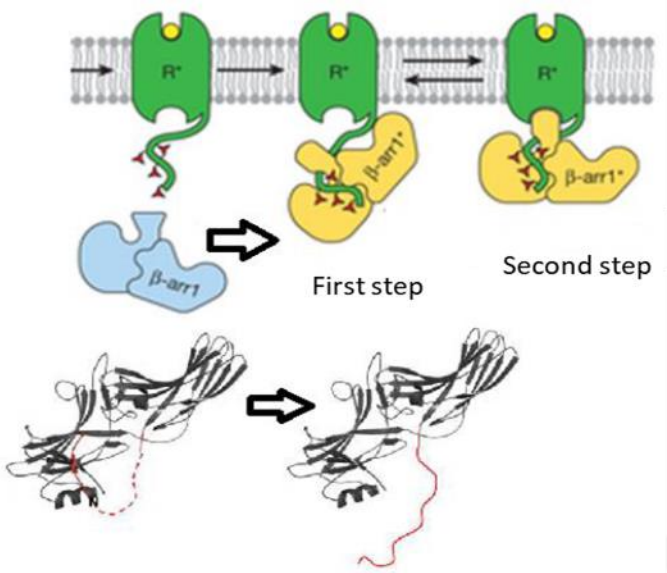

Figure 1.6 Schematic representation of the 2-steps binding mechanism of Arrestin (Top panel) Active and inactive conformations of arrestin shown in yellow and blue respectively, the yellow dot represents the agonist the phosphates group on receptor shown in the red triangle. The detachment of the C-lobe from the N- lobe is shown in the lower panel. Adapted from (Shukla *et al.* 2013).

1.2.1 Beta 2 Adrenergic Receptor and Beta Arrestin 2 Interaction

The β-2-adrenoceptor (β-2AR), a member of the GPCR family, is translated by a gene on chromosome 5 (Yan *et al.* 2011). β-2AR is a key target for catecholamine hormones in metabolic activities such as vascular and trachea smooth muscle cells' relaxation. β-2ARs primarily work by activating adenylyl cyclase via a coupled stimulatory G protein (G_s), resulting in an increase in the intracellular level of cAMP, a secondary messenger that ultimately facilitates several subsequent physiological effects (Moore *et al.* 1999). Anomalies in β-2AR signaling are often associated with diseases such as heart failure and asthma (Fan *et al.* 2016).

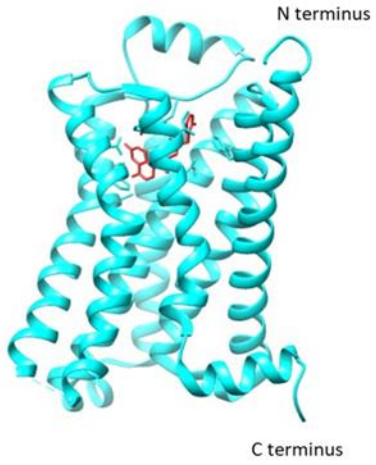

Figure 1.7 Crystal structure of agonist (red) bound human β-2AR. Adapted from PDB 3P0G.

Following prolonged agonist stimulation, GRKs phosphorylate β-ARs, causing the recruitment of multifunctional β-Arrestins (1, 2) and inhibition of further G protein coupling, a mechanism known as desensitization (Rockman, Koch, & Lefkowitz, 2002; Yan *et al.*, 2011). β-2AR C-tail contains 4 aa (at $Ser^{355,356,364}$ and Thr^{360} positions) that can be phosphorylated by GRK2. Following phosphorylation, β-Arrestin binds the receptor and starts internalization (Krasel *et al.* 2008) into endosomes which results in a block of β-2AR overstimulation (Yan *et al.* 2011). A membrane-associated protein phosphatase 2A- like enzyme may dephosphorylate the β2ARs during this trafficking, causing the receptor to return to the membrane at a fully sensitized form. The rate of receptor internalization is relatively faster than its recycling back to the membrane ($t^{1/2}$ < 3 minutes, and $t^{1/2}$ < 8 minutes, respectively) (Moore *et al.* 1999).

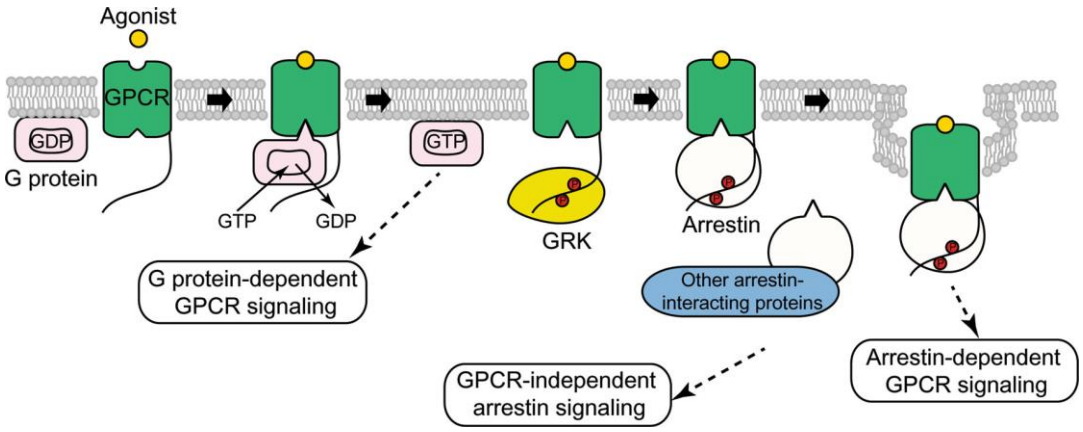

Figure 1.8 An overview of GPCR signaling. (taken from Park, Lee, Kim, Seo, & Chung, 2016).

1.3 **Phosphodeficiency** of GPCRs **Impair Desensitization**

Anomalies that occur in GPCR's phosphorylation pattern have been related to some diseases such mutations in the cytoplasmic site of the receptors can prevent the recognition of these regions by GRKs eventually receptors can not get phosphorylated. As a result, arrestin can not bind to the receptor, and the signal can not be terminated. An example of this situation is an inherited eye disease "retinitis pigmentosa" (night blindness) (Kim *et al.* 1993; Restagno *et al.* 1993; Apfelstedt-Sylla *et al.* 1993). Most commonly, the disease is seen in the autosomal dominant form. The phosphorylable amino acids in the cytoplasmic region of rhodopsin are mutated; therefore, the receptor can not be phosphorylated by the kinase, and it can not bind to the Arr1. As a result, the signal can not be terminated and leads to cell death. In another case, a mutation in the transmembrane region of the GPCR causes the receptor to be activated without the agonist. For example, the R137H mutation in the transmembrane region of the vasopressin receptor causes the activation of the receptor without agonist binding and leads to excessive phosphorylation (nephrogenic diabetes insipidus) (Barak *et al.* 2001). In another case, the amount of synthesis of GPCR-kinase in the cell increases in response to the receptor exposed

to a high concentration of agonist. This situation is seen in congestive heart disease. Over-synthesized GRK2 causes excessive phosphorylation of the β-adrenoceptors. Thus, the receptor, which binds strongly to Arrestin, cannot recycle back to the cell membrane (Mosteller RD 1987; Ungerer *et al.* 1994). In both cases, excessive phosphorylation of the receptor causes the receptor density in the cell membrane to decrease over time (down-regulation) and the cell's inability to respond to the relevant stimulus (Rockman *et al.* 1998; Akhter *et al.* 1999).

It is sufficient that one of the alleles encoding the mutant protein is faulty. In order for the diseases caused by autosomal dominant mutations in the GPCRs mentioned above to be seen in the phenotype; the normal allele cannot suppress the effect of the faulty allele. These anomalies can be removed with gene therapy. For example, a ribozyme for mRNA encoding the faulty allele could be developed, but - given point mutations - it would be very difficult to design a ribozyme that could distinguish between normal and faulty mRNA. In addition, gene therapy has not a therapeutic application yet. Therefore, alternatively, such GPCR-induced anomalies have been attempted to overcome by Arrestin, which can bind to the non-phosphorylated receptor. Arrestin, which can be activated independently of phosphorylation, also prevents the receptor density in the cell membrane from decreasing (down-regulation) as it can prevent excessive phosphorylation of the receptor (Pan, Gurevich, and Gurevich 2003). The reason behind this can be explained by; an arrestin that can be induced independently from receptor phosphorylation that competes with GRK for binding to the receptor. Once the receptor-arrestin complex is formed and targeted for early endosomes, the bound ligand dissociates from the receptor as the ligand-receptor complex faces the low pH of the vesicle lumen. This leads to the transformation of the activated receptor to its inactive form. Eventually, the receptor can be recycled back to the membrane because dissociation of the arrestin-bound inactive and unphosphorylated receptor is 30-50 % faster than the inactive phosphorylated receptor (Pan, Gurevich, and

Gurevich 2003; Celver *et al.* 2002; Gurevich *et al.* 1993, 1995; Kovoor *et al.* 1999).

In the last two decades, there have been several attempts to develop an arrestin that can be activated independently from receptor phosphorylation. Some amino acids in the triple element and polar core regions of arrestin have been mutated in one of these attempts. These mutations led to poor expression of the arrestin and caused its degradation in the cytoplasm (Vishnivetskiy, Chen, *et al.* 2013; Vishnivetskiy, Baameur, *et al.* 2013; Song *et al.* 2009). Moreover, the application of this strategy requires gene manipulation which restricts its therapeutic use. In another study, to mimic receptor attached phosphates molecules, heparin or negatively charged peptides had been used. This strategy failed due to insufficient transportation of these molecules into the cell because of their charges (Palczewski *et al.* 1991). Because of these mentioned issues, there is still no therapeutic method to activate arrestin independently from receptor phosphorylation.

1.4 Protein-Protein Interaction Detection Methods

Protein-protein interactions (PPI) are biochemical reactions that play crucial roles in organisms, and they determine the biological processes, more precisely the metabolic pathways. Understanding these phenomena is a must to understand the biological systems. Many experimental studies have shown that different PPIs involve in response to external stimuli, and they have been related to many diseases, including cancer, metabolic disorders, and neurological diseases. Therefore the comprehensive description of PPI is necessary to expand our understanding of biological phenomena (Oyama, Kitano, Satou, & Ito, 2002; Joy Macalino *et al.*, n.d.).

1.4.1 *In-Silico* Protein-Protein Interaction Detection Methods

The progression of drug discovery and design has been accelerated with the help of *in silico* techniques and the advancement in hardware and computational power (figure 1.9). Even though computation-aided drug discovery (CADD) is in its early stage compared to the traditional methods, it brought numerous successes in the field. CADD has provided an improvement in terms of both labor and cost in the identification of potential therapeutics without intense experimental assays. Computational power relies on many parameters and a vast amount of data on protein and compound structure and the calculation of intramolecular forces and required energies for interaction between any given partners. Computational analyses benefit from structure-activity relationship studies, compound optimization, and prediction of the pharmacokinetic character of the compound. Figure 1.9 summarizes the stages and components of CADD.

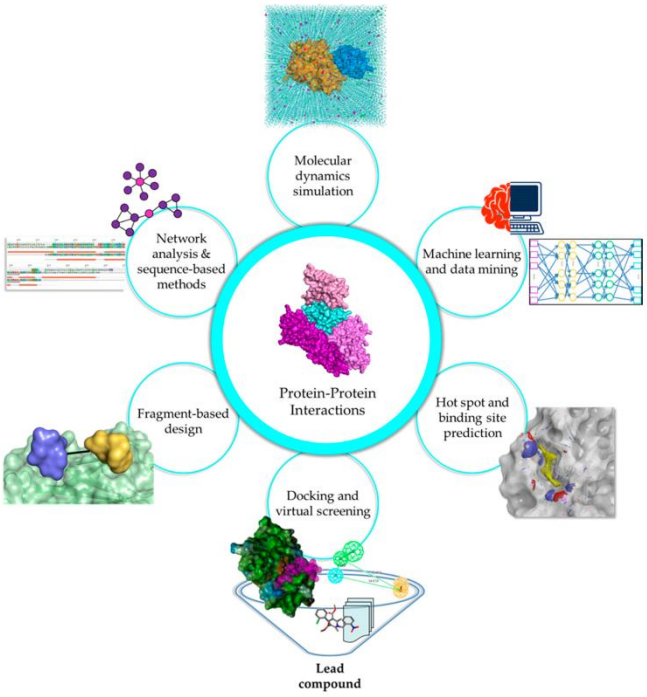

Figure 1.9 The components and the stages of *In silico* strategies for PPI drug discovery. Taken from (Joy Macalino *et al.*, n.d.).

Nonetheless, *in-silico* methods by no doubt, are more reliable and valued along with the other tools. The most popular targets for drug discoveries are the protein-protein interactions for over two decades (Joy Macalino *et al.*, n.d.). Although *in silico* techniques are very useful, they are often required to be confirmed with experimental methods. Some of the experimental methods for the detection of protein-protein interactions are resonance energy transfer-based methods such as Förster Resonance Energy Transfer (FRET) and Bioluminescence Resonance Energy Transfer (BRET).

1.4.2 Resonance Energy Transfer

Traditionally, immunofluorescent microscopy had been a popular technique that is used in fixed samples for the investigation of PPIs *in situ*. The drawback of this technique is the axial- resolution of fluorescent microscopy, which is over 200 nm. while most protein-protein interactions occur around a few nm diameters (Piston and Kremers 2007). The reason for the limited resolution is a physical phenomenon called the diffraction limit that determines the resolution of any light microscope, practically can not be less than 200 nm. and defined by the equation $\lambda/(2NA)$, where λ is denoting the light's wavelength and NA, the numerical aperture of the lens (Willig *et al.* 2007).

Since many cell signaling events occur in common cellular compartments such as clathrin-coated pits, many receptors internalize using this pathway, fluorescent imaging can only suggest at best and mostly misleading regarding a real interaction. Therefore, simple fluorescent imaging gives no information on any given two proteins under investigation that are in fact, interacting. To conclude that two proteins indeed interact rather than being in close vicinity to each other requires more reliable measurements. To that extent, electron microscopy provides a better resolution, yet it has its own limitations such as the lack of specific labeling and its requirement of a sample fixation. Multicolor fluorescent imaging with FPs allows the real-time imaging of live cells, which is crucial for the investigation of

transient interactions, yet the desired resolution cannot be reached with simple fluorescent imaging (Piston and Kremers 2007). Resonance energy transfer (FRET, Förster resonance energy transfer, BRET, Bioluminescence resonance energy transfer or electronic energy transfer, EET) is a physical process that comes as a solution to this problem, where a portion of the excited donor energy is transferred to the acceptor molecule via dipole-dipole couplings (Calçada *et al.* 2019). Förster developed a theoretical explanation and improved his theory of energy transfer. He found that the energy transfer via dipole-dipole couplings depends on two major factors, one of which is the spectral overlap of the two molecules and the other is the distance between them. He discovered the now well-known R^{-6} distance-dependence of RET, and this prediction was verified later on. Because of this characteristic of RET, it has been used as a "spectroscopic ruler" to measure the distance between two chromophores (Calçada *et al.* 2019). Since RET occurs between two molecules that are in close vicinity (less than 10 nm) makes it ideal for the study of PPI which occurs on a similar scale (Piston and Kremers 2007).

Despite the fact that the FRET technique has been widely used in protein-protein interaction studies, it has several drawbacks, including autofluorescence, detector noise, optical noise, and photobleaching. More importantly, spectral bleedthrough (SBT), which is the fluorescent leak of the donor and acceptor fluorescence emission into the FRET channel, is a severe problem that results in the observed FRET signal is larger than the actual FRET intensity. Nevertheless, some approaches and techniques have been developed to tackle these issues. First, a technique was developed to correct SBT and the effect of donor and acceptor concentration on FRET signal and applied to wide-field fluorescent microscopy (Gordon *et al.* 1998; Kraynov *et al.* 2000; Xia and Liu 2001). Later another approach, a new algorithm, was developed, in which correction of SBT and the concentration dependence of the FRET signal for all wide-field, confocal, and multiphoton intensity-based FRET methods. The algorithm calculates percent FRET efficiency by pixel by pixel and gives an estimated distance from the FRET partners from the mathematical calculations of SBT and the concentration effects

of both individual FRET partners. The SBT is evaluated from each donor or acceptor samples, and each partner's contributions on the raw FRET are calculated and eliminated from the raw FRET signal to obtain a net (or precise) FRET signal (Elangovan *et al.* 2003).

1.5 Aim of the Study

Some mutations in the phosphorylation sites of the GPCRs prevent their recognition by kinases (PKA, GRK2). These mutant receptors – called phospho-deficient-, cannot be internalized by arrestin; therefore, the induced signal upon stimuli cannot be terminated. These anomalies cause diseases; several examples have been identified including Rhodopsin and Vasopressin receptors.

Our aim is to activate arrestin independently from receptor phosphorylation with the help of small chemicals that can induce a conformational change in β-Arrestin 2 to its active form. Therefore, it can bind to unphosphorylated receptors. For this purpose, several chemicals were selected from the ZINC database and tested using *in silico* methods by our collaborators at Istanbul Medipol University.

In this study, the selected chemicals were tested *in vivo* using β-2AR-β-Arrestin 2 system. FRET and live-cell fluorescent imaging techniques were used to track the interaction between these two proteins in the presence and absence of the selected compounds. As a result, it was found that one of the compounds facilitates interaction between phospho-deficient β-2AR and β-Arrestin 2.

CHAPTER 2

MATERIALS AND METHODS

2.1 Materials

2.1.1 Bacterial Culture, Media and Conditions

LB medium was prepared according to the instruction given in Appendix B. First, all the ingredients were dissolved in 900 mL deionized water, then pH was adjusted to 7.0 with dilute NaOH. After the pH adjustment volume is completed to 1 L. Sterilization was performed with Nüve OT 40 L autoclave at 121 °C for 20 minutes. For selection purposes, Ampicillin was added to the medium at 100 µg/mL final concentration. Bacterial cultures were grown either on LB containing 2 % agar at 37 °C in Nüve® brand incubator or liquid LB at 37 °C 200 rpm shaking speed in Zheiheng shaker incubator.

2.1.2 N2a Cell Line and Media

To express and visualize fluorescent protein-tagged β-2AR and Arrb2 proteins via transient transfection method, the N2a cell line was chosen. N2a cells were also used in MTT assays. The cell line was purchased from American Tissue and Cell Culture (ATCC).

For maintenance and growing the cell growth medium was prepared from 44.5 % v/v DMEM with L-glutamine (see appendix A) (Gibco, REF 41966-029), 44.5 % v/v Optimem® reduced serum medium with L–glutamine, (Gibco, REF 11058-021), 10 % v/v FBS, (Biological Industries REF 04-127-1B), 1 % v/v

Penicillin/Streptomycin solution, (Biological Industries REF 03-031-1B). After mixing the solutions, complete media was filtered through the Millipore Stericup® Filter unit. For removing cell debris and waste, PBS solution was used (see appendix C). For detaching the cells TrypLE™ (Gibco REF 12605-028) dissociation reagent was used.

2.1.3 HEK 293 Cell Line and Media

For MTT assays and fluorescent microscope imaging of 2s chemical, HEK 293 cells were used. HEK cell line was a kind gift from Erson Lab. METU.

For maintenance and growing the cell growth medium was prepared from 90 % v/v DMEM with L-glutamine (see appendix A) (Gibco, REF 41966-029), 10 % v/v FBS , (Biological Industries REF 04-127-1B), 1 % v/v Penicillin/Streptomycin solution, (Biological Industries REF 03-031-1B). After mixing the solutions, complete media was filtered through a 0.22 μm Millipore Stericup® Filter unit. For removing cell debris and waste, a phenol-free D-MEM solution was used (see appendix A). For detaching the cells TrypLE™ (Gibco REF 12605-028) dissociation reagent was used.

2.1.4 N2a and HEK 293 cell Culture Conditions

Both cell lines were incubated at 37 °C with 5% CO_2 in Nüve® EC160 CO_2 incubator with 5% CO_2 atmosphere. All the cell culture studies were carried out in a Laminar flow cabinet with a Hepa filter.

2.1.5 Other Chemicals and Materials

DNA Polymerases, T4 Ligases, GeneRuler 1kb (#SM0313) and GeneRuler 1kb plus DNA Ladder (Cat. Num. #SM0311) DNA ladders used in the procedures were purchased from Thermo Scientific (MA, USA). New England BioLabs Inc. (MA,

USA) restriction enzymes used in cloning experiments. DNA gel extraction Kits were supplied from Bioteke (#DP1503). Plasmid Miniprep Kit (#K0503) used in plasmid isolation was supplied from Thermo Scientific (MA, USA). Transfection chemicals Lipofectamine® LTX and Plus™ Reagent from Invitrogen (CA, ABD). (#15338-100) used in transfection of N2a and HEK cells.

T-75 and T-25 flasks that were used in mammalian cell culture were obtained from Greiner (Frankfurt Germany). SPL Life sciences Korea, Sterile serological pipettes were also used in cell culture. For live-cell imaging and transfection two types of 35 mm petri dishes were used. Glass bottom ones from In vitro Scientific (CA, USA). Plastic bottom ones were purchased from Corning incorporated NY (USA).

Primer sets used in this study were synthesized by the Oligomer Biotechnology company (Ankara, Turkey). Tagged phosphorylation deficient and wild type-tagged receptors were from previous studies completed in our laboratory. mEGFP and mCherry cDNAs were gifted by Prof. Dr. Henry Lester from the California Institute of Technology (CA, USA).

All the other chemicals used in this work were supplied by Sigma-Aldrich (NY, USA).

Leica Microsystems CMS GmBH's DMI4000B confocal microscope with Andor DSD2 spinning disc confocal device used in fluorescent live-cell imaging. For FRET and other image analyses, Image J software was used for FRET efficiency calculations PixFRET plug-in for Image J was used.

2.2 Methods

2.2.1 Polymerase Chain Reaction

To confirm tagging β-Arrestin 2 from 177^{th} positions and observed 2 separate bands after digestion of β-Arrestin 2 -177-mEGFP is a single gene fragment the

whole insert amplified with Taq polymerase with PcDNA F (binds to T7 promoter) and PcDNA R (binds to poly A signal) the sequence of these primers shown in Appendix E. PCR conditions are given Table 2.1.

Table 2.1 Optimised PCR set-up and thermal Cycling Steps for Taq polymerase.

Components	**Volume**	**Final Concentration**
Nuclease Free Water	Up to 50 µL	-
Template DNA	100 ng	
Primer Forward	1.25 µL	0.5 µM
Primer Reverse	1.25 µL	0.5 µM
Taq polymerase	0,25 µL	
$MgCl_2$ (25 mM)	2 µL	1 mM
Taq buffer 5X	5 µL	
dNTP (10 mM)	1 µL	200 µM

Steps	Temperature	Time	Repeat
Initial Denaturation	95 °C	3 min	-
Denaturation	95 °C	30 sec	33
Annealing *	60 °C	30 sec	
Extension	72 °C	45 sec/kb	
Final Extension	72 °C	4 min	-

2.2.2 Agarose Gel Electrophoresis

Agarose gel electrophoresis was performed for size control of PCR products or confirmation of inserted DNA fragments to the plasmids by a ligation reaction. For this purpose, agarose gel was prepared 1 % or 0.8 % w/v (depends on the expected sizes) in 1X TAE buffer (Appendix C), then 0.5 µg/mL final concentration Ethidium Bromide was added. Samples were mixed with 1x final concentration

DNA loading dye (New England Biolabs cat # B7024S), and the gel was run in 1X TAE at 100-110 V for 45 minutes.

2.2.3 Extraction of DNA from Agarose Gel

PCR products or any insert that has been used in ligation were extracted from the agarose gel electrophoresis by a commercial Bioteke gel extraction kit (cat# DP 1503). After confirming the size of the DNA upon UV excitation, extraction of the DNA was performed according to the user manual.

2.2.4 Quantification of DNA Amount

The amount of isolated plasmids and DNA fragments from PCR amplification and agarose gel electrophoresis were determined by Biodrop µLITE spectrophotometer. 1.5 µL sample was loaded on the device then measurement was performed according to the user's manual. Results were given as ng/µL.

2.2.5 Restriction Enzyme Digestion

All DNA restriction enzymes used in this study were purchased from New England Biolabs (NEB). After adding recognition sequence for each enzyme by PCR, samples were double digested with each enzyme for generating sticky ends to ensure sample annealing to plasmids with the correct orientation.

Two different digestion protocols were used for different purposes. For ligation, 27 µL plasmids and samples were added in different reaction tubes then 3.3 µL of 10X cutsmart® buffer and 15 units of each enzyme were added. For confirmation insert ligation to plasmids reaction component chanced as follows; 200 ng plasmids were used, 2.5 units of each enzyme, and 1.5 µL cutsmart was used. Reaction volume adjusted to 15 µL in insert confirmation restriction. All digestion reactions were

performed at 37 °C for 1.5 hours. Except Dpn1 digestion was performed at 37 °C for 2 hours.

2.2.6 Ligation

After quantification of restricted vector and DNA fragments were ligated in vitro using 1 µL T4 DNA Ligase (NEB, Cat#0202T) in 1X T4 DNA ligase buffer (Appendix C) provided by NEB. For ligation 1:5 vector-insert ratio was chosen. After calculation of vector and insert volumes, the reaction mixture was left at room temperature for 2.5 hours before the transformation of *E. Coli* XL1 blue strain.

2.2.7 Preparation of Competent *E.coli* cells by $RbCl_2$ Method

E. coli XL1 blue strain was used for making competent cells according to the protocol follows;

First, *E. coli* XL1 blue cells were seeded on an agar plate and left for incubation for 16 hours at 37 °C. The next day a single colony was selected and inoculated in a 2.5 mL LB growth medium, then placed in a shaker incubator with 200 rpm shaking speed for 16 hours at 37 °C. The following day, 1 mL of the cell suspension was transferred into sterile Erlenmeyer containing 100 mL LB medium and 0.2 mM $MgSO_4$ then incubated shaker incubator with the same setting until OD_{590} reaches 0.5-0.6. Then the whole suspension was divided into two sterile falcon tubes. Tubes were centrifuged at 4000 rpm for 5 minutes at 4 °C. After discarding the supernatant, cell pellets were resuspended in 40 mL ice-cold TFB1 solution then left in ice for 5 minutes. Next, the solution was centrifuged again with the same settings. The supernatant was replaced with 4 mL ice-cold TFB2 solution

then incubated on ice for 45 minutes. After this final incubation, cells were aliquoted in ice-cold 1.5 mL sterile eppendorf tubes then kept at -80 °C for further use.

2.2.8 Transformation of Competent *E. Coli* cells with Plasmids

E. coli cells were taken from the -80 °C freezer, kept on ice for 15 minutes, then nearly 50 ng DNA sample that needs to be amplified was added on *E. coli* suspension. Then the solution was incubated at 42 °C for 45 seconds to heat shock the cells. Then the solution was kept on ice for another 5 minutes. Next, the volume of the solution was completed 1 mL with LB medium before incubating in an orbital shaker for 30 minutes at 37 °C with 200 rpm shaking speed. Finally, after a portion of the suspension (varying 5 % to 50 %) was seeded on an agar plate that containing ampicillin or kanamycin (for selecting), plates were incubated at 37 °C for 16 hours.

The next day, three selected colonies from agar plates were transferred into a 5 mL LB liquid medium with appropriate selective antibiotic and incubated in an orbital shaker at 200 rpm shaking speed at 37 °C for 16 hours. The following day plasmids were isolated with a commercially available Bioteke plasmid miniprep kit by following the user's manual.

2.2.9 Restriction Free Cloning

Restriction-free cloning or ligation independent cloning is a PCR method that allows insertion of any sequence into any plasmid without needing restriction enzymes. To tag Arrb2 from 177 Glu position RFC was performed. First, a pair of hybrid primers that are complementary to both target sequence and plasmid that

has the protein to tag with fluorescent proteins were designed. Fluorescent proteins or any other sequence was amplified first with these primers. Then the PCR product was extracted from an agarose gel after confirming size, these products were used as a "mega primer" in the second PCR. Dpn1 restriction enzyme was used to get rid of the parental plasmids before transforming *E. coli* cells.

Table 2.2 Optimised first PCR set-up and thermal Cycling Steps for Phire green and Pfu Ultra HS 2 polymerase.

Components	**Volume**	**Final Concentration**
Nuclease Free Water	Up to 50 µL	-
5x Phire Reaction Buffer	10 µL	1x
10 mM dNTPs	1 µL	200 µM
Primer Forward	1.25 µL	0.5 µM
Primer Reverse	1.25 µL	0.5 µM
Template DNA	50 ng	
Phire Hot Start II DNA Polymerase	1 µL	

Steps	**Temperature**	**Time**	**Repeat**
Initial Denaturation	98 °C	3 min	-
Denaturation	98 °C	30 sec	33
Annealing *	55-60 °C	30 sec	
Extension	72 °C	30 sec/kb	
Final Extension	72 °C	4 min	-

Table 2.3 optimized second PCR set up and thermal cycling steps for tagging β-Arrestin 2 from 177th aa. Position.

Components	**Volume**
Nuclease Free Water	Up to 20 µL
5x Phire Reaction Buffer	4 µL
10 mM dNTPs	1,25 µL
Mega primer	50 molar ratio of the template
Template DNA	20-30 ng
Phire Hot Start II DNA Polymerase	1 µL

Steps	**Temperature**	**Time**	**Repeat**
Initial Denaturation	98 °C	3 min	-
Denaturation	98 °C	30 sec	18
Annealing *	54-56 °C	30 sec	
Extension	69 °C	2 min. /kb	
Final Extension	69 °C	14 min	-

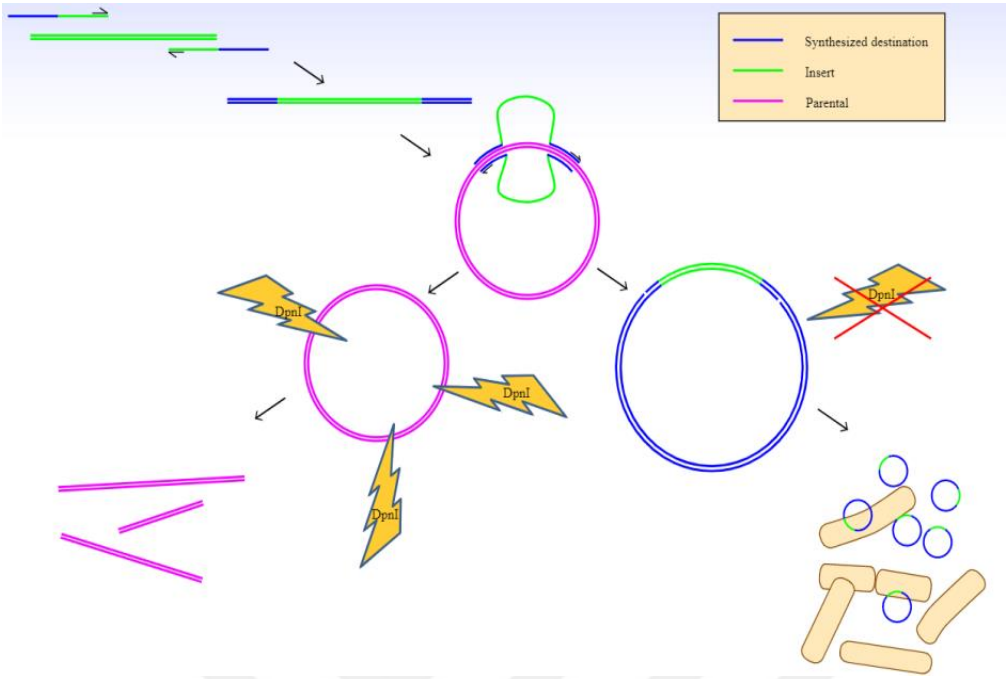

Figure 2.1 Schematic representation of Restriction Free Cloning (RFC). (taken from https://www.rf-cloning.org/QandA.php).

2.2.10 Passage of the N2a and HEK-293 cell Lines

Passaging is necessary to remove cell debris, changing cell media, and provide new space for the cell to proliferate. When cells reach 70 % confluency within 3- or 4-days cells were passaged according to the protocol below,

First cells media aspirated, then N2a Cells washed with PBS, HEK-293 cells washed with DMEM solution. Then washing solutions were removed. For detaching cells from the surface, 0.5 ml TrypLE™ was added directly on top of the cells, then left for incubation for 5 minutes in a 37°C incubator containing humidified air and 5% CO_2.

8 ml fresh media was added to the new T-25 flask. After incubation, the old flask was taken from the incubator then 8 ml fresh media was added. To make a uniform cell suspension, media was added by pipetting several times. Finally, 0.2 ml of N2a

suspension or 0.5 ml HEK-293 suspension was transferred into new flakes and then placed in the incubator.

2.2.11 Transfection of N2a cells with Mammalian Expression Vectors

After passaging 70000 N2a cells were counted via hematocytometer, and they were seeded on 35 mm plastic or glass-bottom petri dishes. Then volume was completed to 2 mL with a growth medium. Petri dishes were placed in the cell culture incubator (37 °C, 5 % CO_2, humidified air) for 24 hours. The following day, cells were chemically transfected with 400 ng of each plasmid by using Lipofectamine LTX and Plus™ reagent according to the protocol below,

First, plasmids were diluted in 75 µL of OptiMEM®I. For 3 plasmids transfection 4 µL, for 2 plasmids transfection 3 µL, for single plasmid transfection 1 µL of Plus™ reagent was added and the mixture was incubated for 15 minutes at room temperature. In another eppendorph tube, 4 µl of Lipofectamine LTX was diluted in 75 µl of Opti-MEM® then both tubes were combined. The final mixture was incubated at room temperature for 15 minutes. During this incubation, media in the sample dish was aspirated and washed with 1 ml of 1X PBS, and 850 µL of OptiMEM® was added to the dish. After the incubation time was over, the transfection mixture was added to the dish. Cells were incubated at 37°C with 5% CO_2 for 3 hours, and then 2 ml of 37°C growth medium was added. The dish was incubated at 37°C with 5% CO_2 for 24 hours; then, the media was replaced with a 2 ml fresh growth medium. Cells were grown at 37°C incubator with 5% CO_2 for another one day before imaging.

2.2.12 Transfection of HEK-293 cells with Mammalian Expression Vectors

After passaging 150000 N2a cells were counted via hematocytometer, and they were seeded on 35 mm plastic or glass-bottom petri dishes. Then volume was completed to 2 mL with a growth medium. Petri dishes were placed in the cell culture incubator (37 °C, 5 % CO_2, humidified air) for 24 hours. The next day cells were chemically transfected with 400 ng of each plasmid by using Lipofectamine LTX and Plus™ reagent according to the protocol explained in section 2.2.11.

2.2.13 Imaging of Transiently Transfected N2a and HEK-293 Mammalian cells with Spinning Disc Confocal Microscope

For β-Arrestin 2 colocalization to cell membrane experiments, 80.000 N2a cells were seeded on 35 mm glass-bottom petri dishes. Twenty-four hours later, cells were transfected with 400 ng each Arrb2-177-mEGFP, B2AR–mCh/B2AR P.D.-mCh. And GRK2 carrying PCDNA 3.1-/PcDNA 3. For imaging of 2s chemical and pH calculation of Golgi organelle in HEK cells, confocal microscopy imaging was performed using Leica DMI 4000 equipped with Andor DsD2 spinning disc confocal microscopy with Leica 63x/1,32 HCX PL APO oil DIC objective or 100x/1.40 HCX APO oil DIC objective. Cells were excited at 365 ± 20 nm emission collected at 470 ± 20 nm (DAPI channel), 480 ± 10 nm emission collected at 525 ± 15 nm (EGFP channel), excitation at 480 ± 10 and emission at 630 ± 20 nm (FRET channel) and excitation at 585 ± 15 nm and emission 630 ± 20 nm (mCherry (mCh.) Channel).

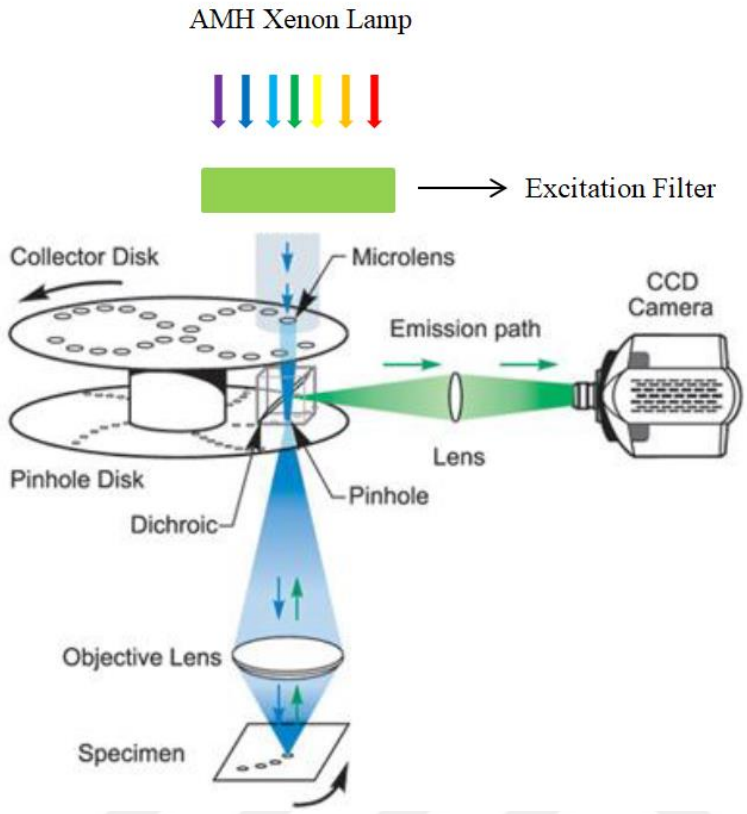

Figure 2.2 Spinning Disc Confocal microscopy configuration (Adapted from LMCF, Duke University).

2.2.14 Image Analysis with ImageJ Pix-FRET Plug-in

The fluorophore pair chosen for this study is mEGFP-mCh. The reason for that is this pair has minimum donor spectral bleed-through (DSBT) and acceptor spectral bleed-through (ASBT).

DSBT is a signal that leaks into the FRET channel, while ASBT is the acceptor emission signal caused by the excitation of the acceptor at the wavelength used for donor excitation. These mentioned signal leaks can be higher when both fluorophore emission maximums are closed to each other.

Since these signals create false FRET, they must be calculated and subtracted from the total FRET signal. Pix FRET (Feige, Sage, Desvergne, & Gelman, 2005) is an image J plug-in that uses an algorithm that calculates this by pixel by pixel in three stacks of microscope images. To use Pix-FRET, 3 separate samples must be prepared.

1. Donor sample to calculate DSBT

It contains only donor-tagged gene transfected cells. Images need to be taken from both the FRET channel (donor excitation and acceptor emission) and the donor channel (donor excitation donor emission).

2. Acceptor sample to calculate ASBT

This sample plate has the cells that express the acceptor-tagged FRET partner. Images from this sample are taken from both the FRET channel and acceptor channel (acceptor excitation acceptor emission).

3. FRET sample

In this sample, cells express both FRET partners to calculate FRET in the tested system. Images from the sample are taken from all three-channel. Both fluorophore's excitation and emission spectrums can be seen in Figure 2.3.

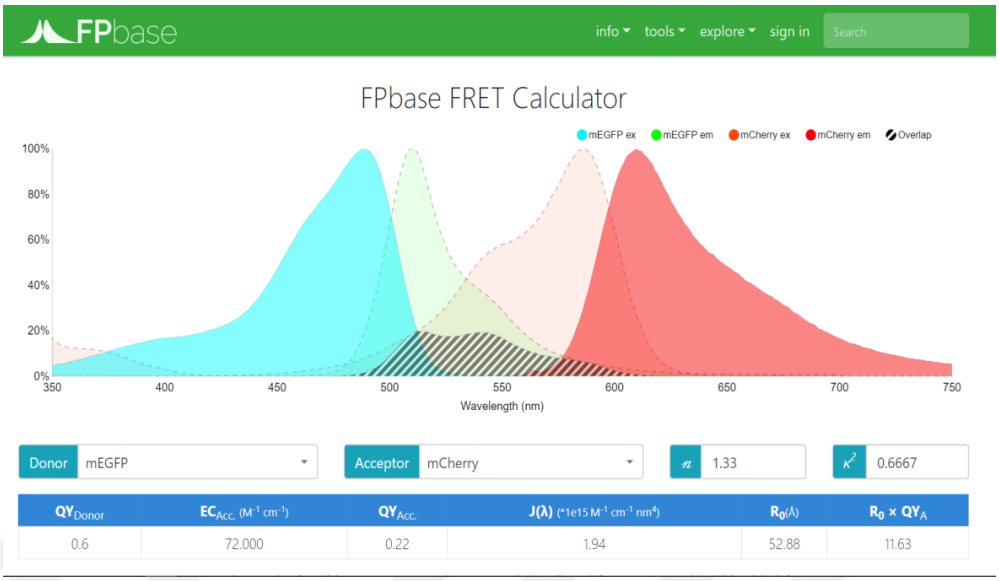

Figure 2.3 mEGFP- mCh. Excitation emission spectrums at 470 nm mEGFP excitation percent is 77.7 while mCh. excites 3.4 %. At 620 nm mCh emission is 87.1 % and mEGFP emission is 1.8 % (taken from https://www.fpbase.org/fret/).

2.2.15 Fluorescence Measurement and FRET Calculation with Multimode Plate Reader

For investigation of the effect of each chemical on FRET, 125 000 N2a cells were seeded on PDL-coated 35 mm plastic petri dishes 24 hours before transfection. A blank plate was prepared for each experiment that was transfected with an empty vector, and sample plates were transfected with either β-2AR-mCh. or P:D. β-2AR-mCh, β-Arrestin 2, and GRK2. After 24 hours transfected cells were washed with PBS then lifted by 140 µL TrypLE™ cells were resuspended in 1.8 mL complete medium then counted. 20 000 N2a cells were seeded each well of PDL coated opac bottom black 96 well plates (SPL Life Sciences F bottom 96 well immunoplate #31496). After 24 hours cells were washed twice with 200 µL HBSS buffer then the final volume was adjusted to 150 µL with HBSS containing either 100 µM each tested chemical or 1 % DMSO (except control groups (Negative). Each chemical was also added to each chemical's blank group. After adding the ligands 96 well

plates were incubated at 37 °C for 30 minutes at incubator then measured for 30 minutes wavelengths as follow mEGFP; 470 ± 15/510 ± 25 FRET; 470 ± 15/610 ± 25 mCherry (mCh.); 570 ± 15/610 ± 25 FRET calculated as the ratio of FRET/Donor. Molecular Device Spectramax ID3 was used for measurement.

2.2.16 MTT Standard Curve

MTT assay was performed to investigate the toxicity of the ligands and to determine the highest concentration to use in further assays. MTT assay is a colorimetric assay that measures the effect of the test compounds on cell metabolism. Through the metabolic activity yellow-colored tetrazolium salt (3-(4,5-dimethylthiazol-2-yl)-2,5-diphenyltetrazolium bromide or MTT) converts to purple color formazan crystals. The assay measures the absorbance of this color at 570 nm.

First, 25 mg of the MTT reagent was dissolved in 5 mL PBS and filtered through a 0.22 μm filter to be sterilized. The detergent solution was prepared by dissolving SDS (Sodium Dodecyl Sulfate) in 0.01 M HCl with the final concentration of 10 % w/v.

To plot the MTT standard curve, 2500, 5000, 7500, 10000, 12500, 15000 N2a cells were plated on plastic clear F bottom 96 well microplate (Sarstedt AG&Co. KG, Germany REF: 83.3924) with the final volume of 100 μL and incubated at 37 °C for 24 h in humidified 5 % CO_2 incubator. The next day plate was taken out and 10 μL MTT reagent (5 mg/mL dissolved in PBS) was added, then moved back to the incubator for another 4 hours of incubation. After incubation, 100 μL of the detergent solution was added (10 % SDS in 0.01 M HCl), shaken for 15 minutes in an orbital shaker, then incubated at room temperature for 16 hours. The next day absorbance was measured with a Thermo Scientific Varioscan Lux microplate reader at 570 nm.

2.2.17 MTT Toxicity Assay

N2a and HEK cells were seeded in clear F bottom plastic 96 well microplates with the density of 10.000 and 20.000 for each cell line respectively, at 100 µL final volume in complete medium, then incubated in cell culture incubator for 20 hours then test compound were added at 50 and 100 µM concentrations then incubated another 4 hours. After that plate was removed from the incubator 10 µL MTT solution was added to each well and incubated for another 4 hours. Finally, 100 µL detergent solution (10 % SDS in 0,01 M HCl) was added to each well to dissolve the formed formazan. The plates were shaken for 5 minutes and incubated at ambient conditions for 16 hours. Absorbance measured at 570 nm. with Thermo Scientific Varioskan Lux microplate reader.

2.2.18 Investigation of the Photochemical Properties of the Test Compounds

Fluorescent emission and Excitation spectrums of the chemicals were measured by Molecular Device Spectramax ID3 at 100 µM concentration of each chemical in SPL life sciences 96 well black imminoplates at 150 µL volume.

Uv-Vis spectrum of the chemicals obtained at 50/100 µM concentration in quartz cuvettes by ThermoFisher Multiskan Go.

2.2.19 Statistical Analysis

All the graphs are plotted in Graphpad Prism version 8.0.1. All experiments were performed in duplicates or triplicates, and the results were presented as mean ±SEM. All the statical analyses were carried out in Graphpad Prism. For a single experiment with 2 or 3 replicas, two-way ANOVA followed by the Tukey test, to analyze two independent experiments Nested t-test was used. Line graphs were tested with the Pearson r correlation test.

CHAPTER 3

RESULTS

The experimental flow of this study starts with tagging of β-Arrestin 2 with mEGFP and mCherry fluorescent proteins followed by imaging and colocalization analysis of β-Arrestin 2 to the cell membrane upon stimulation of β-2 Adrenergic Receptor, microplate reader FRET optimization, characterization, and the toxicity assays of the test compounds, and finally, the interaction between phospho-deficient β-2 Adrenergic Receptor and β-Arrestin 2 in the presence of the test compounds via FRET analysis.

3.1 Tagging of β Arrestin-2 from 177th aa. Position with mEGFP and mCherry Fluorescent Proteins

The coding sequence of β Arrestin 2 (Arrb2) was kindly provided by Mark Scott (CNRS research Associate, Paris, France). Arrb2 is a 1230 bp. long gene. First, it was cloned into PcDNA 3.1- mammalian expression vector (data not shown). Since the Arrestin activation mechanism involves a release of the C tail from the polar core and the three-element region, it 3was decided to tag from alternative positions. Therefore, 2 loops in the C lobe of Arrestin were chosen for tagging. To tag β-Arrestin 2 with mEGFP and mCherry fluorescent protein from 177th aa. and 265th aa. Positions, restriction-free cloning was used with phire green and Pfu Ultra HS 2 polymerases. After Dpn1 digestion, and following agar plate seedings and inoculation to Lb liquid medium, double enzymes digestion was performed to confirm tagging. Results are shown in figure 3.1.

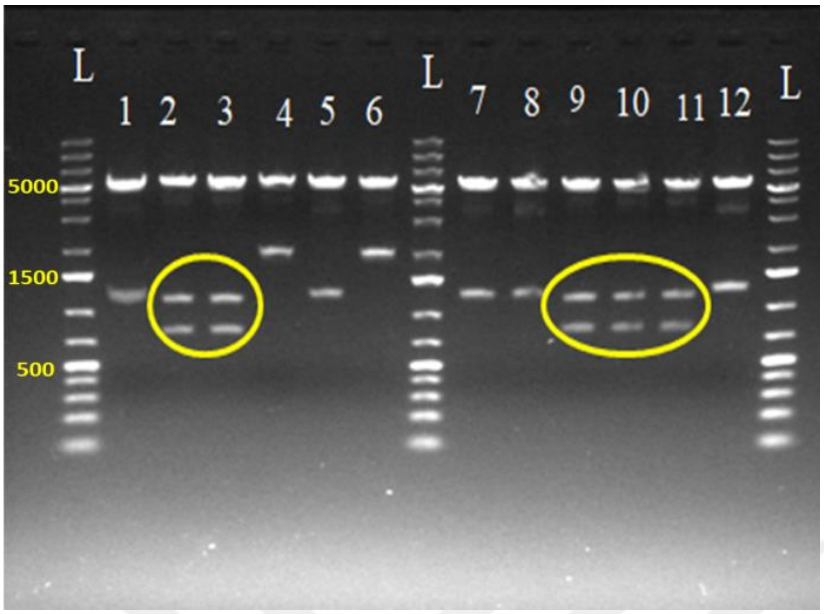

Figure 3.1 0.8 % agarose gel image of double digested Arrb2-177 mEGFP/mCh. in PcDNA 3.1- vector with BamH1 and HindIII. GeneRuler 1 kb plus DNA Ladder was used as a reference (L).

Table 3.1 Layout of Gel in figure 3.1

Enzyme	**Pfu Ultra HS 2**									
Line	L	1	2	3	4	5	6	L	7	8
	Gene Ruler 1 kb plus	Arrb2 177 mEGFP in PcDNA (1)	Arrb2 177 eGFP in PcDNA (2)	Arrb2 177 eGFP in PcDNA (3)	Arrb2 177 mCh in PcDNA (1)	Arrb2 177 mCh. in PcDNA (2)	Arrb2 177 mCh. in PcDNA (3)	Gene Ruler 1 kb plus	Arrb2 265 mCh. İn PcDNA (1)	Arrb2 265 mCh. İn PcDNA (2)
Enzyme	**Phire Green**									
Line	9	10	11	12	L					
	Arrb2 177 eGFP in PcDNA (1)	Arrb2 177 eGFP in PcDNA (2)	Arrb2 177 eGFP in PcDNA (3)	Arrb2 177 mCh in PcDNA (1)	Gene Ruler 1 kb plus					

The size of tagged arrestin either mEGFP or mCh fluorescent proteins is around 1950 bp. According to the results, the insertion of the fluorescent proteins to Arrb2 from 265. aa. was not successful. (lines 7 and 8). Positive results have been seen on Arrb2 177 mEGFP and also insertion of mCh. the 177th position was successful (lines 4 and 6). Unexpectedly, there have been 3 bands for these constructs (Arrb2

177 mEGFP, shown in circles). It was concluded that one of these restriction enzymes may cut the mEGFP gene from one position. To confirm that these two fragments are a single gene, 3 colonies (line 2, 3, 9) were selected, then the whole insert was amplified with Taq polymerase enzyme using PcDNA F (anneals to T7 promoter in PcDNA 3.1-) and PcDNA R primers (anneals to poly-A signal in PcDNA 3.1-). After PCR samples were loaded on an agarose gel. The gel image is shown in Figure 3.2.

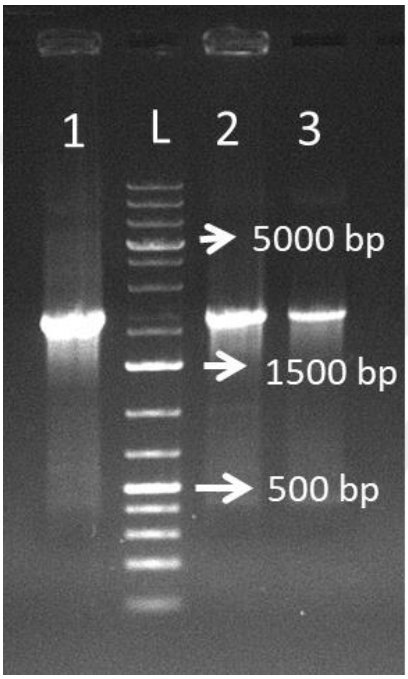

Figure 3.2 1 % agarose gel image of confirming PCR for β-Arrestin 2-177 meGFP constructs with Taq polymerase. GeneRuler 1 kb plus DNA Ladder was used as a reference.

For all Arrb2-177 mEGFP bands are seen between 2000 and 3000 more close to 2000. Later, the HindIII cut site was confirmed in the mEGFP gene via Sanger sequencing.

3.2 Microscope Imaging of β-Arrestin-2 177 mEGFP and β-Arrestin-2 177 mCh. Transfected N2a cells

Tagged Arrestins were sequenced via sanger sequencing. No additional mutations were observed other than the one silent mutation in mEGFP (which creates a HindIII enzyme cut site), and two silent mutations in Arrb2. After that both mEGFP and mCh. tagged arrestins were transfected to N2a cells to confirm localization. As seen in Figure 3.3, both constructs were cytosolicly expressed in the N2a cell line.

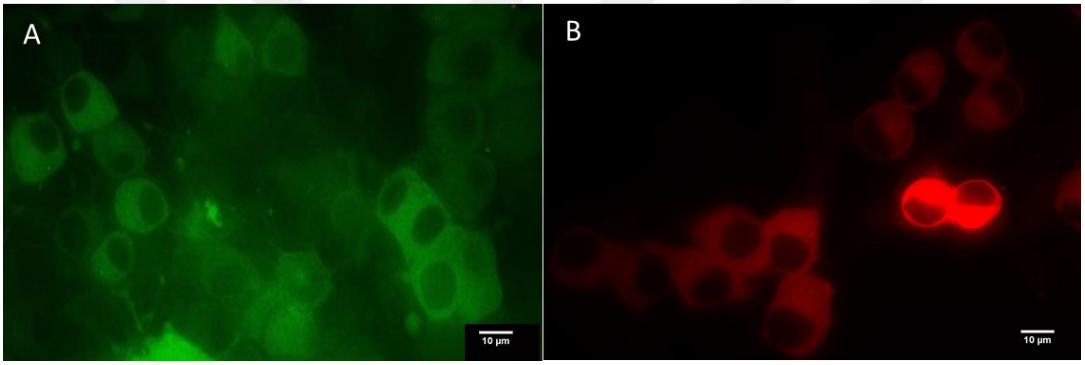

Figure 3.3 Spinning disc confocal microscopy images of Arrb2 tagged with fluorescent proteins from 177th aa. positions. A) Image of N2a cell transfected with Arrb2-177- mEGFP was taken from the microscope's EGFP channel. B) Image of N2a cell transfected with Arrb2-177- mCh. taken from microscope's mCh.channel. (Magnification 63X, scale bars are 10 µm).

3.3 Colocalization of β-Arrestin-2 with β-2AR Upon Stimulation of β-2 Adrenergic Receptor

Both β-2AR-mCh. and β-2AR P.D.-mCh. were constructed in a previous study (Evci 2019). After confirming the sequence and localization of Arrb2-177-mEGFP, the interaction of Arrestin with either P.D. or wt β-2AR was tested in N2a cells. 10 µM Isoproterenol (iso) was used as a β-AR agonist to induce

colocalization of β- Arrestin 2 with β-2AR. Since this interaction requires the phosphorylation of the receptor, GRK2 was also added to the system. As a result, while colocalization of Arrestin occurs in positive test system (β-2AR –mCh., β-Arrestin 2- 177 mEGFP, and GRK2) in Figure 3.4, it was not observed in the negative system (β-2AR –P.D.-mCh., β- Arrestin 2- 177 mEGFP, and GRK2) (Figure 3.5).

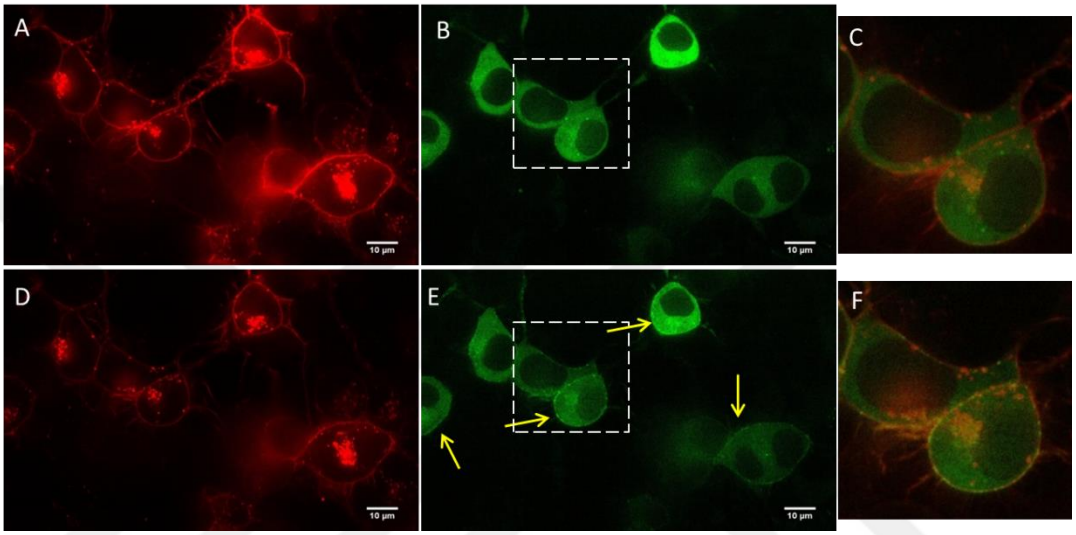

Figure 3.4 Spinning disc confocal microscopy images of N2a cells transfected with β-2AR- mCh., Arrb2-177 mEGFP, and GRK2. A) Taken from mCh. channel after 30-second iso stimulation. B) Taken from EGFP channel after 30-second iso stimulation. C) Overlay of A and B. D) Taken from mCh. channel after 5-minute iso stimulation E) Taken from EGFP channel After 5-minute iso stimulation. Yellow arrows show β-Arrestin 2 colocalization with β-2AR. F) Overlay of D and E. (Magnification 63X, scale bars are 10 µm).

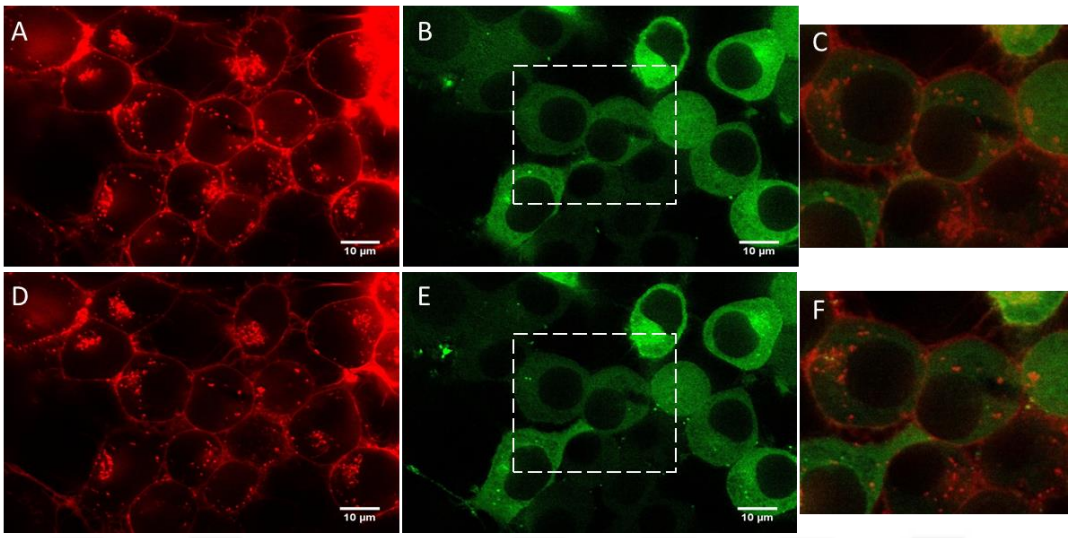

Figure 3.5 Spinning disc confocal microscopy images of N2a cells transfected with β-2AR- P.D.-mCh., Arrb2-177-mEGFP, and GRK2. A) Taken from mCh. channel after 30-second iso stimulation. B) Taken from EGFP channel after 30-second iso stimulation. C) Overlay of A and B. D) Taken from mCh. channel after 5-minute iso stimulation E) Taken from EGFP channel After 5-minute iso stimulation. F) Overlay of D and E. (Magnification 63X, scale bars are 10 µm).

These results suggest that tagged β-2AR and β-Arrestin 2 behave like the wt. of these proteins and the phospho-deficient mutant of the β-2AR impairs the colocalization of β-Arrestin 2 with β-2AR upon stimuli. The FRET analysis of these interactions was shown in section 3.7.

3.4 Microplate Reader Optimization for FRET Analysis

β-2AR and β-Arrestin 2 interaction with or without test compounds and iso, analyzed via FRET method in further experiments. These measurements were performed in a microplate reader. FRET measurement by a microplate reader requires a different FRET calculation method than the 3 cube method, which was used in the fluorescent microscope. For that purpose Gap43-mCh.-meGFP construct was used as a positive FRET control to adapt FRET analysis to microplate reader to use a new FRET calculation in further experiments. Gap43 is a membrane-targeting sequence that fused with mEGFP and mCh. fluorescent

proteins are linked together. First, the FRET efficiency of this construct was calculated from confocal images and compared with the plate reader FRET calculations. Gap43-mEGP and Gap43-mCh. trasfected N2a cells are also imaged and used for bleedthrough calculations (data not shown).

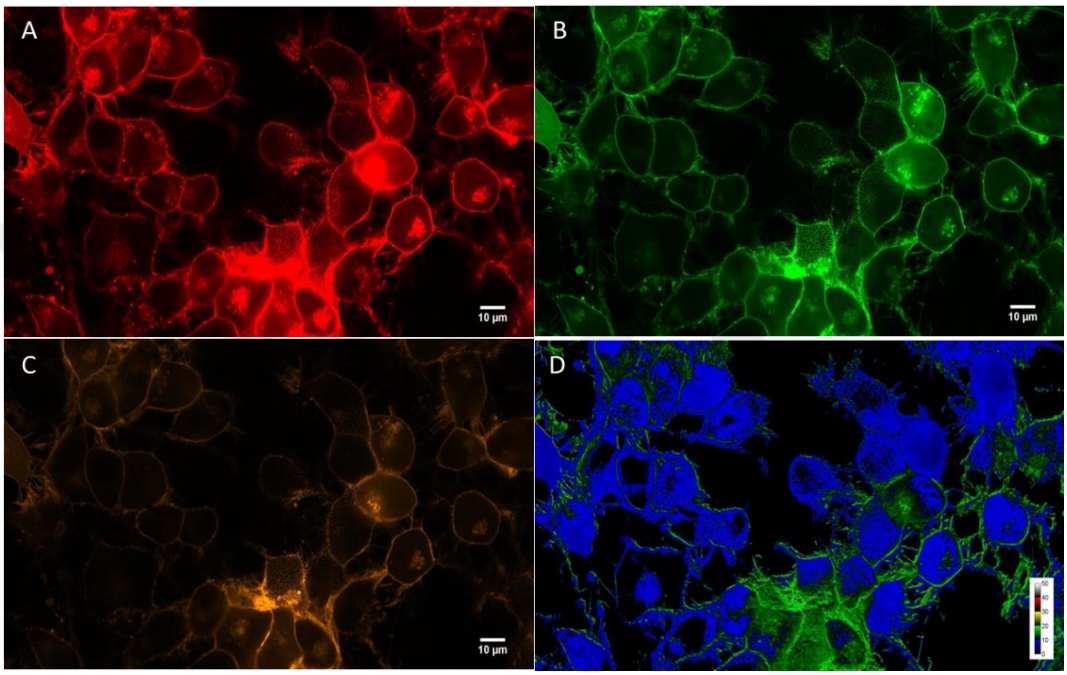

Figure 3.6 Spinning disc confocal microscopy images of N2a cells transfected with Gap43 mCh.-mEGFP. A) Taken from the EGFP channel. B) Taken from mCh. Channel. C) Taken from FRET channel. D) image of FRET efficiency calculated by Image J pixFret plug-in. (Magnification 63X, scale bars are 10 µm).

Figure 3.6 shows the confocal images of Gap43-mCh.-mEGFP and calculated FRET efficiencies via image J pix FRET plug-in. (figure 3.6 D). figure 3.6 A, B, and C shows the membrane localization of this construct in mEGFP, FRET, and mCh. channels, respectively. As a result the FRET efficiency of Gap43 mEGFP-mCh. calculated between 10 and 15 %.

Later on, the same construct was used for FRET calculation in the microplate reader. First, to determine the cell density to use in further experiments, 10000,

15000, and 20000 were tested, and FRET was calculated as FRET intensity/Donor intensity (Figure 3.7).

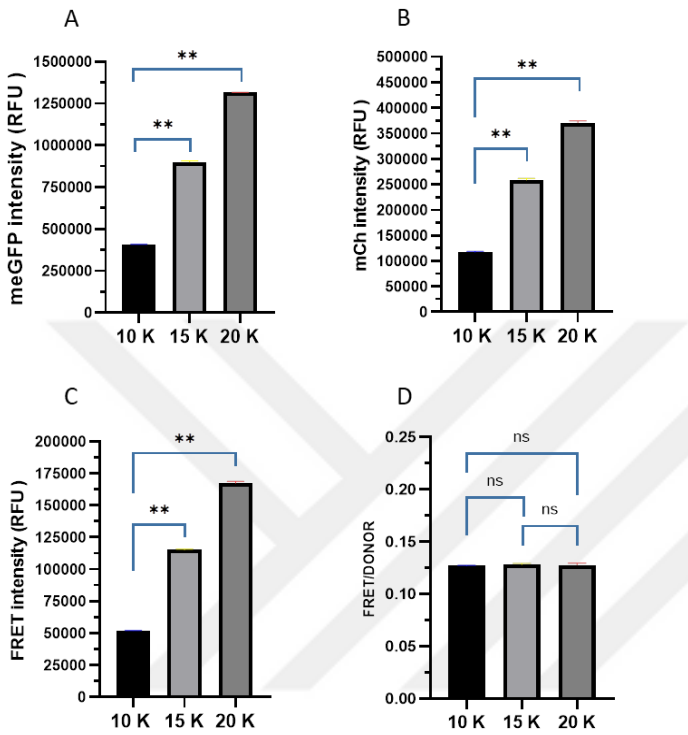

Figure 3.7 Gap 43-mCh –mEGFP FRET calculation in the microplate reader. A) intensty in 470/510 (mEGFP) B) intensty in 570/610 (mCh.) C) intensty in 470/610 (FRET) D) FRET/Donor. **p<0.005, statistically significant differences. ns: no significant differences. Data Mean ± SEM

According to the results increased cell density increase the intensity of each mEGFP, FRET and mCh. Channels (Figure 3.7 A, B, C) but the FRET/Donor ratio does not get affected by the cell density (Figure 3.7 D). FRET/Donor ratio calculated as 0.125, which correlates with the calculated FRET efficiency in a confocal microscope (around 12 % in Figure 3.6 D). 20000 cells for each well in the 96 well plate decided to use in further FRET experiments in the microplate reader.

3.5 Characterization of the Tested Chemicals

In-silico part of this work was conducted by Asst. Prof. Dr. Özge Şensoy and her students at İstanbul Medipol University as a part of the TUBİTAK 117Z245 1001 project. The chosen compounds were taken from the ZINC database and were tested by in-silico molecular dynamics simulations. Then selected four compounds were tested by in-vivo FRET analysis during this work.

All the chemicals were dissolved in 100 % DMSO at 10 mM concentration, then aliquoted at 10 µL in PCR tubes, and kept in a -80 °C freezer for further use.

Following experiments were performed to characterize the compounds, such as photochemical properties and the toxicity of each chemical.

The below figure shows the chemical structures of the chemicals and their names along with ZINC codes.

1. ZINC 06812752 (2s)

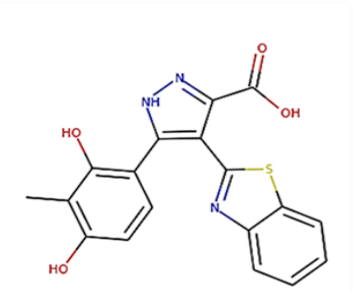

1*H*-Pyrazole-3-carboxylic acid, 4-(2-benzothiazolyl)-5-(2,4-dihydroxy-3-methylphenyl)-

2. ZINC 31135800 (3s)

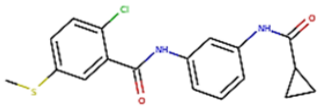

Benzamide, 2-chloro-*N*-[3-[(cyclopropylcarbonyl)amino]phenyl]-5-(methylthio)-

4. ZINC 67490967 (4s)

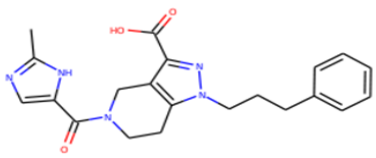

1*H*-Pyrazolo[4,3-*c*]pyridine-3-carboxylic acid, 4,5,6,7-tetrahydro-5-[(2-methyl-1*H*-imidazol-5-yl)carbonyl]-1-(3-phenylpropyl)-

3. ZINC 36365956 (6s)

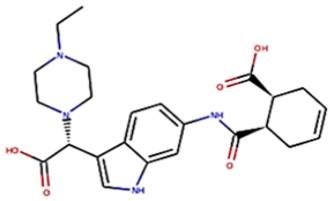

1*H*-Indole-3-acetic acid, 6-[[(6-carboxy-3-cyclohexen-1-yl)carbonyl]amino]-α-(4-ethyl-1-piperazinyl)-

Figure 3.8 Chemical structures of tested molecules (Taken from ZINC database). CAS Registry numbers for 2s, 3s, 4s, and 6s chemicals are as follows 384367-09-3, 1386112-75-9, 1309319-17-2, 1214645-87-0, respectively. Each chemical's absorbance spectrum is shown in figure 3.9.

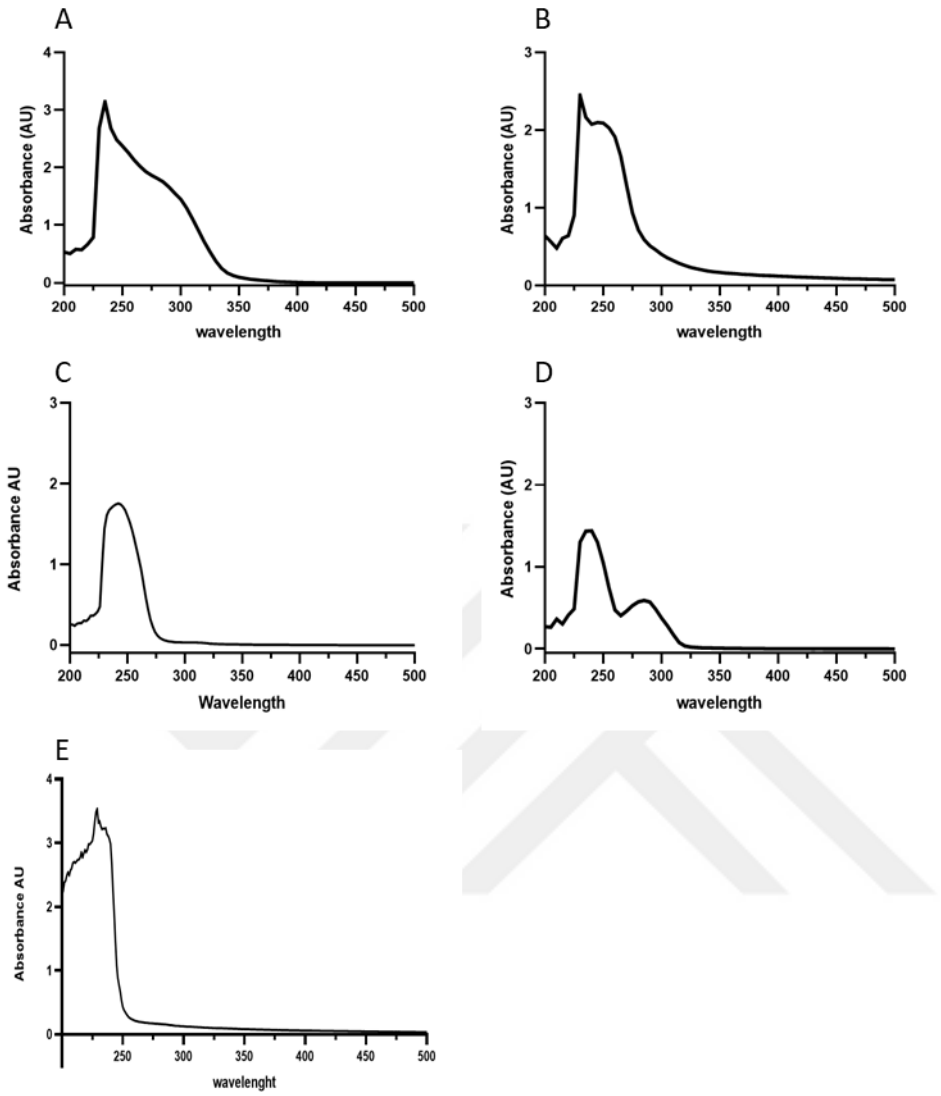

Figure 3.9 Absorbance spectrums of the tested chemicals and acetic acid.

A) 2s; B) 3s; C) 4s; D) 6s; E) 25 % Acetic acid (v/v). 2s absorption peak was observed around 240 nm. 3s; peak was observed around 250 nm. 4s; peak was observed around 250 nm. 6s; two peaks were observed, one is around 250 nm. The other one is approximately 290 nm. Acetic acid absorbance spectrum was obtained as a control since all the tested compounds have at least one carbonyl group. Acetic acid absorption peak was observed around 250 nm.

Fluorescent properties of the chemicals were also investigated to have an idea of the chemical's interference in the further FRET experiments. Figure 3.10 shows the fluorescent spectrum of the 3s, 4s, and 6s chemicals.

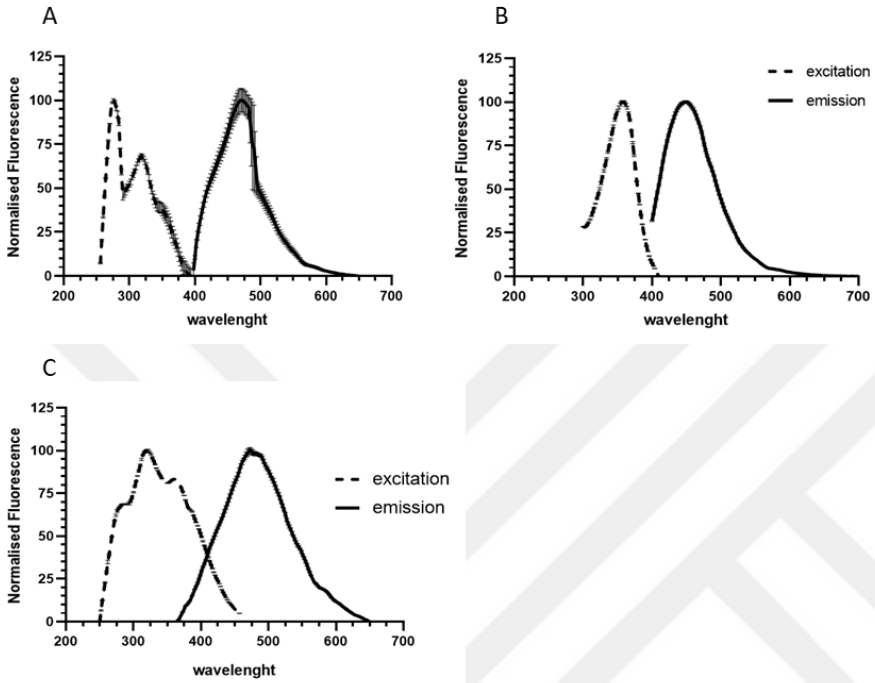

Figure 3.10 Fluorescent excitation and Emission spectrums of the test compounds. A) 3s B) 4s C) 6s the experiment was performed in duplicate with 100 μM of each chemical in HBSS. Data ± SEM

As a result, it was found that all the tested compounds have a fluorescent character. For 3s chemical two excitation peaks were observed first around 276 nm., second excitation peak 320 nm. and emission peak 470 nm. For 4s the excitation maximum for this chemical is determined as 358 nm. and the emission maximum was detected at 450 nm. 6s chemical has an emission peak at around 473 nm and an excitation peak around 320 nm.

While obtaining 2s chemical's fluorescent spectra, it was found that the fluorescent character of this chemical changes over time in HBSS solutions. Later, the reason for this observation was found to be due to pH change. Both absorption and fluorescent spectrum of 2s chemicals were obtained in pH 4.0 (50 mM Acetic

acid), 7.0 (50 mM Tris-HCl), and 10.0 (50 mM Glycine -NaOH) with or without 30 minutes incubation in 37 °C. Figure 3.11 shows the absorption spectrum of the chemical.

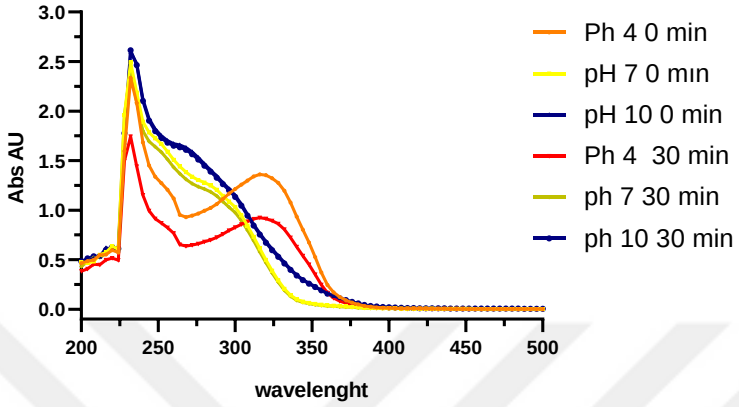

Figure 3.11 The UV-Visible absorbance spectrum of 2s chemical at pH 4.0, 7.0, and 10.0

The chemical showed absorbance maximum at 232 nm. in all conditions tested. Additionally, a second peak was observed at around 315 nm. in pH 4.0 buffer but not at higher pHs.

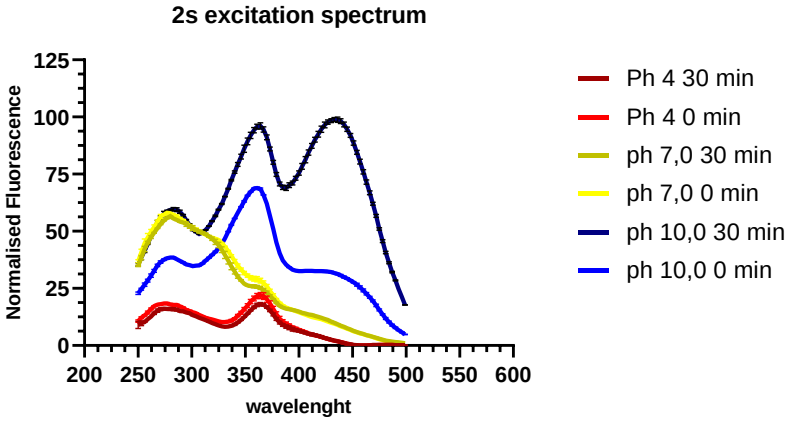

Figure 3.12 Fluorescence excitation spectrum of 2s (1*H*-Pyrazole-3-carboxylic acid, 4-(2-benzothiazolyl)-5-(2,4-dihydroxy-3-methylphenyl)) at 30 °C in pH 4.0, 7.0 and 10.0 and time. Emission was fixed to 540 nm. The experiment was performed in duplicate with 100 µM chemical in HBSS.

According to figure 3.12, increasing pH improves fluorescence and changes the excitation spectra. At low pH, two separate peaks were observed, one at around 250 nm other at around 340 nm. At neutral pH, the first peak increases significantly. At high pH, both of these peaks increase while another peak emerges at 450 nm. Incubation time does not affect the intensity of the first two peaks while it dramatically increases the third peak around 450 nm. at pH 10.0.

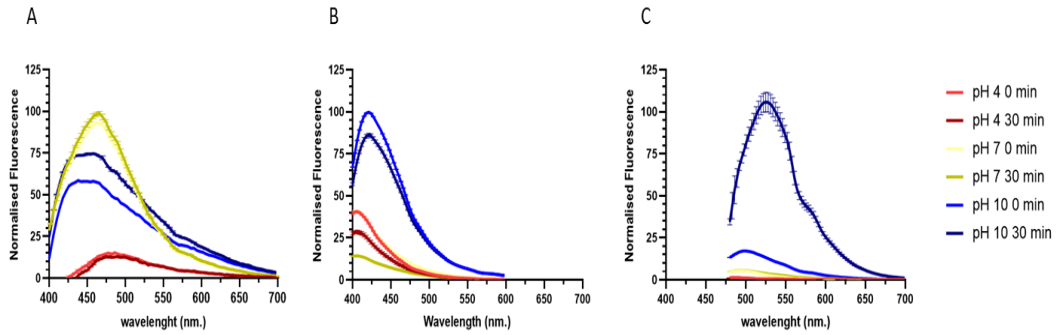

Figure 3.13 Fluorescent emission spectrum of 2s chemical. (1*H*-Pyrazole-3-carboxylic acid, 4-(2-benzothiazolyl)-5-(2,4-dihydroxy-3-methylphenyl)- at pH 4.0, 7.0, and 10.0. A) Excitation wavelength was set to 310 nm. B) Excitation wavelength was set to 360 nm. C) Excitation wavelength was set to 450 nm.

The emission spectrum for all these excitation peaks was obtained separately (figure 3.13A, 3.13B, 3.13C, respectively). At pH 4.0 relatively low emission intensities were observed in all excitation wavelengths, while at 360 and 450 nm, excitation wavelength pH 10.0 results in higher fluorescence intensity compared to 310 nm excitation wavelength in which pH 7.0 shows higher intensity. At 450 nm excitation wavelength emission peak was observed at 520 nm, while at 310 and 450 nm excitation results in emission max at 450 nm incubation for 30 minutes at pH 10.0 significantly improves fluorescence at emission 520 nm wavelength.

3.6 Toxicity of the Test Compounds

To measure the toxicity of the tested chemicals, an MTT test was performed. First, to determine the density of the cells that are going to be used, MTT standard curves were plotted for each N2a and HEK cell line. For N2a cells calibration curve was plotted with 2500, 5000, 7500, and 10000 cell densities. The graph fits a linear curve between absorbance values ranging 0.2 - 0.8 figure 3.14A. For HEK cell line calibration curve plotted with the density of 4000, 8000, 12000, 16000, 20000, and 24000. The graph fits a linear curve between absorbance values ranging 0.5 – 0.9 figure 3.14B. As a result, 10.000 for N2a, and 20.000 for HEK cell density were decided to be used in further assays.

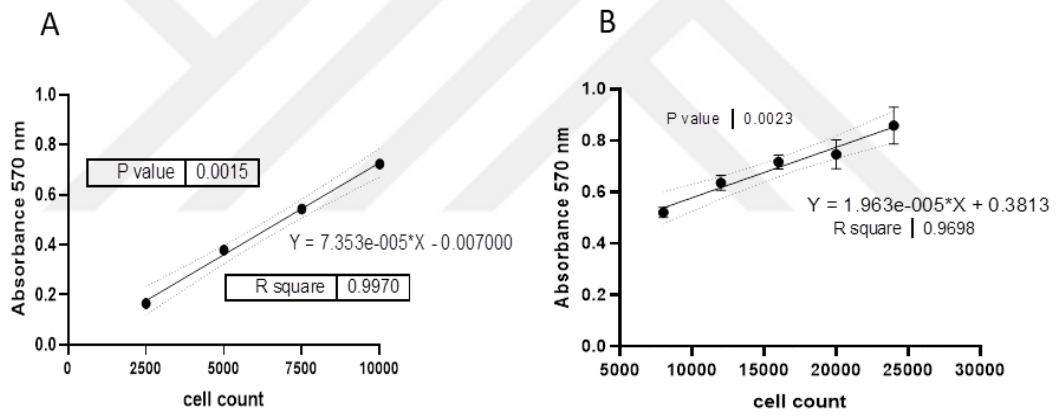

Figure 3.14 MTT toxicity assay standard curves. A) N2a cells MTT Toxicity assay standard curve B) HEK cells MTT Toxicity assay standard curve.

Toxicity of each chemical tested at 50 and 100 μM concentration, the aim here was to determine the maximum non-toxic concentration to use in the FRET experiment. Since each chemical dissolved in 100 % DMSO additional test group, 1 % DMSO, was added to the assay (Control DMSO/ veh.) and each chemical test group compared with control veh. Figure 3.15 shows the toxicity of the chemicals in N2a cells.

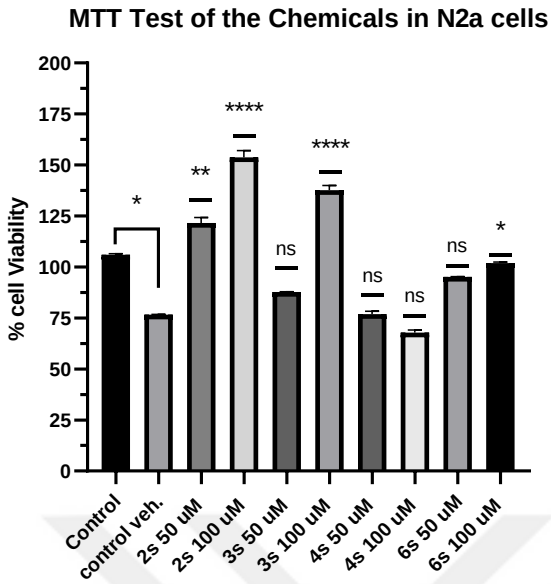

Figure 3.15 Toxicity test of the chemicals in N2a cells. The final DMSO concentration is 1 % in all groups except the control. *p<0.05, **P<0.005, ****p<0.0001 statistically significant differences. ns: no significant differences. Data Mean ± SEM

According to MTT test results, 1% DMSO results in nearly 25 % toxicity (compared to the control group). 2s compound increase cell viability by about 70 % at 50 μM and nearly 90 % at 100 μM concentration (compared to control veh.). 3s chemical does not affect cell viability at the 50 μM concentration but increases nearly 80 % at 100 μM concentration (compared to control veh.). 4s chemicals do not affect cell viability at either concentration. 6s chemical does not affect cell viability at 50 μM where areas increase nearly 35 % at 100 μM concentration (compared to control veh.).

After observing this data, another control experiment was performed to determine the observed increased cell viability of some of the tested compounds is not due to nonenzymatic oxidation of the MTT reagent with the test compounds. For this purpose, an MTT test was performed in a noncell containing N2a media and a control group with untreated N2a cells added to the test group. Figure 3.16 shows that there is no such interaction.

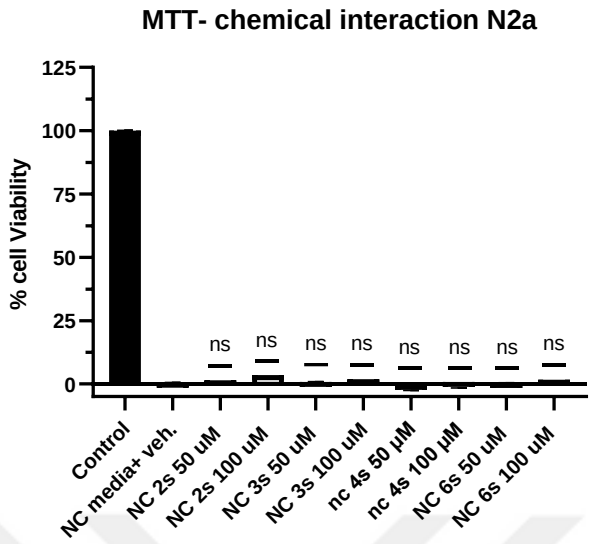

Figure 3.16 Bar graph representation of MTT reagent and chemicals interaction test. 2s, 3s, 4s, and 6s compounds without cells in N2a cell media and control group. ns: no significant differences. Data Mean ± SEM

All the test groups compared with the NC (No cell media) veh. As a result, no significant differences were observed. These results confirm that there is no interaction between the MTT reagent and the test compounds.

To determine key components of this observed increased cell viability effect of the 2s, 3s, and 6s chemicals, MTT assay was performed in N2a cells that transiently transfected with empty vector, β-2AR, Arrb2, or co-transfected with β-2AR and β-Arrestin 2 together. To use the same amount of DNA in each test group, the empty vector test group was transfected with 800 ng. PcDNA 3.1- vector, single protein-expressing test groups were transfected with 400 ng. either of the β-2AR or β-Arrestin 2 carrying plasmids, and 400 ng PcDNA3.1- vector, and β-Arrestin 2 and β-2AR co-expressing N2a cells were transfected with 400 ng. of each protein's gene carrying plasmids. The results are shown in figure 3.17.

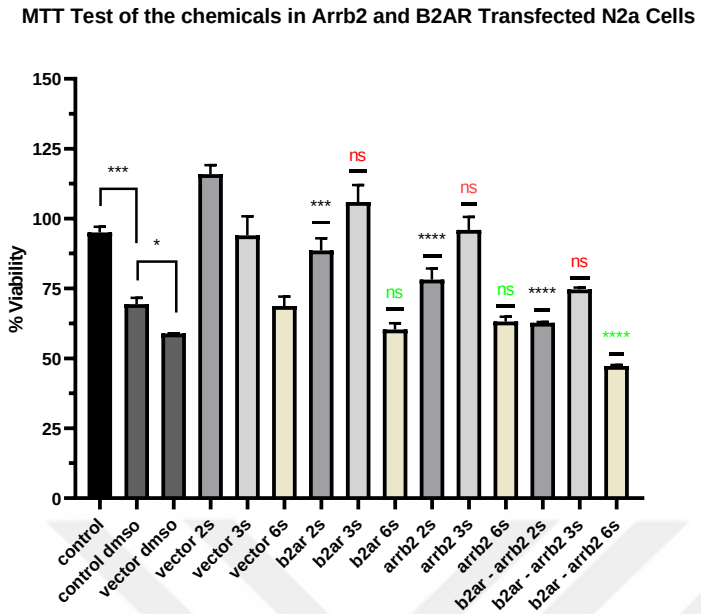

Figure 3.17 The effects of the compounds on cell viability in N2a cells overexpress β-2AR, Arrb2, or β-2AR and Arrb2. Transfected samples were compared to corresponding empty vector samples. The final DMSO concentration is 1 % in all groups except the control group. *P < 0.05, ***p<0.001, ****p<0.0001 statistically significant differences. ns: no significant differences. Data Mean ± SEM

Empty vector-transfected N2a cells treated with 100 µM each chemical show increased cell viability except 6s (compared to vector-DMSO). This data correlates with the data shown in figure 3.15. In cells overexpressing β-2AR, 2s chemical effect on increased cell viability decreases significantly. This effect becomes more severe in the presence of β-Arrestin 2 protein. Moreover, in the N2a cells co-express these 2 proteins, 2s chemical's effect on increased cell viability almost vanishes. 3s chemical's effect on cell viability does not change in the N2a cells either transfected with β-Arrestin 2 and β-2AR or co-transfected with those 2 genes. 6s chemical does not chance cell viability in the cells that overexpress either these proteins alone, but this chemical shows toxic effect in the cells overexpresses these 2 proteins.

MTT test of the compounds was also performed in the HEK cell line figure 3.18 shows the toxicity of these chemicals significantly different for 2s and 3s

chemicals, yet it is similar for 4s and 6s chemicals. According to MTT test results, 1% DMSO results in nearly 30 % toxicity (compared to the control group). 2s, 4s, and 6s chemicals do not affect cell viability at both concentrations (compared to the control vehicle). 3s compound increased cell viability by about 35 % at both tested concentrations. (compared to control vehicle).

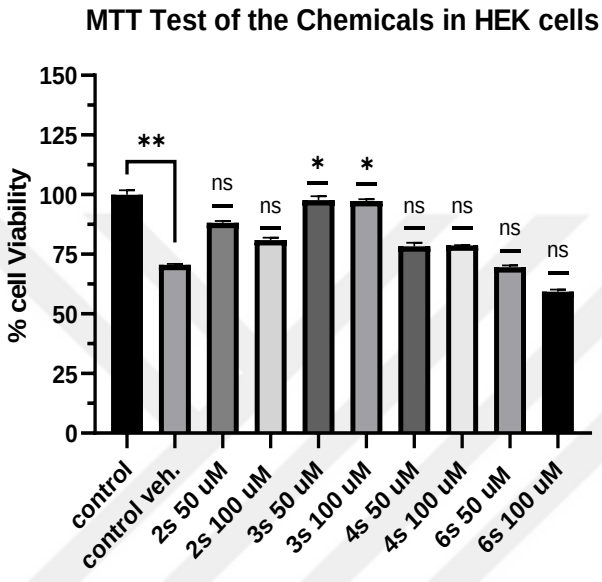

Figure 3.18 Bar graph representation of the effect of tested chemicals on cell viability in HEK cells. *p<0.05, **p<0.005, statistically significant differences. ns: no significant differences. Data Mean ± SEM

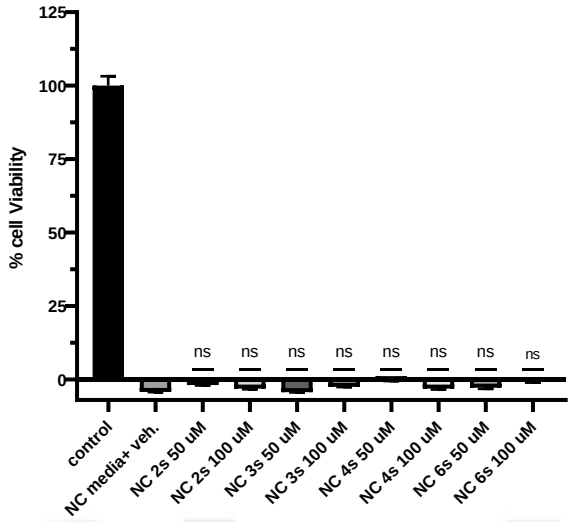

Figure 3.19 Bar graph representation of MTT reagent and test compounds interaction test.2s, 3s, 4s, and 6s ligands without cells in HEK cell media and control group. ns: no significant differences. Data Mean ± SEM

Figure 3.19 shows that there is no interaction between the MTT reagent and the test compounds in HEK cell media. After the MTT test, it was decided to use 100 μM of each chemical in the FRET experiments.

3.7 FRET Analysis of the Iso Response and Test Compounds in β-2AR, β-Arrestin-2 System

3.7.1 FRET Analysis of the Iso response in Negative and Positive system

In the previous sections, plate reader FRET analysis was done, and FRET/Donor was chosen to be used for microplate reader FRET calculations. Before testing the chemicals in the P.D. β-2AR system, β-2AR-β-Arrestin 2 and P.D. β-2AR-β-Arrestin basal FRET levels (before stimuli) and iso response measured. 20 μM iso used for stimulation.

Figure 3.20 shows that there is a significant difference in basal FRET levels between the negative and positive systems.

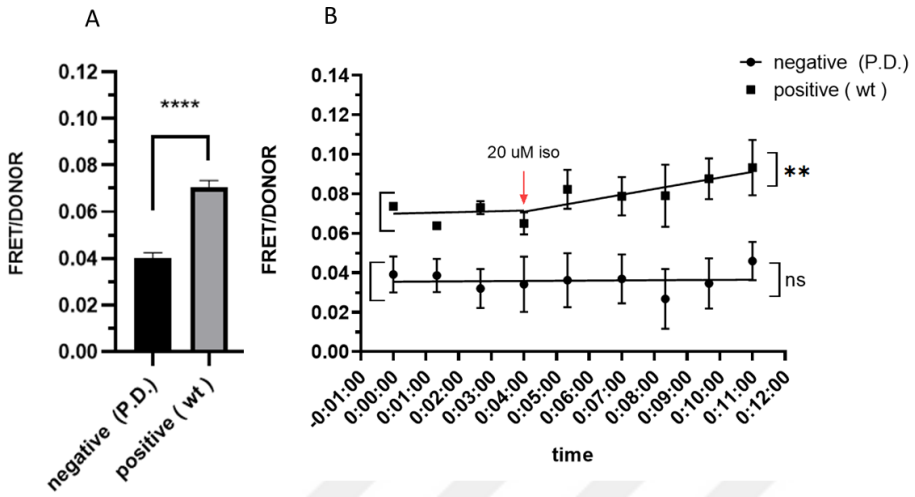

Figure 3.20 Calculated basal FRET levels in N2a cells transfected with B2AR P.D mCherry, Arrb2 177-mEGFP, GRK2 (negative), or β-2AR-mCh., Arrb2-177-mEGFP, GRK2 (positive wt.). B) calculated FRET levels in N2a cells before and after 20 µM iso stimulation. *p<0.05 ****p<0.0001 statistically significant differences. ns: no significant differences. Data Mean ± SEM

For the negative system, the basal FRET/Donor value was calculated as 0.04 and for the positive system, it was found to be 0.07. Figure 3.20 B shows the iso response of both negative and positive systems. While iso stimulation increases FRET/Donor value in the positive system, it does not change in the negative system. These results correlate with the results shown in 3.4 in which it was shown that iso stimulation triggers β-Arrestin 2 co-localization with the β-2AR.

3.7.2 FRET Analysis of the Test Compounds in Negative System

The FRET analysis of the test compounds was performed in a plate reader at 100 μM of each chemical. The experimental setup of FRET analysis is shown in figure 3.21

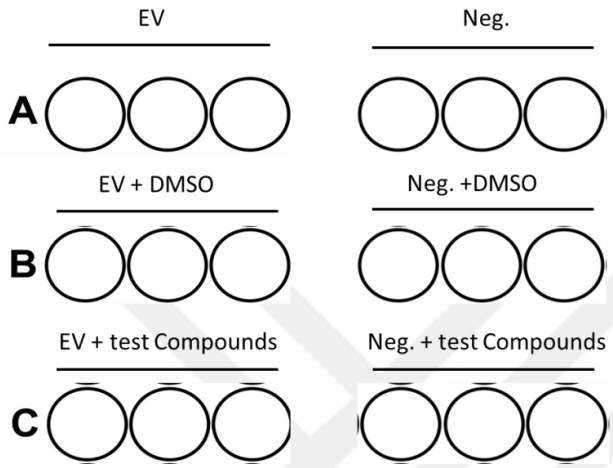

Figure 3.21 Experimental setup for testing each chemical in P.D. β-2AR system. EV: empty vector, Neg.: P.D. β-2AR-mCh., β-Arrestin 2-177-mEGFP, GRK2.

Since all the chemicals have fluorescent character, 3 different blanks were prepared with 1200 ng PcDNA 3.1- vector, and the samples were transfected with 400 ng. of each P.D. β-2AR-mCh., β-Arrestin 2-177-mEGFP, and GRK2 constructs. Each blank was used in the subtraction of corresponding samples in all channels.

First, the FRET analysis was conducted after adding each chemical then measured for 30 minutes. In this first trial of the experiments, no differences were found. After this observation, it was reasoned to incubate the samples for 30 minutes and measure for 30 minutes.

In FRET experiments it was observed that the 2s chemical has huge interference in both mEGFP and FRET channels, and in the first trial of the experiment, no significant differences were observed. For this reason, 2s chemical was not included in the results. Figure 3.22 shows the FRET measurement of the 3s, 4s, and 6s chemicals. Each of these compounds was tested twice in separate experiments.

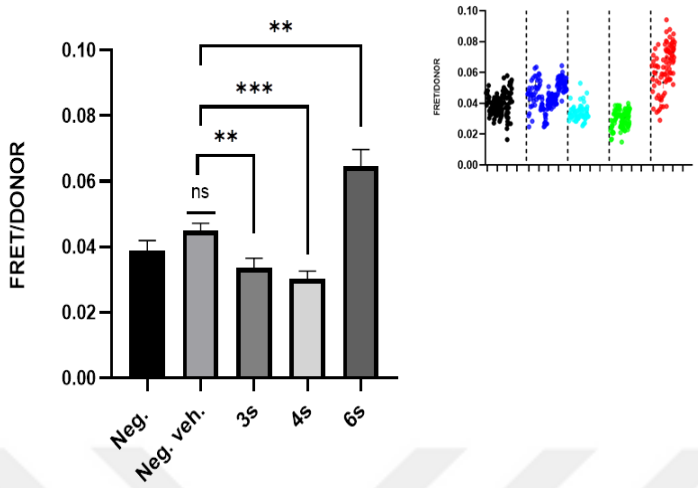

Figure 3.22 FRET analysis of the test chemicals in the Negative system. Each chemical was tested in two separate experiments n=6. **p<0.005, ***p<0.001 statistically significant differences. ns: no significant differences.

According to the results shown in figure 3.22 FRET/Donor values for Negative and Negative veh. (1 % DMSO) calculates as 0.038, and 0.044, respectively, and no significant differences were observed between these samples. FRET/Donor values for 3s, 4s, and 6s were found to be 0.033, 0.030, and 0.064 respectively. It was observed that 3s and 4s decreased FRET 25 and 30 %, respectively, the 6s chemical increased FRET by nearly 50 %, which strongly suggests that 6s chemical initiate interaction between P.D. β-2AR and β-Arrestin 2.

To confirm that the results shown in figure 3.22 were not due to an interference of the test chemicals, all 3 chemicals were tested in a membrane-targeted positive FRET construct (Gap43 mCh-mEGFP). N2a cells were transfected with Positive FRET construct, and before FRET measurement in a microplate reader, 96 well plate was incubated for 1 hour with each chemical (100 µM) in cell culture incubator then measured. Results are shown in figure 3.23.

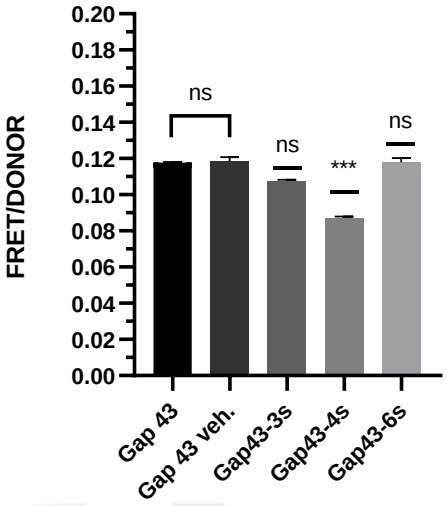

Figure 3.23 Chemical interaction with membrane targetting sequence fused mCh. and mEGFP transfected N2a cells. Data Mean ± SEM ***p<0.001, statistically significant differences, ns: no significant differences. Chemical treated samples were compared with Gap 43 veh. (1% DMSO).

Results indicate that 3s and 6s chemical does not interfere with the positive construct while 4s chemical decreases FRET over 25 %.

3.8 Further Characterization of 2s Chemical

After the observation of the 2s chemical's fluorescent character is shifted to green from blue by increased pH, it was reasoned that this compound might be a pH sensor. To test this possibility several experiments were performed. First, the pKa value of the chemical was calculated from over the intensity of λex: 450/360 nm. λem: 520 nm. ($I_{450/360}$). The rationale for choosing these wavelengths is that most of the fluorescence microscope has light sources around these wavelengths and avoiding exposing living cells to intense UV light (275 nm.).

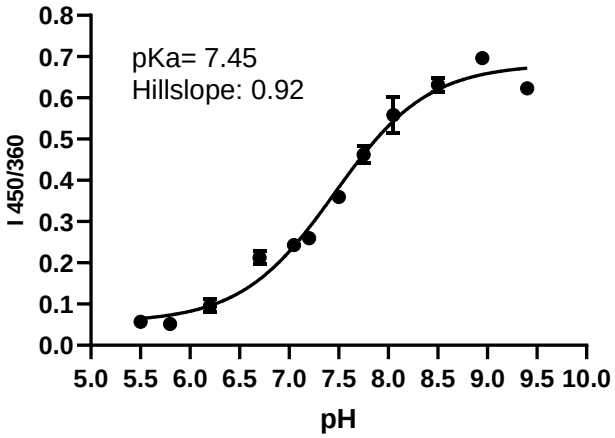

Figure 3.24 Plot of pH versus $I_{450/360}$ λem = 520 nm. data mean ± SEM experiment performed duplicate.

The ratio over 450/ 360 increases from 0.05 to 0.6 between pH: 4.8 and 9.40 (± 0.02). The pKa value is calculated to be 7.45 (figure 3.24) and it has an over 2-fold increase between pH 7.0 and 8.0.

The interference of a redox species, H_2O_2 at 100 µM, and the most abundant elements in cell Na^+, K^+, Ca^{2+}, and Mg^{2+} were tested at 50 mM, 150 mM, 1 µM, and 1 mM respectively. The chosen concentrations are based on free intracellular concentrations of these elements. Also, we tested some of the trace elements Al^{3+}, Cu^{2+}, Fe^{3+}, Ni^{2+} at 1 µM (above intracellular concentrations). Results indicated that $Ni^{2+}$and Cu^{2+} showed a little decreasing effect on the $I_{450/360}$ while other elements have no such interference (Figure 3.25). We also investigated the concentration of the probe does not alter the $I_{450/360}$ ratio. 3 different concentrations, 25, 50, and 75 µM of the probe investigated at pH 7.20 and $I_{450/360}$ ratio compared to each other (Figure 3.26).

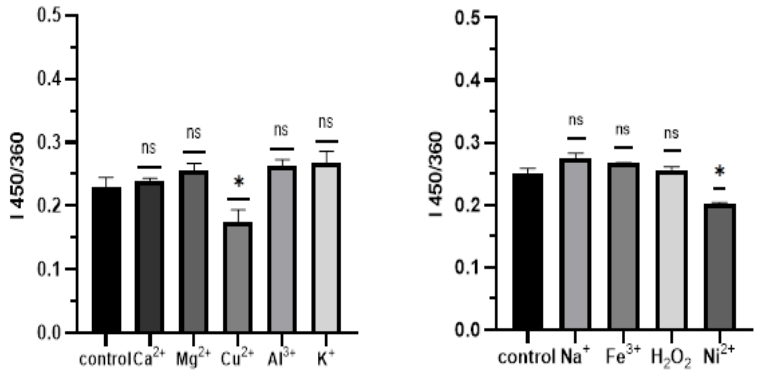

Figure 3.25 The interference of some metal ions and molecules on ThiAKS Green at different concentrations in 250 mM Tris HCl buffer solution (pH=7.35) 150 mM K^+, 1 μM Ca^{2+}, 1 mM Mg^{2+}, 1 μM Cu^{2+}, 1 μM Al^{3+} 50 mM Na^+, 1 μM Ni^{2+}, 1 μM Fe^{3+} and 100 μM H_2O_2. *p<0.05, statistically significant differences, ns: no significant differences. Data Mean ± SEM experiment performed duplicate replicas.

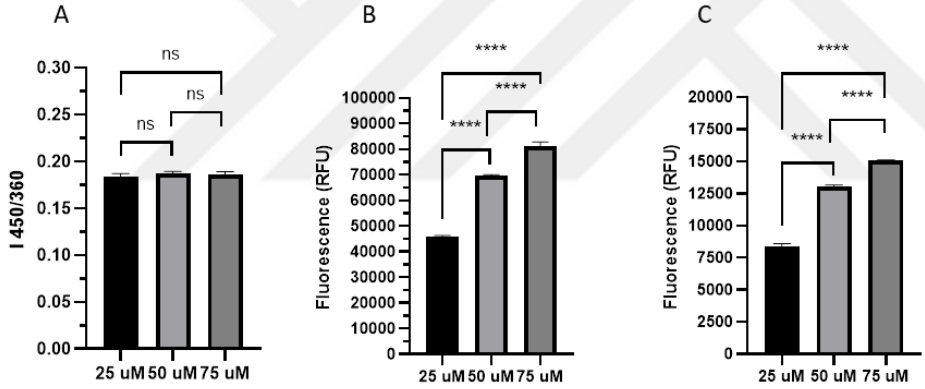

Figure 3.26 Concentration effect of the 2s chemical on $I_{450/360}$ ratio at pH 7.20. The experiment was performed in triplicate. ****p<0.0001 statistically significant differences. ns: no significant difference. Data Mean ± SEM experiment performed triplicate replicas.

The intracellular localization of the chemical was determined by the fluorescent microscope using HEK cells transfected with the nucleus targeted mCh. After 1.5 hours of exposure to 50 μM of the probe or 0.5 %, DMSO samples were imaged in Bright-Field, DAPI, EGFP, and mCh. channels (Figure 3.26). The results show that the chemical is mainly localized in the cytoplasm.

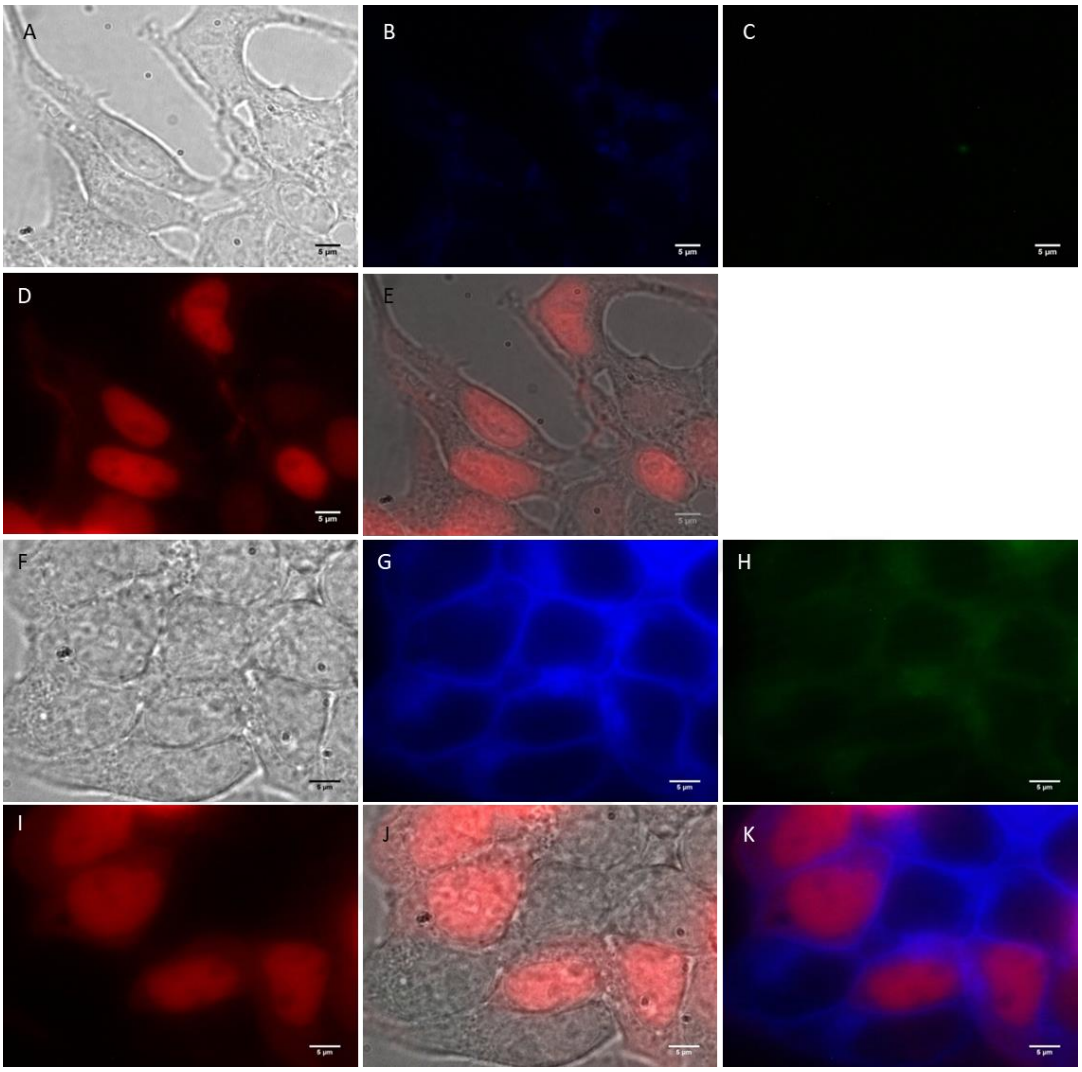

Figure 3.27 Fluorescent microscope image of HEK 293 cells treated with 0.5 % DMSO (A-E) or 50 μM ThiAKS Green (F-K) for 1.5 hours. A) Bright-field image B) DAPI channel. C) EGFP channel. D) mCh. channel E) overlay of A and D. F) Bright-field image G) DAPI channel. H) EGFP channel. I) mCh. channel J) overlay of F and I. K) overlay of G and I. (Magnification 100X, scale bars are 5 μm).

After observing the cell-penetrating character of the chemical, it was also tested for pH measurement in live cells. To measure intracellular pH, HEK 293 cells were used as a model system to measure the pH of the Golgi by using fluorescent microscopy. For that purpose, a modified excitation and emission wavelength compared to $I_{450/360}$ had to be used as most of the fluorescent microscopes lack light sources and filters suitable for these wavelengths. First, calibration studies were

performed and a curve plotted that is suitable for our microscope and making comparative measurements with a plate reader.

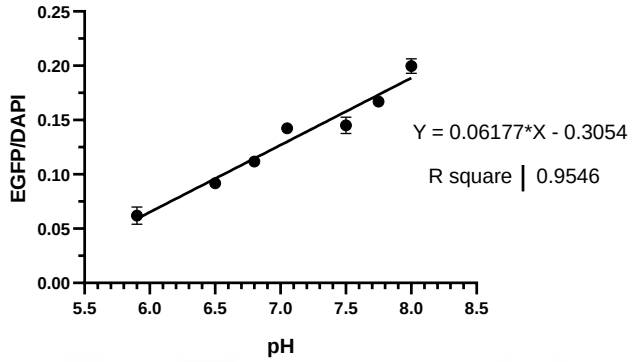

Figure 3.28 Calibration curve EGFP 450-510 DAPI 360-470 excitation bandwidth is 15 nm emission bandwidth is 25 nm.

Results indicate DAPI and EGFP channels (360-470, 450-510, respectively) are the most suitable settings in the microscope for this purpose. The plotted linear curve (R^2 = 0.9546) between pH 5.9 and 8.0 using EGFP/DAPI ratio in a plate reader (Figure 3.28) had good agreement with the microscope readings. However, our microscope has different light sources and filters for DAPI and EGFP channels. The intensity of the light coming out of the objective lens (both LUX and Photon count) was measured with the help of a luminometer for each channel. To make each channel's intensity comparable, the excitation power of each line was adjusted accordingly.

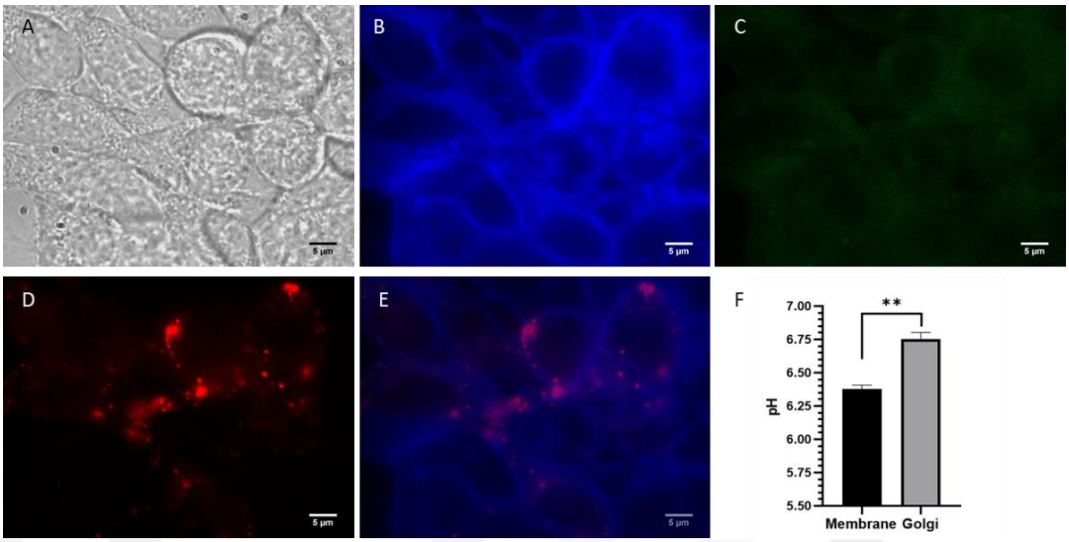

Figure 3.29 Fluorescent images of HEK cells transfected with Golgi targeted mCh. and treated with 50 μM 2s chemical. A) Bright Field image B) DAPI channel C) EGFP Channel D) image from mCh. Channel. E) overlay of B and D. F) calculated pH values of intermembrane space and Golgi (Magnification 100X, scale bars are 5 μm). *p<0.005 statistically significant differences. Data Mean ± SEM

Using above mentioned corrections, to measure the pH of cellular organelles such as the Golgi (taking advantage of a Golgi-targeted mCh. fluorescent protein for localization purposes) with 50 μM of the 2s compound following the necessary background calculations (from DMSO treated Golgi marker transfected HEK cells, figure 3.30), the value of $I_{EGFP/DAPI}$ was calculated and extrapolated with the equation of the calibration curve (Fig. 3.28). Our calculated results showed that the pH of Golgi was 6.75 the pH for the intermembrane space was also calculated as 6.38 (Fig. 3.29).

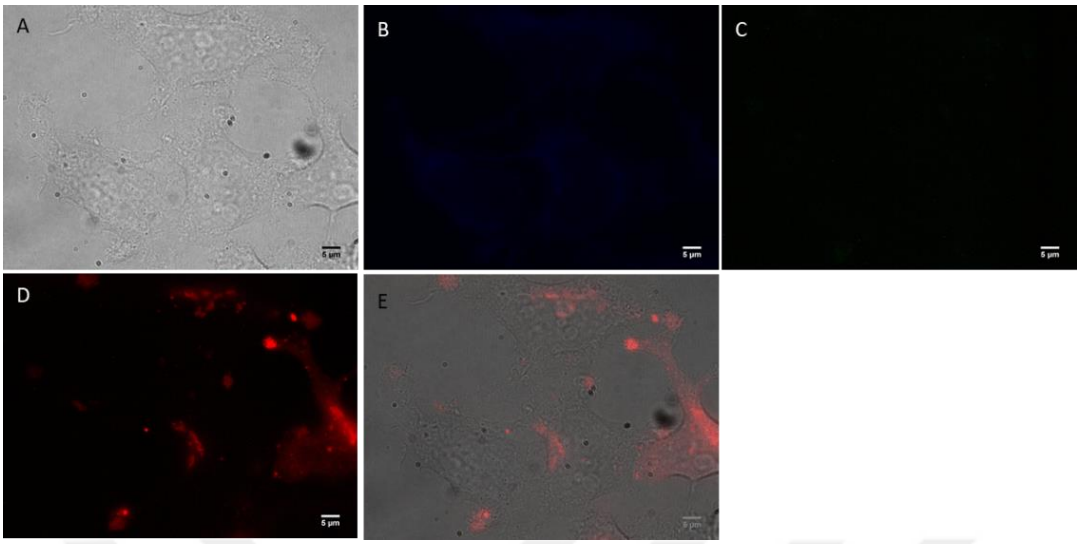

Figure 3.30 Fluorescent images of HEK cells transfected with Golgi targeted mCh. and treated with 0.5% DMSO. A) Bright Field image B) DAPI channel C) EGFP Channel D) image from mCh. Channel. E) overlay of A and D. (Magnification 100X, scale bars are 5 μm).

CHAPTER 4

DISCUSSION

In order to study interactions of β-Arrestin 2 with the receptors in live cells, fluorescent protein tagging was preferred in our laboratory. As the fluorescent protein has the potential to disrupt the function and localization of the tagged protein we select several tagging positions and test the functionality of the tagged protein and compare it with wild-type untagged protein before starting our interaction analysis. In this study tagging at 177^{th} and 265^{th} aa. positions were chosen to tag β-Arrestin 2. Tagging from the 265^{th} aa. position was not successful. After observing the colocalization of β-Arrestin 2- 177-mEGFP with the β-2AR-mCh. upon stimulation, this construct was preferred to be used in further assays and tagging from 265^{th} aa. position was not pursued.

The test compounds were partially characterized during this thesis work. Absorbance spectrums of the compounds showed that when dissolved in HBSS solution none of the chemicals have absorbance at wavelengths longer than 400 nm. This ensures us that these compounds will not interfere with the MTT assay (which requires 570 nm. excitation) due to their absorbance.

MTT assay was performed to assess the toxicity of the test chemicals and to determine the maximum non-toxic concentrations that can be used in further experiments. In N2a cells none of the chemicals were determined to be toxic and three of the chemicals resulted in increased cell viability at 100 μM concentration. In the presence of β-2AR or β-Arrestin 2, these chemicals show a reduced cell viability effect, which suggests a possible alternative pathway competing with the β-2AR and β-Arrestin 2 interaction. With the overexpression of β-2AR or β-Arrestin 2, 2s compounds preference through these possible pathways decreased. To further evaluate this possibility, an MTT assay was also performed in second

cell culture (HEK293 cells). Results in HEK cells suggest that the 4s chemical does not increase the cell viability as in the N2a cells, yet 2s does not activate that suggested pathway in N2a cells. While 3s chemical still activates this pathway slightly. 6s chemical showed neither increased cell viability nor toxicity in this cell line. These results suggest that this mentioned pathway's components may be less active (or not expressed) in the HEK cell line.

FRET calculation by the three cube method in confocal microscopy is a well-adapted technique in our laboratory. Nevertheless, it requires an image process and some corrections. The main drawback is microscope imaging allows gathering only a few cell images at a time. On the other hand, FRET calculation in a microplate reader allows measuring the fluorescent of the samples on a larger scale (thousands of cells in a much shorter time). And it does not require image processing also minimizes the environmental effect on the fluorescent such as reflection of daylight. The chosen fluorophores (mEGFP and mCh.) have good spectral overlap and minimum fluorescent leakage to each other's spectrum. The total leakage of this FRET pair at chosen wavelengths is around 8 %. By the three cube method, the FRET is calculated as % FRET efficiency which gives the percentage energy transferred from the donor to acceptor fluorophore and it is independent of the concentration of the fluorophores. Because of this low bleed trough noise, very similar data could be obtained when the FRET is calculated as FRET/Donor in a microplate reader compared to a microscope image processing. Similar to microscope results, plate reader results are also independent of the concentration of fluorophores.

Colocalization analysis of β-Arrestin 2 with P.D. β-2AR-mCh. and β-2AR-mCh. show that agonist stimulation induces the colocalization of β-Arrestin 2 only with wt. β-2AR-mCh. Although, these results alone cannot prove the interaction between these two proteins, further evaluation of this interaction, by FRET analysis using both microscopy and plate reader systems was tested. The basal FRET levels between wt. and P.D. with β-Arrestin 2 was found to be significantly different. Our results suggest that basal activity between these two proteins is higher than

expected. Similar results have been shown in the literature. It was shown that some GPCRs exhibit basal activity towards G protein or β-Arrestin mediated pathways without a stimulus. Iso stimulation of the wt. system increases FRET only around 15%. This observed result might be due to several reasons. First, the basal activity indicates that some of the β-2AR on the cell membrane is already occupied with β-Arrestin 2. Second, the agonist used in this study (iso) is a balanced agonist that induces G protein and Arrestin mediated pathways equally. Moreover, it is not a specific ligand for β-2AR. It also activates the β-1AR and β-3AR. When the cells are exposed to this ligand it may induce the interaction of β-Arrestin 2 with all the endogenous β-ARs.

Chemical FRET assays in the P.D. β-2AR system were performed after 30 minutes of incubation. In the first trial of experiments, FRET analysis was conducted without incubation. In these experiments, it was observed that none of the chemicals affect the FRET level of the P.D. β-2AR system. This may suggest that the transportation of the chemicals into the cells takes nearly 30 minutes and we do not know how much of the chemicals get inside the cells. After increasing the incubation to 30 minutes in HBSS solutions, only 6s chemical resulted in an increase on the FRET by 50% while 2s and 4s compounds decrease it.

To evaluate the chemical's interference with mEGFP and mCh. fluorescent proteins, another FRET experiment performed with the test compounds in positive FRET construct (Gap43-mCh.-mEGFP) the results suggest 3s and 6s effect seen in figure 3.22 is not due to such interaction and confirms 6s increases FRET by bringing the tested two proteins closer to each other. The decreasing effect of 3s might be due to a pathway suggested in MTT results. Interestingly 4s decreases FRET 25 % as seen in figure 3.22 indicating that this decrease might be caused by blocking energy transfer between the fluorescent proteins.

2s chemical spectrums in different pH solutions suggest that high pH induces a conformational change that results in a red-shifted fluorescence and this transformation seems to be slow because it reaches equilibrium between 1 and 1.5

hours. For that reason, all the experiments on further characterization of this compound were conducted after 1.5 hours of incubation. After showing that 2s chemical (later named as ThiAKS Green) has a pH-dependent fluorescent emission, it was hypothesized that it may be used as a pH probe for intracellular pH measurement. First, the cell penetration capability of the probe was investigated in HEK cells. This cell line was chosen for this experiment as a model system because this chemical does not increase cell viability in this cell line.

HEK cells were exposed to the probe then imaged by fluorescent microscopy the probe exhibit cytoplasm and membrane localization. The localization of the probe seems to be not uniform and high intensities observed around the membrane may suggest that the probe accumulates around the membrane. To show that the property of this probe does not impair pH measurement the $I_{450/360}$ ratio was calculated at pH=7.20 in three different concentrations. This pH was chosen because it reflects the pH of the cell cytoplasm. As a result, it was shown that $I_{450/360}$ value is independent of the concentration of the probe.

Later the probe was used to measure the pH of the intracellular pH measurement and Golgi organelle was chosen for this purpose. Because the $I_{450/360}$ ratio was not compatible with our microscope, an alternative calibration graph had to be plotted. DAPI and EGFP channels of our microscope were chosen and a calibration curve was plotted from the intensity ratio EGFP/DAPI channels. Finally, the pH of the Golgi was calculated as 6.75 which agrees with the literature.

CONCLUSION

The aim of this work was to facilitate the interaction between P.D. β-2AR, β-Arrestin 2 with the help of small compounds. In the literature to achieve this interaction, several strategies were tested. Our strategy differs from the previous attempts. We hypothesized that changing the confirmation of arrestin to its active form by small chemicals could initiate the interaction with β-2AR. To that extent, four molecules were chosen by computational tools then tested by *in-vitro* FRET analysis during this work.

The chosen compounds were partially characterized and it was found that all the chemicals have fluorescent character around the blue and green spectrum. The toxicity of the chemicals was also investigated by MTT assay. The results show that all the chemicals were non-toxic at 50 and 100 μM concentrations. Moreover, 2 of the chemicals show increasing cell viability effects by unknown mechanisms.

Further characterization of 2s chemical revealed that this molecule can be used as a pH probe later named "ThiAKS Green" is suitable for intracellular pH measurements. This new probe has no cell toxicity and good cell-penetrating properties. Moreover, its pKa value (7.45) makes it ideal for intracellular pH measurement. Another advantage of the probe is that it allows not only the intracellular pH but also the pH of the intermembrane space, which indicated that the probe could also be used for cancer research. The flexibility of the ratios that could be used to calculate pH changes makes this probe suitable for various instruments that could have limited excitation and emission capabilities.

After characterization studies, the chemicals were tested in fluorescent protein-tagged P.D. β-2AR and β-Arrestin 2, and untagged GRK2 transfected N2a cells. The results show that while the 6s compound increases FRET, 3s and 4s compounds decrease it. 6s compound does not alter the FRET of Gap43-mCh.-mEGFP which strongly suggests that the 6s compound initiates the interaction

between P.D. β-2AR and β-Arrestin 2. This observed effect seems much slower than iso stimulation. This might be because of the slow rate of transportation of this compound into the cell. Because this chemical has two carboxylic acid groups that can donate protons under physiologic pH. Also, it is yet unknown how 6s initiates this interaction.

Together these data indicate 6s chemical might be a potential drug for such diseases caused by anomalies in the desensitization of GPCRs.

FUTURE PERSPECTIVES

FRET calculation in microplate reader can be further improved by calculation of the fluorescent leakage into FRET channel in different concentrations of each fluorophore and by subtracting this leakage, % FRET efficiency can be calculated in a microplate reader.

2s and 3s chemicals increase cell viability by an unknown pathway, which seems to compete with β-2AR and β-Arrestin 2 signaling. The function of β-Arrestin 2 and the proteins involved in this pathway are unknown. These proteins can be identified by proximity ligation assay by tagging β-Arrestin 2.

6s compound seems to be a potential drug for P.D. β-2AR and β-Arrestin 2 interaction. In further studies, the activation mechanism of this interaction and the co-localization of the receptor-arrestin complex in early endosomes can be analyzed. Furthermore, the Kd value of the chemical can be investigated. Further characterization of the 6s compound is also needed. EC_{50} and LD_{50} values of this compound can be assessed to evaluate its therapeutic index. Kd value of the 6s compound can be found by in-vitro and in-vivo experiments. For in-vitro analysis β-Arrestin 2 protein must be purified and a titration curve may be plotted by calorimetric measurements. Also, the conformational change induced by the 6s chemical can be monitored by a β-Arrestin 2 FRET sensor.

Intermembrane localization of the ThiAKS Green pH probe can be detected by co-localization analysis of the probe with intermembrane space markers.

REFERENCES

Akhter, Shahab A., Andrea D. Eckhart, Howard A. Rockman, Kyle Shotwell, Robert J. Lefkowitz, and Walter J. Koch. 1999. "In Vivo Inhibition of Elevated Myocardial β-Adrenergic Receptor Kinase Activity in Hybrid Transgenic Mice Restores Normal β-Adrenergic Signaling and Function." *Circulation* 100 (6): 648–53. https://doi.org/10.1161/01.CIR.100.6.648.

Anderson, Richard G.W. 1998. "The Caveolae Membrane System." *Annual Review of Biochemistry* 67: 199–225. https://doi.org/10.1146/annurev.biochem.67.1.199.

Apfelstedt-Sylla, Eckart, Markus Kunisch, Monika Horn, Klaus Rüther, Heinrich Gerding, Andreas Gal, and Eberhart Zrenner. 1993. "Ocular Findings in a Family with Autosomal Dominant Retinitis Pigmentosa and a Frameshift Mutation Altering the Carboxyl Terminal Sequence of Rhodopsin." *British Journal of Ophthalmology* 77 (8): 495–501. https://doi.org/10.1136/bjo.77.8.495.

Attramadal, H., J. L. Arriza, C. Aoki, T. M. Dawson, J. Codina, M. M. Kwatra, S. H. Snyder, M. G. Caron, and R. J. Lefkowitz. 1992. "β-Arrestin2, a Novel Member of the Arrestin/β-Arrestin Gene Family." *Journal of Biological Chemistry* 267 (25): 17882–90. https://doi.org/10.1016/S0021-9258(19)37125-X.

Audet, Martin, and Michel Bouvier. 2012. "Restructuring G-Protein- Coupled Receptor Activation." *Cell* 151 (1): 14–23. https://doi.org/10.1016/j.cell.2012.09.003.

Azzi, Mounia, Pascale G. Charest, Stéphane Angers, Guy Rousseau, Trudy Kohout, Michel Bouvier, and Graciela Piñeyro. 2003. "β-Arrestin-Mediated Activation of MAPK by Inverse Agonists Reveals Distinct Active Conformations for G Protein-Coupled Receptors." *Proceedings of the*

National Academy of Sciences of the United States of America 100 (20): 11406–11. https://doi.org/10.1073/pnas.1936664100.

Baker, Jillian G, Ian P Hall, and Stephen J Hill. 2003. “Agonist and Inverse Agonist Actions of β-Blockers at the Human B₂-Adrenoceptor Provide Evidence for Agonist-Directed Signaling.” *Molecular Pharmacology* 64 (6): 1357 LP – 1369. https://doi.org/10.1124/mol.64.6.1357.

Barak, Larry S., Robert H. Oakley, Stéphane A. Laporte, and Marc G. Caron. 2001. “Constitutive Arrestin-Mediated Desensitization of a Human Vasopressin Receptor Mutant Associated with Nephrogenic Diabetes Insipidus.” *Proceedings of the National Academy of Sciences of the United States of America* 98 (1): 93–98. https://doi.org/10.1073/pnas.98.1.93.

Beaulieu, Jean Martin, Tatyana D. Sotnikova, Sébastien Marion, Robert J. Lefkowitz, Raul R. Gainetdinov, and Marc G. Caron. 2005. “An Akt/β-Arrestin 2/PP2A Signaling Complex Mediates Dopaminergic Neurotransmission and Behavior.” *Cell* 122 (2): 261–73. https://doi.org/10.1016/j.cell.2005.05.012.

Bennett, Nelly, and Ari Sitaramayya. 1988. “Inactivation of Photoexcited Rhodopsin in Retinal Rods: The Roles of Rhodopsin Kinase and 48-KDa Protein (Arrestin).” *Biochemistry* 27 (5): 1710–15. https://doi.org/10.1021/bi00405a049.

Benovic, J. L., H. Kühn, I. Weyand, J. Codina, M. G. Caron, and R. J. Lefkowitz. 1987. “Functional Desensitization of the Isolated Beta-Adrenergic Receptor by the Beta-Adrenergic Receptor Kinase: Potential Role of an Analog of the Retinal Protein Arrestin (48-KDa Protein).” *Proceedings of the National Academy of Sciences of the United States of America* 84 (24): 8879–82. https://doi.org/10.1073/pnas.84.24.8879.

Calçada, Marcos, José T. Lunardi, Luiz A. Manzoni, Wagner Monteiro, and Marciano Pereira. 2019. “A Distributional Approach for the One-Dimensional

Hydrogen Atom." *Frontiers in Physics* 7 (JULY): 1–19. https://doi.org/10.3389/fphy.2019.00100.

Calebiro, Davide, Viacheslav O. Nikolaev, Maria Cristina Gagliani, Tiziana De Filippis, Christian Dees, Carlo Tacchetti, Luca Persani, and Martin J. Lohse. 2009. "Persistent CAMP-Signals Triggered by Internalized G-Protein-Coupled Receptors." *PLoS Biology* 7 (8). https://doi.org/10.1371/journal.pbio.1000172.

Celver, Jeremy, Sergey A. Vishnivetskiy, Charles Chavkin, and Vsevolod V. Gurevich. 2002. "Conservation of the Phosphate-Sensitive Elements in the Arrestin Family of Proteins." *Journal of Biological Chemistry* 277 (11): 9043–48. https://doi.org/10.1074/jbc.M107400200.

Charest, Pascale G., and Michel Bouvier. 2003. "Palmitoylation of the V2 Vasopressin Receptor Carboxyl Tail Enhances β-Arrestin Recruitment Leading to Efficient Receptor Endocytosis and ERK1/ 2 Activation." *Journal of Biological Chemistry* 278 (42): 41541–51. https://doi.org/10.1074/jbc.M306589200.

Cherezov, Vadim, Daniel M Rosenbaum, Michael Hanson, Seren GF Rasmussen, Hee-Jung Choi, Peter Kuhn, William Weis, Brian Kobika, and Raymond C Stevens. 2007. "High-Resolution Crystal Structure of an Engineered Human β." *Science* 318 (5854): 1258–65. https://doi.org/10.1126/science.1150577.High.

Chini, B., and M. Parenti. 2004. "G-Protein Coupled Receptors in Lipid Rafts and Caveolae: How, When and Why Do They Go There?" *Journal of Molecular Endocrinology* 32 (2): 325–38. https://doi.org/10.1677/jme.0.0320325.

Choe, Hui Woog, Yong Ju Kim, Jung Hee Park, Takefumi Morizumi, Emil F. Pai, Norbert Krau, Klaus Peter Hofmann, Patrick Scheerer, and Oliver P. Ernst. 2011. "Crystal Structure of Metarhodopsin II." *Nature* 471 (7340): 651–55. https://doi.org/10.1038/nature09789.

Craft, Cheryl M., Donald H. Whitmore, and Allan F. Wiechmann. 1994. “Cone Arrestin Identified by Targeting Expression of a Functional Family.” *Journal of Biological Chemistry* 269 (6): 4613–19. https://doi.org/10.1016/s0021-9258(17)41820-5.

Drake, Matthew T., Jonathan D. Violin, Erin J. Whalen, James W. Wisler, Sudha K. Shenoy, and Robert J. Lefkowitz. 2008. “B-Arrestin-Biased Agonism At the B2-Adrenergic Receptor.” *Journal of Biological Chemistry* 283 (9): 5669–76. https://doi.org/10.1074/jbc.M708118200.

Elangovan, Masilamani, H Wallrabe, Y E CHEN, R N Day, MARGARIDA BARROSO, and A PERIASAMY. 2003. “FRETImgProc_Elangovan2003.” *Methods* 29: 58–73.

Evci, Hüseyin. 2019. “Analysis of Interactions between Beta-2 Adrenergic Receptor & Beta Arrestin-2 Using Förster Resonance Energy Transfer (Fret) Method in Live Cells.” Middle East Technical University. http://etd.lib.metu.edu.tr/upload/12623559/index.pdf %0Ahttps://hdl.handle.net/11511/43784.

Fan, Xiaofang, Xuejiang Gu, Ru Zhao, Qingqing Zheng, Lan Li, Wenbing Yang, Lu Ding, *et al.* 2016. “Cardiac 2-Adrenergic Receptor Phosphorylation at Ser355/356 Regulates Receptor Internalization and Functional Resensitization.” *PLoS ONE* 11 (8). https://doi.org/10.1371/journal.pone.0161373.

Freeman. 2018. “乳鼠心肌提取 HHS Public Access.” *Physiology & Behavior* 176 (1): 139–48. https://doi.org/10.1117/12.2549369.Hyperspectral.

Funk JL, Frye JB, Oyarzo JN, Timmermann BN. 2014. “基因的改变NIH Public Access.” *Bone* 23 (1): 1–7. https://doi.org/10.1126/science.1232807.Structural.

Gahbauer, Stefan, and Rainer A Böckmann. 2016. “Membrane-Mediated

Oligomerization of G Protein Coupled Receptors and Its Implications for GPCR Function" 7 (October): 1–17. https://doi.org/10.3389/fphys.2016.00494.

Galandrin, Ségolène, Geneviève Oligny-Longpré, and Michel Bouvier. 2007. "The Evasive Nature of Drug Efficacy: Implications for Drug Discovery." *Trends in Pharmacological Sciences* 28 (8): 423–30. https://doi.org/10.1016/j.tips.2007.06.005.

Gimenez, Luis E., Seunghyi Kook, Sergey A. Vishnivetskiy, M. Rafiuddin Ahmed, Eugenia V. Gurevich, and Vsevolod V. Gurevich. 2012. "Role of Receptor-Attached Phosphates in Binding of Visual and Non-Visual Arrestins to G Protein-Coupled Receptors." *Journal of Biological Chemistry* 287 (12): 9028–40. https://doi.org/10.1074/jbc.M111.311803.

Gordon, Gerald W, Gail Berry, Xiao Huan Liang, Beth Levine, and Brian Herman. 1998. "Using Fluorescence Microscopy" 74 (May): 2702–13.

Gurevich, V. V., S. B. Dion, J. J. Onorato, J. Ptasienski, C. M. Kim, R. Sterne-Marr, M. M. Hosey, and J. L. Benovic. 1995. "Arrestin Interactions with G Protein-Coupled Receptors. Direct Binding Studies of Wild Type and Mutant Arrestins with Rhodopsin, B2-Adrenergic, and M2 Muscarinic Cholinergic Receptors." *Journal of Biological Chemistry* 270 (2): 720–31. https://doi.org/10.1074/jbc.270.2.720.

Gurevich, V. V., R. M. Richardson, C. M. Kim, M. M. Hosey, and J. L. Benovic. 1993. "Binding of Wild Type and Chimeric Arrestins to the M2 Muscarinic Cholinergic Receptor." *Journal of Biological Chemistry* 268 (23): 16879–82. https://doi.org/10.1016/s0021-9258(19)85275-4.

Jacobson, Kenneth A. 2015. "New Paradigms in GPCR Drug Delivery." *Biochem Pharmacol.* 98 (4): 541–55. https://doi.org/10.1002/aur.1474.Replication.

Joy Macalino, Stephani Y, Shaherin Basith, Nina B Abigail Clavio, Hyerim Chang, Soosung Kang, and Sun Choi. n.d. "Molecules Evolution of In Silico

Strategies for Protein-Protein Interaction Drug Discovery." https://doi.org/10.3390/molecules23081963.

Kahsai, Alem W., Kunhong Xiao, Sudarshan Rajagopal, Seungkirl Ahn, Arun K. Shukla, Jinpeng Sun, Terrence G. Oas, and Robert J. Lefkowitz. 2011. "Multiple Ligand-Specific Conformations of the B2-Adrenergic Receptor." *Nature Chemical Biology* 7 (10): 692–700. https://doi.org/10.1038/nchembio.634.

Kang, Yanyong, Oleg Kuybeda, Parker W. de Waal, Somnath Mukherjee, Ned Van Eps, Przemyslaw Dutka, X. Edward Zhou, *et al.* 2018. "Erratum to: Cryo-EM Structure of Human Rhodopsin Bound to an Inhibitory G Protein (Nature, (2018), 558, 7711, (553-558), 10.1038/S41586-018-0215-Y)." *Nature* 561 (7724): E44. https://doi.org/10.1038/s41586-018-0302-0.

Kenakin, Terry. 2007. "Functional Selectivity through Protean and Biased Agonism: Who Steers the Ship?" *Molecular Pharmacology* 72 (6): 1393 LP – 1401. https://doi.org/10.1124/mol.107.040352.

Kim, Robert Y, Mai Al-Maghtheh, Fred W Fitzke, Geoffrey B Arden, Marcelle Jay, Shomi S Bhattacharya, and Alan C Bird. 1993. "Dominant Retinitis Pigmentosa Associated With Two Rhodopsin Gene Mutations: Leu-40-Arg and an Insertion Disrupting the 5′-Splice Junction of Exon 5." *Archives of Ophthalmology* 111 (11): 1518–24. https://doi.org/10.1001/archopht.1993.01090110084030.

Kopecky, Stephen L. 2006. "Effect of Beta Blockers, Particularly Carvedilol, on Reducing the Risk of Events After Acute Myocardial Infarction." *American Journal of Cardiology* 98 (8): 1115–19. https://doi.org/10.1016/j.amjcard.2006.05.039.

Kovoor, Abraham, Jeremy Celver, Ravil I. Abdryashitov, Charles Chavkin, and Vsevolod V. Gurevich. 1999. "Targeted Construction of Phosphorylation-Independent β-Arrestin Mutants with Constitutive Activity in Cells." *Journal*

of Biological Chemistry 274 (11): 6831–34. https://doi.org/10.1074/jbc.274.11.6831.

Krasel, Cornelius, Ulrike Zabel, Kristina Lorenz, Susanne Reiner, Suleiman Al-Sabah, and Martin J. Lohse. 2008. "Dual Role of the B2-Adrenergic Receptor C Terminus for the Binding of β-Arrestin and Receptor Internalization." *Journal of Biological Chemistry* 283 (46): 31840–48. https://doi.org/10.1074/jbc.M806086200.

Kraynov, Vadim S, Chester Chamberlain, Gary M Bokoch, Martin A Schwartz, Sarah Slabaugh, and Klaus M Hahn. 2000. "Localized Rac Activation Dynamics Visualized in Living Cells." *Science* 290 (5490): 333 LP – 337. https://doi.org/10.1126/science.290.5490.333.

Kuhn, H. n.d. "D E a C T I V a T I O N of Photoactivated" 7: 283–98.

Lebon, Guillaume, Tony Warne, Patricia C. Edwards, Kirstie Bennett, Christopher J. Langmead, Andrew G.W. Leslie, and Christopher G. Tate. 2011. "Agonist-Bound Adenosine A2A Receptor Structures Reveal Common Features of GPCR Activation." *Nature* 474 (7352): 521–26. https://doi.org/10.1038/nature10136.

Lefkowitz, Robert J, and Sudha K Shenoy. 2005. "Transduction of Receptor Signals by SS-Arrestins." *Science* 308 (5721): 512 LP – 517. https://doi.org/10.1126/science.1109237.

Li, Shane, Tong Sun Kobilka, Brian K Kobilka, and Georgios Skiniotis. 2017. "With G Protein" 546 (7657): 248–53. https://doi.org/10.1038/nature22394.Cryo-EM.

Liang, Yi Lynn, Maryam Khoshouei, Mazdak Radjainia, Yan Zhang, Alisa Glukhova, Jeffrey Tarrasch, David M. Thal, *et al.* 2017. "Phase-Plate Cryo-EM Structure of a Class B GPCR-G-Protein Complex." *Nature* 546 (7656): 118–23. https://doi.org/10.1038/nature22327.

Lohse, M. J., J. L. Benovic, M. G. Caron, and R. J. Lefkowitz. 1990. “Multiple Pathways of Rapid B2-Adrenergic Receptor Desensitization. Delineation with Specific Inhibitors.” *Journal of Biological Chemistry* 265 (6): 3202–11. https://doi.org/10.1016/s0021-9258(19)39754-6.

Lohse, Martin J, Jeffrey L Benovic, Juan Codina, Marc G Caron, J Lefkowitz, Martin J Lohse, Jeffrey L Benovic, and Juan Codina. 2017. “β-Arrestin : A Protein That Regulates β-Adrenergic Receptor Function Published by : American Association for the Advancement of Science Stable URL : Http://Www.Jstor.Org/Stable/2874766 , 1-Arrestin : A Protein That Regulates , -Adrenergic Receptor Functio” 248 (4962): 1547–50.

Luttrell, Louis M., Francine L. Roudabush, Eric W. Choy, William E. Miller, Michael E. Field, Kristen L. Pierce, and Robert J. Lefkowitz. 2001. “Activation and Targeting of Extracellular Signal-Regulated Kinases by β-Arrestin Scaffolds.” *Proceedings of the National Academy of Sciences of the United States of America* 98 (5): 2449–54. https://doi.org/10.1073/pnas.041604898.

McDonald, Patricia H, Chi-Wing Chow, William E Miller, Stéphane A Laporte, Michael E Field, Fang-Tsyr Lin, Roger J Davis, and Robert J Lefkowitz. 2000. “β-Arrestin 2: A Receptor-Regulated MAPK Scaffold for the Activation of JNK3.” *Science* 290 (5496): 1574 LP – 1577. https://doi.org/10.1126/science.290.5496.1574.

Moore, Robert H., Amjad Tuffaha, Ellen E. Millman, Wenping Dai, Hassan S. Hall, Burton F. Dickey, and Brian J. Knoll. 1999. “Agonist-Induced Sorting of Human B2-Adrenergic Receptors to Lysosomes during Downregulation.” *Journal of Cell Science* 112 (3): 329–38.

Mosteller RD. 1987. “The New England Journal of Medicine Downloaded from Nejm.Org at DUKE MEDICAL CENTER LIBRARY on November 25, 2012. For Personal Use Only. No Other Uses without Permission. From the NEJM

Archive. Copyright © 2010 Massachusetts Medical Society. All Rights Re." *The New England Journal of Medicine*, no. 307: 2012.

Murakami, Akira, Toshihiro Yajima, Hitoshi Sakuma, Margaret J. McLaren, and George Inana. 1993. "X-Arrestin: A New Retinal Arrestin Mapping to the X Chromosome." *FEBS Letters* 334 (2): 203–9. https://doi.org/10.1016/0014-5793(93)81712-9.

Nobles, Kelly N., Ziqiang Guan, Kunhong Xiao, Terrence G. Oas, and Robert J. Lefkowitz. 2007. "The Active Conformation of β-Arrestin1: Direct Evidence for the Phosphate Sensor in the N-Domain and Conformational Differences in the Active States of β-Arrestins1 and -2." *Journal of Biological Chemistry* 282 (29): 21370–81. https://doi.org/10.1074/jbc.M611483200.

Oyama, T, K Kitano, K Satou, and T Ito. 2002. "Extraction of Knowledge on Protein-Protein Interaction by Association Rule Discovery." *BIOINFORMATICS*. Vol. 18.

Packer, Milton, Michael R. Bristow, Jay N. Cohn, Wilson S. Colucci, Michael B. Fowler, Edward M. Gilbert, and Neil H. Shusterman. 1996. "The Effect of Carvedilol on Morbidity and Mortality in Patients with Chronic Heart Failure." *New England Journal of Medicine* 334 (21): 1349–55. https://doi.org/10.1056/nejm199605233342101.

Palczewski, K., T. Kumasaka, T. Hori, C. A. Behnke, H. Motoshima, B. A. Fox, I. Le Trong, *et al.* 2000. "Crystal Structure of Rhodopsin: A G Protein-Coupled Receptor." *Science* 289 (5480): 739–45. https://doi.org/10.1126/science.289.5480.739.

Palczewski, K., A. Pulvermuller, J. Buczylko, and K. P. Hofmann. 1991. "Phosphorylated Rhodopsin and Heparin Induce Similar Conformational Changes in Arrestin." *Journal of Biological Chemistry* 266 (28): 18649–54. https://doi.org/10.1016/s0021-9258(18)55112-7.

Pan, Ling, Eugenia V. Gurevich, and Vsevolod V. Gurevich. 2003. "The Nature of

the Arrestin·receptor Complex Determines the Ultimate Fate of the Internalized Receptor." *Journal of Biological Chemistry* 278 (13): 11623–32. https://doi.org/10.1074/jbc.M209532200.

Park, Ji Young, Su Youn Lee, Hee Ryung Kim, Min Duk Seo, and Ka Young Chung. 2016. "Structural Mechanism of GPCR-Arrestin Interaction: Recent Breakthroughs." *Archives of Pharmacal Research* 39 (3): 293–301. https://doi.org/10.1007/s12272-016-0712-1.

Pierce, Kristen L., Richard T. Premont, and Robert J. Lefkowitz. 2002. "Seven-Transmembrane Receptors." *Nature Reviews Molecular Cell Biology* 3 (9): 639–50. https://doi.org/10.1038/nrm908.

Piston, David W., and Gert Jan Kremers. 2007. "Fluorescent Protein FRET: The Good, the Bad and the Ugly." *Trends in Biochemical Sciences* 32 (9): 407–14. https://doi.org/10.1016/j.tibs.2007.08.003.

Poole-Wilson, Philip A., Karl Swedberg, John G.F. Cleland, Andrea Di Lenarda, Peter Hanrath, Michel Komajda, Jacobus Lubsen, *et al.* 2003. "Comparison of Carvedilol and Metoprolol on Clinical Outcomes in Patients with Chronic Heart Failure in the Carvedilol Or Metoprolol European Trial (COMET): Randomised Controlled Trial." *Lancet* 362 (9377): 7–13. https://doi.org/10.1016/S0140-6736(03)13800-7.

Rasmussen, Sŏren G.F., Brian T. Devree, Yaozhong Zou, Andrew C. Kruse, Ka Young Chung, Tong Sun Kobilka, Foon Sun Thian, *et al.* 2011. "Crystal Structure of the β 2 Adrenergic Receptor-Gs Protein Complex." *Nature* 477 (7366): 549–57. https://doi.org/10.1038/nature10361.

Rasmussen, Søren G F, Hee-jung Choi, Juan Jose Fung, Els Pardon, Pil Seok Chae, Brian T Devree, Daniel M Rosenbaum, *et al.* 2011. "HHS Public Access" 469 (7329): 175–80. https://doi.org/10.1038/nature09648.Structure.

Restagno, G., M. Maghtheh, S. Bhattacharya, M. Ferrone, S. Garnerone, R. Samuelly, and A. Carbonara. 1993. "A Large Deletion at the 3′ End of the

Rhodopsin Gene in an Italian Family with a Diffuse Form of Autosomal Dominant Retinitis Pigmentosa." *Human Molecular Genetics* 2 (2): 207–8. https://doi.org/10.1093/hmg/2.2.207.

Rockman, Howard A., Dong Ju Choi, Shahab A. Akhter, Mohamed Jaber, Bruno Giros, Robert J. Lefkowitz, Marc G. Caron, and Walter J. Koch. 1998. "Control of Myocardial Contractile Function by the Level of β-Adrenergic Receptor Kinase 1 in Gene-Targeted Mice." *Journal of Biological Chemistry* 273 (29): 18180–84. https://doi.org/10.1074/jbc.273.29.18180.

Rockman, Howard A., Walter J. Koch, and Robert J. Lefkowitz. 2002. "Seven-Transmembrane-Spanning Receptors and Heart Function." *Nature* 415 (6868): 206–12. https://doi.org/10.1038/415206a.

Rosenbaum, Daniel M., Vadim Cherezov, Michael A. Hanson, Søren G.F. Rasmussen, Sun Thian Foon, Tong Sun Kobilka, Hee Jung Choi, *et al.* 2007. "GPCR Engineering Yields High-Resolution Structural Insights into B2-Adrenergic Receptor Function." *Science* 318 (5854): 1266–73. https://doi.org/10.1126/science.1150609.

Rosenbaum, Daniel M, Cheng Zhang, Joseph A Lyons, Ralph Holl, David Aragao, Daniel H Arlow, Søren G F Rasmussen, *et al.* 2011. "Adrenoceptor Complex." *Nature* 469 (7329): 236–40. https://doi.org/10.1038/nature09665.Structure.

Santos, Geisa A., Diego A. Duarte, Lucas T. Parreiras-e-Silva, Felipe R. Teixeira, Rafael Silva-Rocha, Eduardo B. Oliveira, Michel Bouvier, and Claudio M. Costa-Neto. 2015. "Comparative Analyses of Downstream Signal Transduction Targets Modulated after Activation of the AT1 Receptor by Two SS-Arrestin-Biased Agonists." *Frontiers in Pharmacology* 6 (JUL). https://doi.org/10.3389/fphar.2015.00131.

Schiöth, Helgi B., and Malin C. Lagerström. 2008. "Structural Diversity of g Proteincoupled Receptors and Significance for Drug Discovery." *Nature*

Reviews Drug Discovery 7 (4): 339–57. https://doi.org/10.1038/nrd2518.

Sensoy, Ozge, Irina S. Moreira, and Giulia Morra. 2016. "Understanding the Differential Selectivity of Arrestins toward the Phosphorylation State of the Receptor." *ACS Chemical Neuroscience* 7 (9): 1212–24. https://doi.org/10.1021/acschemneuro.6b00073.

Shukla, Arun K., Aashish Manglik, Andrew C. Kruse, Kunhong Xiao, Rosana I. Reis, Wei Chou Tseng, Dean P. Staus, *et al.* 2013. "Structure of Active β-Arrestin-1 Bound to a G-Protein-Coupled Receptor Phosphopeptide." *Nature* 497 (7447): 137–41. https://doi.org/10.1038/nature12120.

Shukla, Arun K., Jonathan D. Violin, Erin J. Whalen, Diane Gesty-Palmer, Sudha K. Shenoy, and Robert J. Lefkowitz. 2008a. "Distinct Conformational Changes in β-Arrestin Report Biased Agonism at Seven-Transmembrane Receptors." *Proceedings of the National Academy of Sciences of the United States of America* 105 (29): 9988–93. https://doi.org/10.1073/pnas.0804246105.

Shukla, Arun K, Jonathan D Violin, Erin J Whalen, Diane Gesty-Palmer, Sudha K Shenoy, and Robert J Lefkowitz. 2008b. "Distinct Conformational Changes in β-Arrestin Report Biased Agonism at Seven-Transmembrane Receptors." *Proceedings of the National Academy of Sciences* 105 (29): 9988 LP – 9993. https://doi.org/10.1073/pnas.0804246105.

Song, Xiufeng, Sergey A. Vishnivetskiy, Owen P. Gross, Katrina Emelianoff, Ana Mendez, Jeannie Chen, Eugenia V. Gurevich, Marie E. Burns, and Vsevolod V. Gurevich. 2009. "Enhanced Arrestin Facilitates Recovery and Protects Rods Lacking Rhodopsin Phosphorylation." *Current Biology* 19 (8): 700–705. https://doi.org/10.1016/j.cub.2009.02.065.

Standfuss, Jörg, Patricia C. Edwards, Aaron D'Antona, Maikel Fransen, Guifu Xie, Daniel D. Oprian, and Gebhard F.X. Schertler. 2011. "The Structural Basis of Agonist-Induced Activation in Constitutively Active Rhodopsin." *Nature* 471

(7340): 656–60. https://doi.org/10.1038/nature09795.

Sterne-Marr, R., V. V. Gurevich, P. Goldsmith, R. C. Bodine, C. Sanders, L. A. Donoso, and J. L. Benovic. 1993. “Polypeptide Variants of β-Arrestin and Arrestin3.” *Journal of Biological Chemistry* 268 (21): 15640–48. https://doi.org/10.1016/s0021-9258(18)82304-3.

Ungerer, Martin, Giustino Parruti, Michael Böhm, Mechthild Puzicha, Antonio DeBlasi, Erland Erdmann, and Martin J. Lohse. 1994. “Expression of β-Arrestins and β-Adrenergic Receptor Kinases in the Failing Human Heart.” *Circulation Research* 74 (2): 206–13. https://doi.org/10.1161/01.RES.74.2.206.

Vishnivetskiy, Sergey A., Faiza Baameur, Kristen R. Findley, and Vsevolod V. Gurevich. 2013. “Critical Role of the Central 139-Loop in Stability and Binding Selectivity of Arrestin-1.” *Journal of Biological Chemistry* 288 (17): 11741–50. https://doi.org/10.1074/jbc.M113.450031.

Vishnivetskiy, Sergey A., Qiuyan Chen, Maria C. Palazzo, Evan K. Brooks, Christian Altenbach, Tina M. Iverson, Wayne L. Hubbell, and Vsevolod V. Gurevich. 2013. “Engineering Visual Arrestin-1 with Special Functional Characteristics.” *Journal of Biological Chemistry* 288 (5): 3394–3405. https://doi.org/10.1074/jbc.M112.445437.

Wacker, Waldon B, Larry A Donoso, Carolyn M Kalsow, John A Yankeelov, and Daniel T Organisciak. 1977. “Experimental Allergic Uveitis. Isolation, Characterization, and Localization of a Soluble Uveitopathogenic Antigen from Bovine Retina.” *The Journal of Immunology* 119 (6): 1949 LP – 1958. http://www.jimmunol.org/content/119/6/1949.abstract.

Wilden, Ursula, Eduard Wüst, Ingo Weyand, and Hermann Kühn. 1986. “Rapid Affinity Purification of Retinal Arrestin (48 KDa Protein) via Its Light-Dependent Binding to Phosphorylated Rhodopsin.” *FEBS Letters* 207 (2): 292–95. https://doi.org/10.1016/0014-5793(86)81507-1.

Willig, Katrin I., Benjamin Harke, Rebecca Medda, and Stefan W. Hell. 2007. "STED Microscopy with Continuous Wave Beams." *Nature Methods* 4 (11): 915–18. https://doi.org/10.1038/nmeth1108.

Wisler, James W., Howard A. Rockman, and Robert J. Lefkowitz. 2018. "Biased G Protein-Coupled Receptor Signaling: Changing the Paradigm of Drug Discovery." *Circulation* 137 (22): 2315–17. https://doi.org/10.1161/CIRCULATIONAHA.117.028194.

Wisler, James W, Scott M DeWire, Erin J Whalen, Jonathan D Violin, Matthew T Drake, Seungkirl Ahn, Sudha K Shenoy, and Robert J Lefkowitz. 2007. "A Unique Mechanism of β-Blocker Action: Carvedilol Stimulates β-Arrestin Signaling." *Proceedings of the National Academy of Sciences* 104 (42): 16657 LP – 16662. https://doi.org/10.1073/pnas.0707936104.

Xia, Zongping, and Yuechueng Liu. 2001. "Reliable and Global Measurement of Fluorescence Resonance Energy Transfer Using Fluorescence Microscopes." *Biophysical Journal* 81 (4): 2395–2402. https://doi.org/10.1016/S0006-3495(01)75886-9.

Xu, Fei, Huixian Wu, Vsevolod Katritch, Gye Won Han, Kenneth A. Jacobson, Zhan Guo Gao, Vadim Cherezov, and Raymond C. Stevens. 2011. "Structure of an Agonist-Bound Human A2A Adenosine Receptor." *Science* 332 (6027): 322–27. https://doi.org/10.1126/science.1202793.

Yan, Biao, Zhaoxia Huo, Ying Liu, Xiaoping Lin, Jun Li, Luying Peng, Hong Zhao, *et al.* 2011. "Prolyl Hydroxylase 2: A Novel Regulator of B2-Adrenoceptor Internalization." *Journal of Cellular and Molecular Medicine* 15 (12): 2712–22. https://doi.org/10.1111/j.1582-4934.2011.01268.x.

Yun, Youngjoo, Dong Kyun Kim, Min Duk Seo, Kyeong Man Kim, and Ka Young Chung. 2015. "Different Conformational Dynamics of β-Arrestin1 and β-Arrestin2 Analyzed by Hydrogen/Deuterium Exchange Mass Spectrometry." *Biochemical and Biophysical Research Communications* 457 (1): 50–57.

https://doi.org/10.1016/j.bbrc.2014.12.079.

Zhang, Xin, and Ulrike S. Eggert. 2013. “Non-Traditional Roles of G Protein-Coupled Receptors in Basic Cell Biology.” *Molecular BioSystems* 9 (4): 586–95. https://doi.org/10.1039/c2mb25429h.

Zuckerman, Ralph, and James E. Cheasty. 1986. “A 48 KDa Protein Arrests CGMP Phosphodiesterase Activation in Retinal Rod Disk Membranes.” *FEBS Letters* 207 (1): 35–41. https://doi.org/10.1016/0014-5793(86)80008-4.

APPENDICES

A. MAMMALIAN CELL CULTURE SOLUTIONS

Table A 1 Composition of D-MEM with high glucose

Components	Concentration (mg/L)
Amino Acids	
Glycine	30
L-Arginine.HCl	84
L- Cysteine.2HCl	63
L-Glutamine	580
L- Histidine Hydrochloride-H_2O	42
L-Isoleucine	105
L-Leucine	105
L-Lysine.HCl	146
L-Methionine	30
L-Phenylalanine	66
L-Serine	42
L-Threonine	95
L-Tryptophan	16
L-Tyrosine	72
L-Valine	94
Vitamins	
Choline Chloride	4
D-Calcium Pantothenate	4
Folic acid	4
Niacinamide	4
Pyridoxine hydrochloride	4
Riboflavin	0,4

Thiamine hydrochloride	4
I-İnositol	7,2
Inorganic salts	
Calcium Chloride	264
Ferric Nitrate	0,1
Magnesium Sulfate	200
Potassium chloride	400
Sodium bicarbonate	3700
Sodium chloride	6400
Sodium phosphate monobasic	141
Other components	
D-Glucose (dexrose)	4500
Phenol Red	15
Sodium pyruvate	110

Table A 2 Composition of 1X PBS Solution

NaCl	8 g/L
KCl	0,2 g/L
Na_2HPO_4	1,44 g/L
KH_2PO_4	0,24 g/L

All the components dissolved in 900 mL deionized water then pH adjusted to 7,4 by adding diluted HCl, after pH adjustment final volume was completed to 1 L then the solution was autoclaved.

Table A 3 Composition of HBSS Solution

NaCl	8 g/L
KCl	400 mg/L
$Na_2HPO_4.2H_2O$	60 mg/L
$KH_2PO_4.2H_2O$	60 mg/L
$CaCl_2$	140 mg/L
$MgCl_2.6H_2O$	100 mg/L
$MgSO_4.7H_2O$	100 mg/L
Glucose anhydrous	1 g/L
$NaHCO_3$	350 mg/L

All the components were dissolved in 800 mL of deionized water then pH adjusted to 7,4 by adding 1 M HCl, after pH adjustment final volume was completed to 1000 mL then the solution was filtered through a PES membrane 0,22 μm filter.

B. PREPARATION OF BACTERIAL CULTURE MEDIUM

LB Medium

10 g Tryptone (enzymatically digested)

5 g yeast extract

5 g NaCl

The components are dissolved in deionized water 20g/L agar was added for solid agar plate preparation, After adjustment of pH to 7,0 solution was autoclaved.

C. COMPOSITION OF BUFFERS AND SOLUTIONS

1X NEB CutSmart ™ Buffer

50 mM Potassium Acetate

20 mM Tris-acetate

10 mM Magnesium Acetate

100 μg/mL BSA

1X T4DNA Ligase Reaction Buffer

50 mM Tris-HCl

10 mM $MgCl_2$

1 mM ATP

10 mM Dithiothreitol

6x Loading Dye

10 mM Tris-HCl

003 % Bromophenol Blue

003 % Xylene Cyanol FF

60 % glycerol

60 mM EDTA

1x TAE (Tris Acetic acid EDTA) Buffer

40 mM Tris base

20 mM Acetic acid (From Glacial Acetic acid)

1 mM EDTA

Table C 1 Composition of TFBI and TFBII.

TFB1	**Final Concentration**	**Prepared Stock**	**For 100 mL Solution take from prepared Stock**
KOAc	30 mM	300 mM	10 mL
RbCl	100 mM	1000 mM	10 mL
$CaCl_2$	10 mM	1000 mM	1 mL
$MnCl_2$	50 mM	1000 mM	5 mL
Glycerol	15 %	87 %	17,2 mL
TFB2	**Final Concentration**	**Prepared Stock**	**For 10 mL Solution take from prepared Stock**
MOPS/PIPES	10 mM	1000 mM	0,1 mL
RbCl	10 mM	1000 mM	0,1 mL
$CaCl_2$	75 mM	1000 mM	0,75 mL
Glycerol	15 %	87 %	1,7 mL

The TFB1 solution completed to 100 mL, the TFB2 solution was completed to 10 mL with deionized water and the pH adjusted to 5,8. After pH adjustment both solutions filtered through a 0,22 µm filter.

Table C 2 Composition of 50 mM Acetic Acid/ Acetate (pH 4.0, 4.8, 5.5) Buffers

pH	$CH_3COONa.3H_2O$	Glacial Acetic Acid	Deionised Water
4.0	76.7 mg	110,5 µL	Up to 50 mL
4.8	49.05 mg	46.7 µL	
5.5	305 mg	14.7 µL	

Table C 3 Composition of 50 mM Glycine/NaOH (pH 8.25, 8.50, 8.95, 9.40 and 10.0) Buffers

pH	Glycine	NaOH (1M)	Deionized water
8.25	187.5 mg	X µL	Up to 50 mL
8.50		X µL	
8.95		X µL	
9.40		X µL	
10.0		X µL	

Table C 4 Composition of 1X PBS (pH 5.8, 6.2, 6.8) Buffers

pH	1X PBS	1 M HCl
5.8	50 mL	X µL
6.2	50 mL	X µL
6.8	50 mL	X µL

Table C 5 Composition of 50 mM Tris / HCl (pH 7.05, 7.20, 7.50, 7.75 and 8.05) Buffers

pH	Trizma Base	HCl (1M)	Deionised water
7.05	303 mg.	X µL	Up to 50 mL
7.20		X µL	
7.5		X µL	
7.75		X µL	
8.05		X µL	

D. PLASMID MAPS

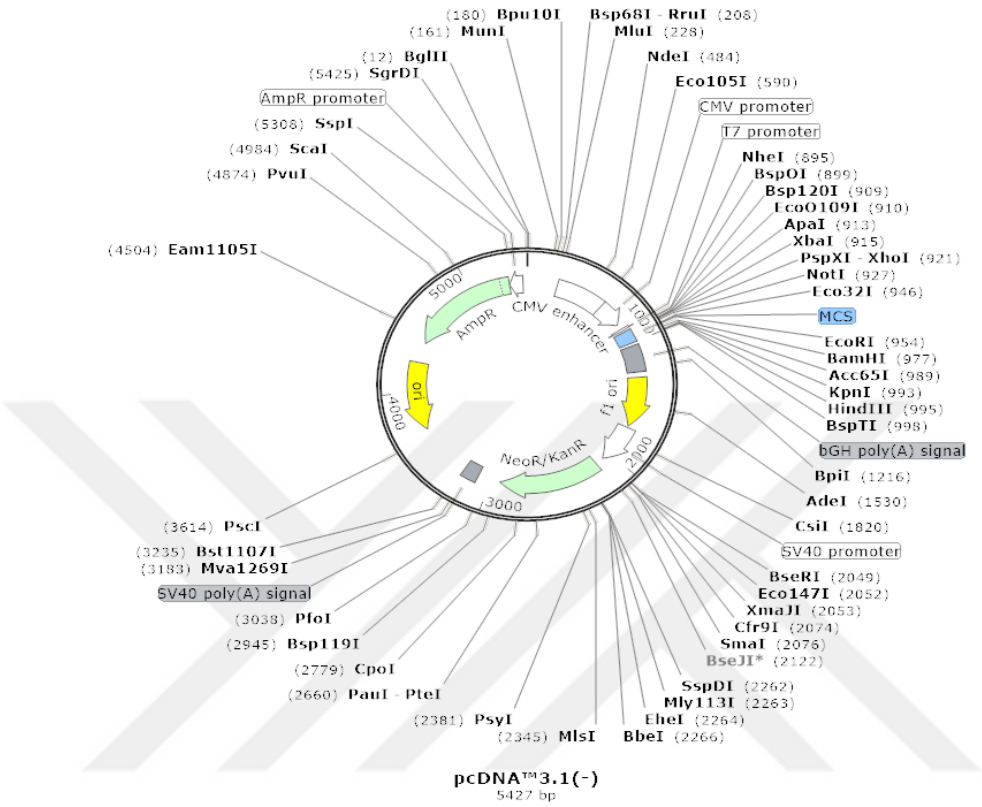

Figure D 1 Plasmid map of PcDNA 3.1- (from Snapgene)

E. PRIMERS

Table E 1 RFC primers used in tagging of Arrb2 from 177th amino acid position

Cloning method and description	Primer name	Pimer Sequence 5'-3'
RFC	Arrb2_177_mEGFP_F	**Ggtgatccgaaaggtgcagttcgccccgg**ag **ATGGTGAGCAAGGGCGAGGAG**
RFC	Arrb2_177_mEGFP_R	**Tggtttcggctgaaggctgggggccgggttt** **CTTGTACAGCTCGTCCATGCCG**

Green letters represent the sequences that anneal the mEGFP and mCh. Fluorescent proteins.

Table E 2 primers that used in confirmation of tagging of Arrb2 from 177th amino acid position

Description	Primer name	Pimer Sequence 5'-3'
Sequencing primer	PcDNA F	GTGTACGGTGGGAGGTCTAT
Sequencing primer	PcDNA R	TTCCAGGGTCAAGGAAGGC

F. CODING SEQUENCES OF FUSION PROTEINS

Coding Sequence of β-Arrestin 2

atgggggagaaacccgggaccagggtcttcaagaagtcgagccctaactgcaagctcaccgtgtacttgggcaagc
gggacttcgtagatcacctggacaaagtggaccctgtagatggcgtggtgcttgtggaccctgactacctgaaggacc
gcaaagtgtttgtgaccctcacctgcgccttccgctatggccgtgaagacctggatgtgctgggcttgtccttccgcaaa
gacctgttcatcgccacctaccaggccttccccccggtgcccaacccaccccggcccccccacccgcctgcaggaccg
gctgctgaggaagctgggccagcatgcccacccctttcttcttcaccataccccagaatcttccatgctccgtcacactgc
agccaggcccagaggatacaggaaaggcctgcggcgtagactttgagattcgagccttctgtgctaaatcactagaag
agaaaagccacaaaaggaactctgtgcggctggtgatccgaaaggtgcagttcgccccggagaaacccggccccca
gccttcagccgaaaccacacgccacttcctcatgtctgaccggtccctgcacctcgaggcttccctggacaaggagct
gtactaccatggggagcccctcaatgtaaatgtccacgtcaccaacaactccaccaagaccgtcaagaagatcaaagt
ctctgtgagacagtacgccgacatctgcctcttcagcaccgcccagtacaagtgtcctgtggctcaactcgaacaagat
gaccaggtatctcccagctccacattctgtaaggtgtacaccataaccccactgctcagtgacaaccgggagaagcgg
gtctcgccctggatgggaaactcaagcacgaggacaccaacctggcttccagcaccatcgtgaaggagggtgcca
acaaggaggtgctgggaatcctggtgtcctacagggtcaaggtgaagctggtggtgtctcgaggcggggatgtctctg
tggagctgccttttgttcttatgcaccccaagccccacgaccacatccccctccccagaccccagtcagccgctccgga
gacagatgtccctgtggacaccaacctcattgaatttgataccaactatgccacagatgatgacattgtgtttgaggacttt
gcccggcttcggctgaaggggatgaaggatgacgactatgatgatcaactctgctag

ggc and agt are silent mutations, gag tagged position.

Coding Sequence of Arrb2 177 mEGFP:

atgggggagaaacccgggaccagggtcttcaagaagtcgagccctaactgcaagctcaccgtgtacttgggcaagc
gggacttcgtagatcacctggacaaagtggaccctgtagatggcgtggtgcttgtggaccctgactacctgaaggacc
gcaaagtgtttgtgaccctcacctgcgccttccgctatggccgtgaagacctggatgtgctgggcttgtccttccgcaaa
gacctgttcatcgccacctaccaggccttccccccggtgcccaacccaccccggcccccccacccgcctgcaggaccg
gctgctgaggaagctgggccagcatgcccacccccttcttcttcaccataccccagaatcttccatgctccgtcacactgc
agccaggcccagaggatacaggaaaggcctgcggcgtagactttgagattcgagccttctgtgctaaatcactagaag
agaaaagccacaaaaggaactctgtgcggctggtgatccgaaaggtgcagttcgccccggagATGGTGAGC
AAGGGCGAGGAGCTGTTCACCGGGGTGGTGCCCATCCTGGTCGAGCTG
GACGGCGACGTAAACGGCCACAAGTTCAGCGTGTCCGGCGAGGGCGAG
GGCGATGCCACCTACGGCAAGCTGACCCTGAAGTTCATCTGCACCACCG
GCAAGCTGCCCGTGCCCTGGCCCACCCTCGTGACCACCCTGACCTACGG
CGTGCAGTGCTTCAGCCGCTACCCCGACCACATGAAGCAGCACGACTTC
TTCAAGTCCGCCATGCCCGAAGGCTACGTCCAGGAGCGCACCATCTTCT
TCAAGGACGACGGCAACTACAAGACCCGCGCCGAGGTGAAGTTCGAGG
GCGACACCCTGGTGAACCGCATCGAGCTGAAGGGCATCGACTTCAAGG
AGGACGGCAACATCCTGGGGCACAAGCTGGAGTACAACTACAACAGCC
ACAACGTCTATATCATGGCCGACAAGCAGAAGAACGGCATCAAGGTGA
ACTTCAAGATCCGCCACAACATCGAGGACGGCAGCGTGCAGCTCGCCG
ACCACTACCAGCAGAACACCCCCATCGGCGACGGCCCCGTGCTGCTGC
CCGACAACCACTACCTGAGCACCCAGTCCAAGCTGAGCAAAGACCCCA
ACGAGAAGCGCGATCACATGGTCCTGCTGGAGTTCGTGACCGCCGCCG
GGATCACTCTCGGCATGGACGAGCTGTACAAGaaacccggcccccagccttcagccga
aaccacacgccacttcctcatgtctgaccggtccctgcacctcgaggcttccctggacaaggagctgtactaccatggg
gagcccctcaatgtaaatgtccacgtcaccaacaactccaccaagaccgtcaagaagatcaaagtctctgtgagacagt
acgccgacatctgcctcttcagcaccgcccagtacaagtgtcctgtggctcaactcgaacaagatgaccaggtatctcc
cagctccacattctgtaaggtgtacaccataaccccactgctcagtgacaaccgggagaagcggggtctcgccctgga
tgggaaactcaagcacgaggacaccaacctggcttccagcaccatcgtgaaggagggtgccaacaaggaggtgctg
ggaatcctggtgtcctacagggtcaaggtgaagctggtggtgtctcgaggcggggatgtctctgtggagctgccttttgt
tcttatgcaccccaagccccacgaccacatccccctccccagaccccagtcagccgctccggagacagatgtccctgt
ggacaccaacctcattgaatttgataccaactatgccacagatgatgacattgtgtttgaggactttgcccggcttcggct
gaaggggatgaaggatgacgactatgatgatcaactctgctag

green letter sequence represents the mEGFP sequence ggc and agt are silent mutation

G. FILTERS USED IN SPINNING DISC CONFOCAL FLUORESCENT MICROSCOPY

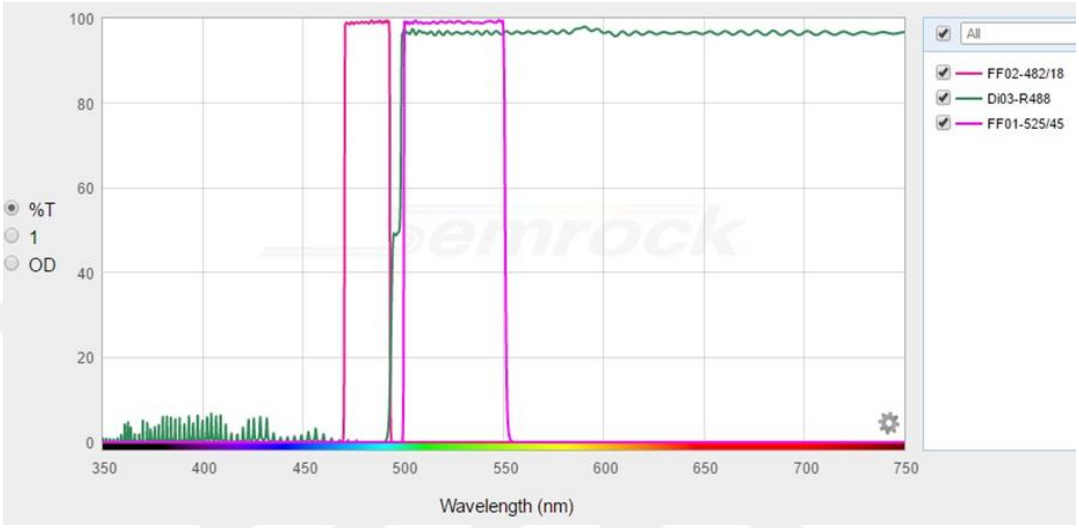

Figure G 1 Excitation and emission ranges of EGFP filter used in Leica DMI4000 B with Andor DSD2 Confocal device.

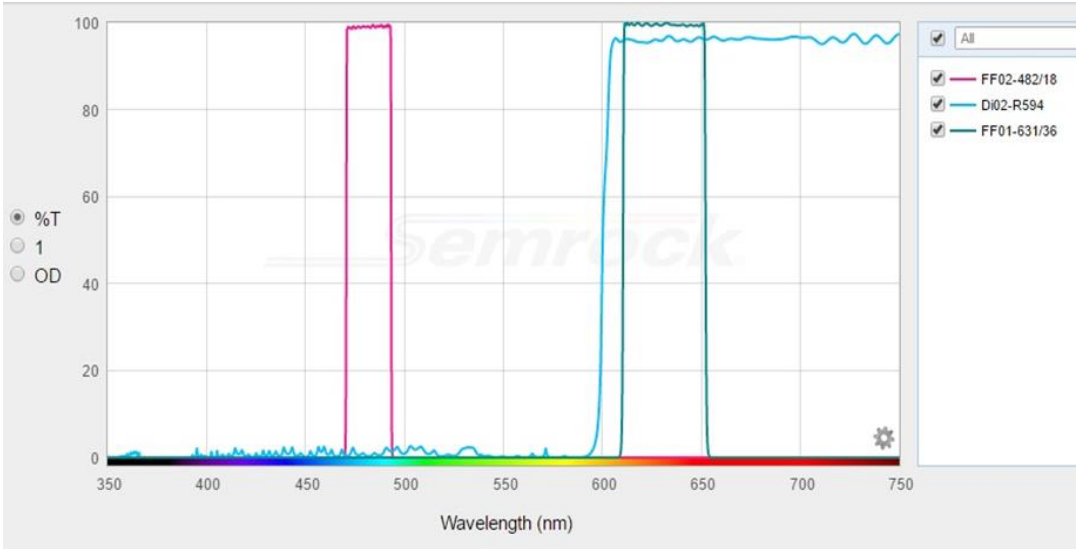

Figure G 2 Excitation and emission ranges of FRET configuration (EGFP excitation, mCherry emission) used in Leica DMI4000 B with Andor DSD2 Confocal device

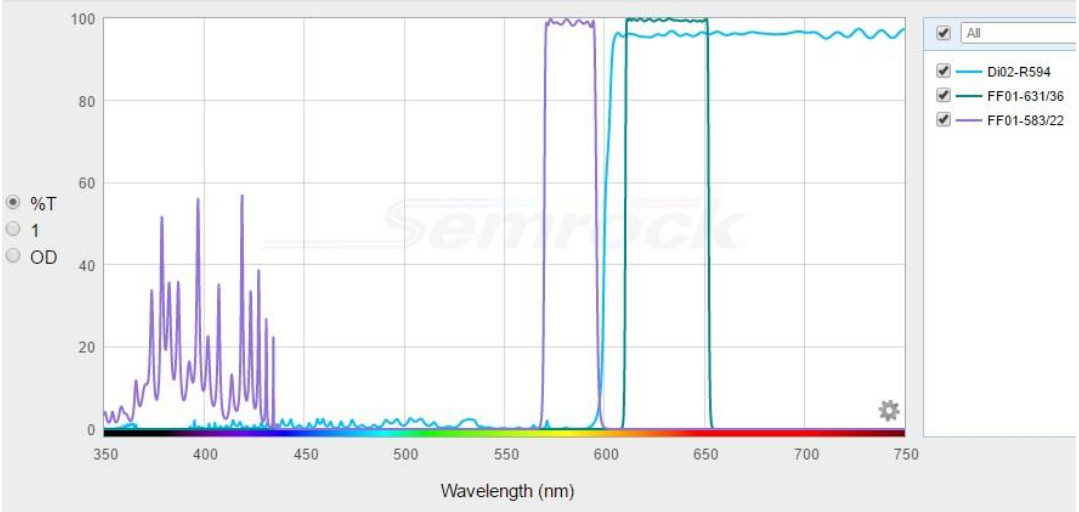

Figure G 3 Excitation and emission ranges of mCherry filter used in Leica DMI4000 B with Andor DSD2 Confocal device